Doctoral School of Geosciences

THE ACCUMULATION HISTORY OF THE PÉCEL LOESS-PALEOSOL PROFILE

A PÉCELI LÖSZ-PALEOTALAJ SZELVÉNY AKKUMULÁCIÓS TÖRTÉNETE

PhD Dissertation

Author

László Makó

Supervisor

Dr. Dávid Molnár

Assistant professor, University of Szeged, Department of Geology and Paleontology

University of Szeged

Faculty of Science and Informatics

Department of Department of Geology and Paleontology

Szeged

2023

TABLE OF CONTENTS

List of Figures

LIST OF TABLES

CHAPTER I.

Introduction and aims

Today's climatic changes make researches that process and model processes in the past increasingly important. Loess and loess-like sediments are the most important preserves of the changes that took place in the recent past – Quaternary period. By examining them in sufficient detail, we are able to examine the paleoenvironment and the factors influencing it at a resolution of decades to centuries. A large percentage of Hungary's surface is covered by loess or loess-like formations, however, it is possible to study them in walls mainly along the Danube, and most of them have already been the subject of research.

The loess is a yellowish-brownish sediment, which accumulates nearby to periglacial territories during glacial periods, mostly made of medium and coarse silt (Pye, 1995). As the dust falls, it conserves all the fauna and flora it covers, which helps us to investigate for example Molluscs. From Molluscs, we can infer the vegetation cover nearby, as well as the average temperature prevailing in the given period and of course, we can use the Molluscs shells to measure radiocarbon ages. In the warm periods, the dust falling slows and the soil formation prevails.

During my research, different loess-paleosol sequences were investigated, including some new sequences, which were not described before. The first aim was to (I) compare different chronometric methods (radiocarbon, OSL) in one sequence. The next one (II) was to investigate the Pécel site weathering degree after the first sampling period with geochemical indices. These geochemical measurements also showed that (III) there is a change in the source of the dust. After the weathering degree has been identified, the whole 26 meters high sequence was sampled and the whole grain size distribution was revealed. There were 20 radiocarbon measurements were made and the whole sequence was measured with magnetic susceptibility. It occurred from all these relative and absolute ages that the Pécel sequence started to accumulate (IV) at least in the Middle Pleistocene (between 300-400 ka.). After all, three more sequences were sampled in the Tolna hills of the Transdanubian region. These sequences were smaller, between 6-12 meters, so there were no preliminary weathering investigations. During the results processing, it occurred that there is a dominant difference between the north-eastern and the south-western sequences grain size distribution. With all the five sequences data (V) the difference in wind directions became apparent. The prevailing wind direction in the Carpathian Basin is western-northwestern, but the coarser grains in some sequences shows that

there was a period when this direction was opposite, south-southeast. In the Bodrogkeresztúr and Pécel sequences there were no well-developed paleosol layers, but in the Transdanubian sequences 1-3 meters thick paleosols were described which (VI) can be explained by the regionality of hilly areas.

To investigate all these results, grain size distribution, loss on ignition, geochemical investigation (XRF), magnetic susceptibility, chronometric analysis (radiocarbon and OSL ages) were performed. From the chronometric data there were age-depth models and accumulation rates were made and calculated.

CHAPTER II.

MAR COMPARISONS BETWEEN DIFFERENT CHRONOMETRIC METHODS FOR TWO PROFILES IN THE BODROGKERESZTÚR AREA

László Makó
Department of Geology and Paleontology, University of Szeged, Hungary
makol@geo.u-szeged.hu
Dávid Molnár
Department of Geology and Paleontology, University of Szeged, Hungary
molnard@geo.u-szeged.hu
Péter Cseh
Department of Geology and Paleontology, University of Szeged, Hungary
cspeti94@gmail.com
Pál Sümegi
Department of Geology and Paleontology, University of Szeged, Hungary
sumegi@geo.u-szeged.hu

Studia Quaternaria
Volume 38, no. 1, 2021
DOI: 10.24425/sq.2020.133761

MAR comparisons between different chronometric methods for two profiles in the Bodrogkeresztúr area

László Makó, Dávid Molnár, Péter Cseh, Pál Sümegi

Abstract

The deepening and exploration of the loess-paleosol section at the foot of the Kopasz Hill at Bodrogkeresztúr have been carried out to expand the existing knowledge of the Carpathian foothill paleoenvironmental factors and their impact. The study deals with particle size analysis, organic matter, and carbonate content. For the presentation of age-depth models, the OSL dates of Bodrogkeresztúr (BKT) and the ^{14}C dates of Bodrogkeresztúr, brickyard 1 were used-, and the diagrams of the Accumulation Rates (AR) derived from them. These were compared with Mass Accumulation Rate (MAR) calculations based on OSL and ^{14}C data from BKT and ^{14}C data from Bodrogkeresztúr, brickyard 1. It became evident that there is a significant difference between the two sections, which may be due to the upland position, the overlap, or the wind tunnel effect.

Sedimentological studies revealed coarser grain composition, however, the nearly complete absence of coarser sand fraction is also noticeable in the case of BKT. Also, the entire section is characterized by increased carbonate content due to post-sedimentation processes, recarbonization and leaching. The AR and MAR results show the difference between the suitability of different chronometric methods, indicating that the top of both sections may have been redeposited or eroded.

II.1. Introduction

The loess-paleosol profile of Bodrogkeresztúr (BKT; Bösken et al. 2019) (Fig. II.1), located near Bodrogkeresztúr in the north-eastern part of Hungary at 48° 8’ 50” N and 21°21’ 49” E, was modelled in 2014 by a German-Hungarian research team (University of Aachen and University of Szeged). The primary purpose of sampling and analysis was to supplement the previously surveyed area with data from a new section (Sümegi and Hertelendi, 1998; Sümegi and Rudner, 2001; Sümegi and Krolopp, 2002; Sümegi, 2005; Schatz et al., 2011, 2012, 2015; Sümegi et al., 2016). The previously investigated Bodrogkeresztúr, brickyard 1 profile – which radiocarbon data was also used to create an age-depth model and MAR for the comparison –, is located 100 meters away from this new site. With the use of these two sections we aimed to

compare the AR, MAR and the usage of age-depth models with different chronometric methods on these two profiles.

As a result, a summary article was published in 2019, in which the authors discuss the chronological, sedimentological and geochemical parameters and features of the section (Bösken et al., 2019). To complement these assays, new assays such as organic and carbonate contents (LOI – loss on ignition; Dean, 1974), particle composition analysis, age-depth model and accumulation rate diagrams were made. The samples were taken in 4 cm resolution, from the 592 cm high wall, resulting 148 samples, but the uppermost 8 cm was not sampled.

For the study, the research team obtained three OSL dates, which can be used to produce today's depth models which show only a low degree of accuracy. Thus, we used the radiocarbon dating of the Bodrogkeresztúr, brickyard 1, similar to BKT, which was previously explored in its structure and composition to make the model. Neither the Bodrogkeresztúr, brickyard 2 would have been suitable because of its diverse composition, nor the Henye Hill section -which is a typical locality of Gravettian culture where minor scattered bone and silica fragments were found (Sümegi et al., 2016) with its only one piece of radiocarbon dating.

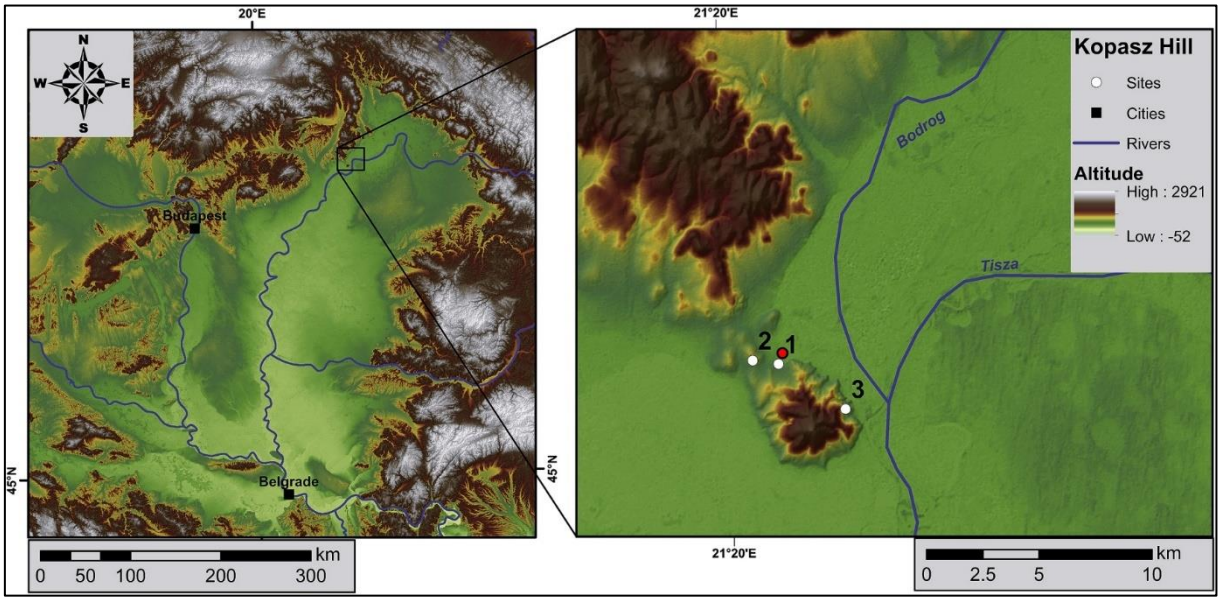

Fig. II.1 The position of the Kopasz Hill in the Carpathian Basin (1. BKT, 2. Bodrogkeresztúr-Henye, 3. Tokaj, Patkó quarry, red dot: Bodrogkeresztúr, brickyard 1; modified after Bösken et al. (2019)

II.2. Methods

The particle size analysis of the samples collected from the BKT section was carried out based on the method of Bokhorst et al., 2011. Organic and carbonate matter values were obtained by using the Dean weight loss method (LOI; Dean, 1974). Measurements were made

with the Omec Easysizer 20 Laser Sedigraph and with a furnace at the Department of Geology and Paleontology (University of Szeged). The values of the laser sedigraph are plotted on a 100% stacked graph divided by the particle size ranges of the Wentworth scale (Wentworth, 1922). By analyzing the particle fractions in the diagram, the positions of loess and paleosol horizons can be observed. In loess-paleosol profiles, increased organic matter content may represent paleosol horizons, as the result of the organic matter enrichment processes of pedogenesis. At the same time the weathering results a decrease in carbonate content. Therefore, carbonate accumulation zones appear due to the development of advanced paleosols (Dokuchaev, 1879; Ding et al., 2001).

II.2.1. Absolute dating

Knowledge of the ages is essential for the timely placement of the section and thus for correlation with each other (Sümegi, 2005). Two age determination methods were used on the examined segment, OSL (optically stimulated luminescence; Huntley et al., 1985) from three depths and radiocarbon dating from one (Bösken et al., 2019). For the BKT OSL measurement methodology see Bösken et al. (2019). The radiocarbon ages from the two sections were calibrated using IntCal13 calibration curve with OxCal (Bronk Ramsey and Lee, 2013) and Calib 7.10 (Stuiver and Reimer, 1993) softwares. OSL measurements are reliable for up to 350,000 years and can vary by up to 5-10% (Rhodes, 2011).

II.2.2. Age-depth models

There are many age-depth models, from simpler (linear interpolation) to more complex ones. The essence of each model is to plot the values between the measurement points according to the given calculation method (Bennett, 1994). In the simplest approaches, sediment formation is uniform between the measured points, but this is not the actual case either since the rate of sediment accumulation is fluctuating. Therefore, models that rely on historical error values also consider previous data. The models were constructed with Bacon (Blaauw, Christen, 2011) program, used Bayesian MCMC (Markov Chain Monte Carlo) calculations. Both models were calculated in 4 cm sections, as the samples were taken and 100% of the results were fit in the 9% confidence interval (CI) ranges. In the BKT case, only the OSL ages were used, because the upward aging was distorted the result. In 592 cm, 149 sections were calculated by 33.22 mln iterations. At the Bodrogkeresztúr, brickyard 1 profile, the 700 cm resulted 176 sections by 39.16 mln iterations. The OSL and IRSL dates do not require calibration, but the uncertainty of the absolute dates obtained from them greatly influences the accuracy of the model. From this

point of view, both OSL and IRSL (post-IR IRSL) measurements are unsuitable for making this type of model.

II.2.3. MAR calculation

By calculating the MAR (Mass Accumulation Rate), it shows the extent of sedimentation between two ages, considering the height of the section, sample density, and fraction size. Method of calculation:

$$MAR = LSR \cdot \rho_{dry} \cdot f_{eol} \quad \left[\frac{gramm}{m^2 \cdot age}\right]$$

The LSR (Linear Sedimentation Rate) in the formula gives the thickness of the sediment formed over time (m a-1). The ρ_{dry} is the dry bulk density (g m^{-3}), which for loess sediment is 1.5 g cm-3 according to Újvári et al. (2010). The f_{eol} parameter is the mass concentration of aeolian materials (Kohfeld and Harrison, 2001), which in case of loess is 1. The final result is obtained with the dimension g m^{-2} a^{-1} (Újvári et al., 2010; Sümegi et al., 2016, 2019).

II.3. Results

Since the predominant particle size range of loess is medium and coarse silt (Pécsi, 1993), these fractions are present in the graph in increased amounts, whereas the increas of clay fraction is due to postgenetic processes. The presence of smaller grain fractions compared to sand may indicate weathering, but higher sand content may be a signal of a change in the energy of the transportation material (Pye, 1995).

II.3.1. Particle composition

In the publication of Bösken et al. (2019), based on grain composition results, the BKT profile was divided into 4 parts, which, can be further subdivided into a minimum of 7 (Fig. II.2). The lowest of it, between 570-592 cm is a lower clayey fluvial sediment with high organic matter content (4%) and carbonate (7-8%) values. The part between 400 and 570 cm is an advanced paleosol with upwardly increasing organic matter content (from 2.5 to 3.5%) and a significant proportion of coarse grain size (between 23-32%). Besides, loess aggregates appear between 520 and 540 cm. The next part (340-400 cm), which is a loess body, is marked by a coarser grain size upwards, with the highest fraction of sand (~15% very fine sand and ~0.5% fine and medium sand) in this section. Based on the increasing carbonate and decreasing organic matter values, this horizon may have been the carbonate accumulation zone of the poorly developed paleosol above it.

Between 270 and 340 cm in the loess body, a poorly developed paleosol can be defined according to the granular refinement, the increasing of organic matter and the decreasing of carbonate content. Above, between 240-270 cm a peak of organic matter with almost 3%, can be found. Between 70-200 cm a homogeneous loess body with low sand content (5-10%), 2% organic matter and 3-4% carbonate content can be defined. The upper 70 cm is loose soil, where both organic matter, grain size increase upwards and carbonate also increases till the top 16 cm, when it decreases due to leaching.

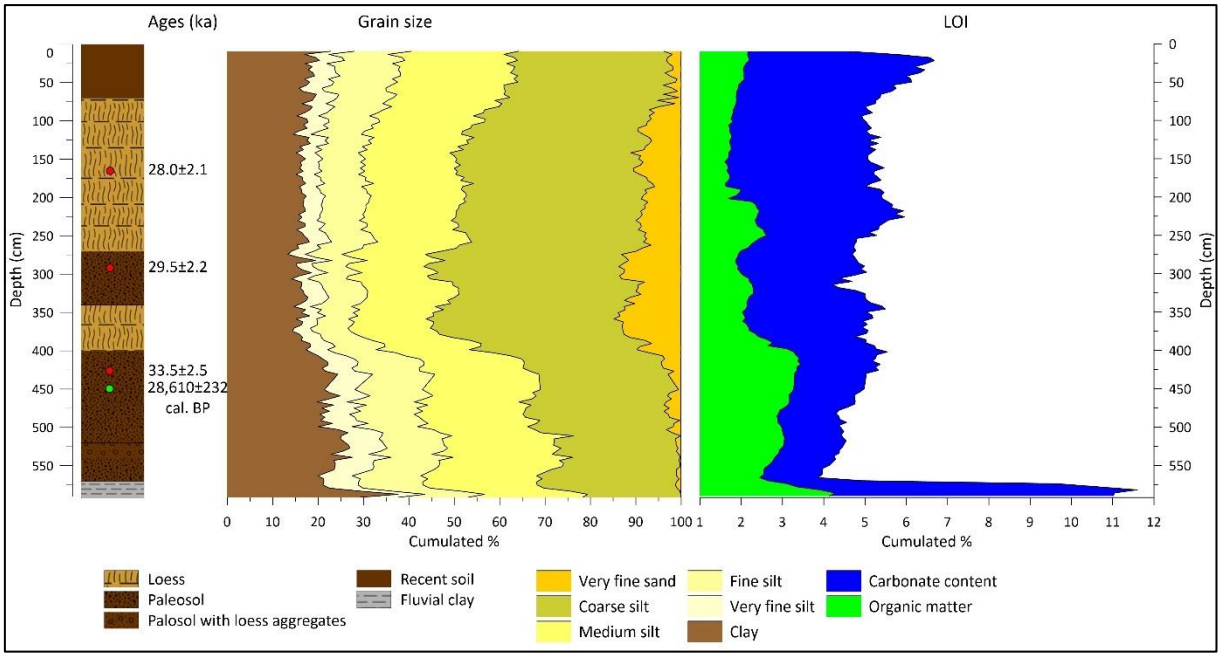

Fig. II. 2. Sedimentological (left) and LOI (right) results of the BKT section

II.3.2. Age-depth models

Table II. 1. OSL and radiocarbon data from BKT and Bodrogkeresztúr, brickyard 1 sections

Profile	Depth (cm)	OSL ages (ka)	Uncal age (years)	Cal BP age (years)	Lab code
BKT (Bösken et al. 2019)	169	28000±2.1	-	-	C-L3799
BKT (Bösken et al. 2019)	290	29500±2.2	-	-	C-L3797
BKT (Bösken et al. 2019)	427	33500±2.5	-	-	C-L3795
BKT (Bösken et al. 2019)	451	-	24580±90	28610±232	Beta-454081
Bodrogkeresztúr, brickyard 1 (Sümegi, 2005)	125-150	-	15388±147	18633±305	Deb-4358
Bodrogkeresztúr, brickyard 1 (Sümegi, 2005)	325-350	-	19813±170	23885±421	Deb-4335
Bodrogkeresztúr, brickyard 1 (Sümegi, 2005)	500-525	-	26851±398	30895±647	Deb-3049

For the profiles, shown in Figure II.3 and II.4, age models were constructed using Bacon (Blaauw and Christen, 2011) program to obtain minimum, average, and maximum accumulation values per centimeter, and the charts were created with Grapher. Figure II.3 shows the section of BKT, including the OSL and the radiocarbon ages (Table II.1), but the model was generated only by the OSL data which cause the homogeneity, because of its high (approx. 10%) error values. The mean accumulation is 0,49 mm/year, but the CI in one point reaches the 2 mm/year maximum value.

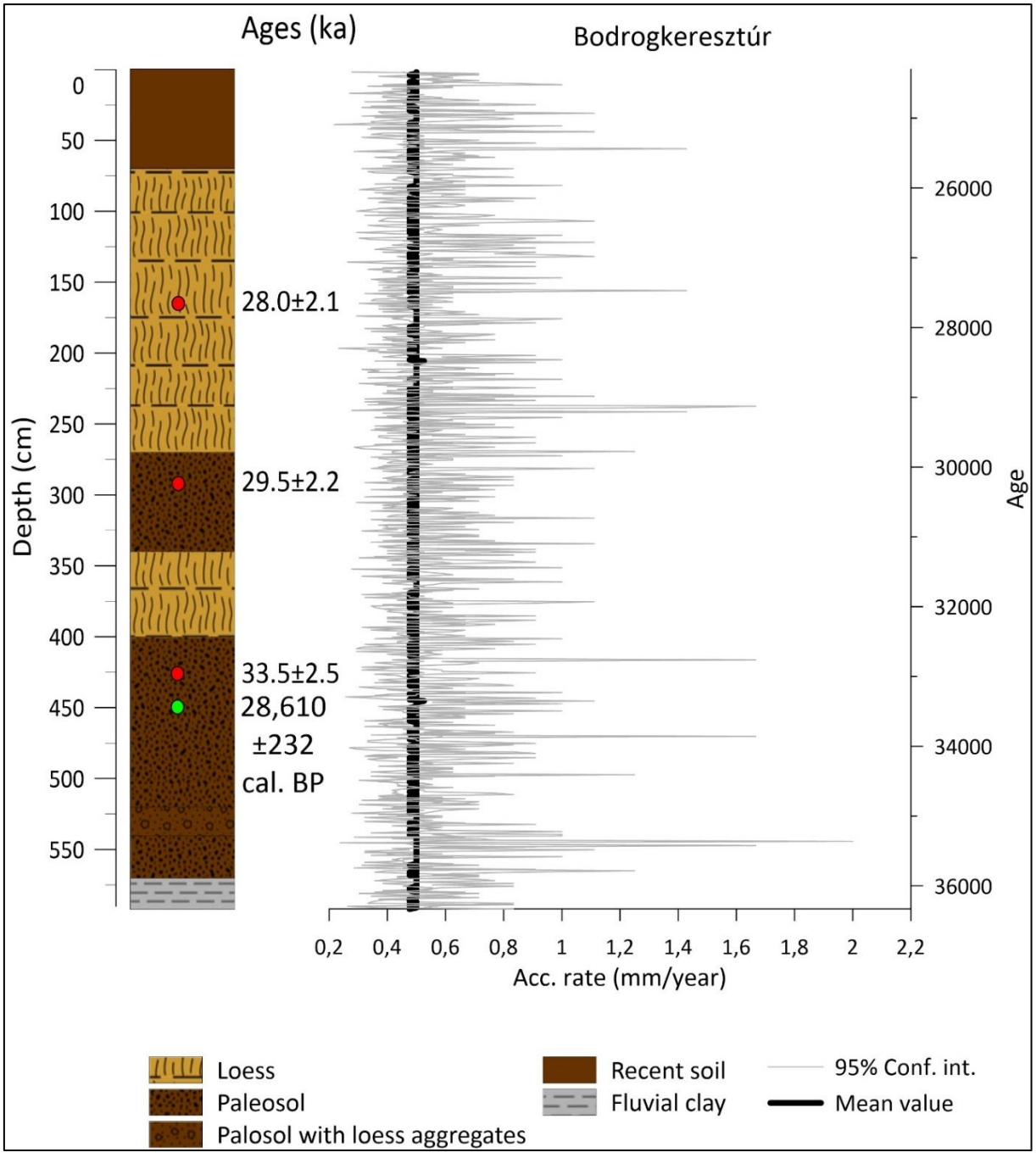

Fig. II. 3. BKT section with its OSL and radiocarbon dates and accumulation rate diagram

In contrast, on Figure II.4 (Bodrogkeresztúr, brickyard 1) a more differentiated accumulation diagram can be observed. Its mean value is 0,28 mm/year which is almost half of the BKT's result. Usable information about the accumulation cannot be obtained from the lower loess body, because of the absence of any age data. The accumulation of the upper loess body is a little higher than the mean (~0,29 mm/year) but between 18,000-24,000 cal. BP yr. a more dominant, 0.34-0.36 mm/year rate appears. Above that, the accumulation falls back to 0.23-0.24 mm/year.

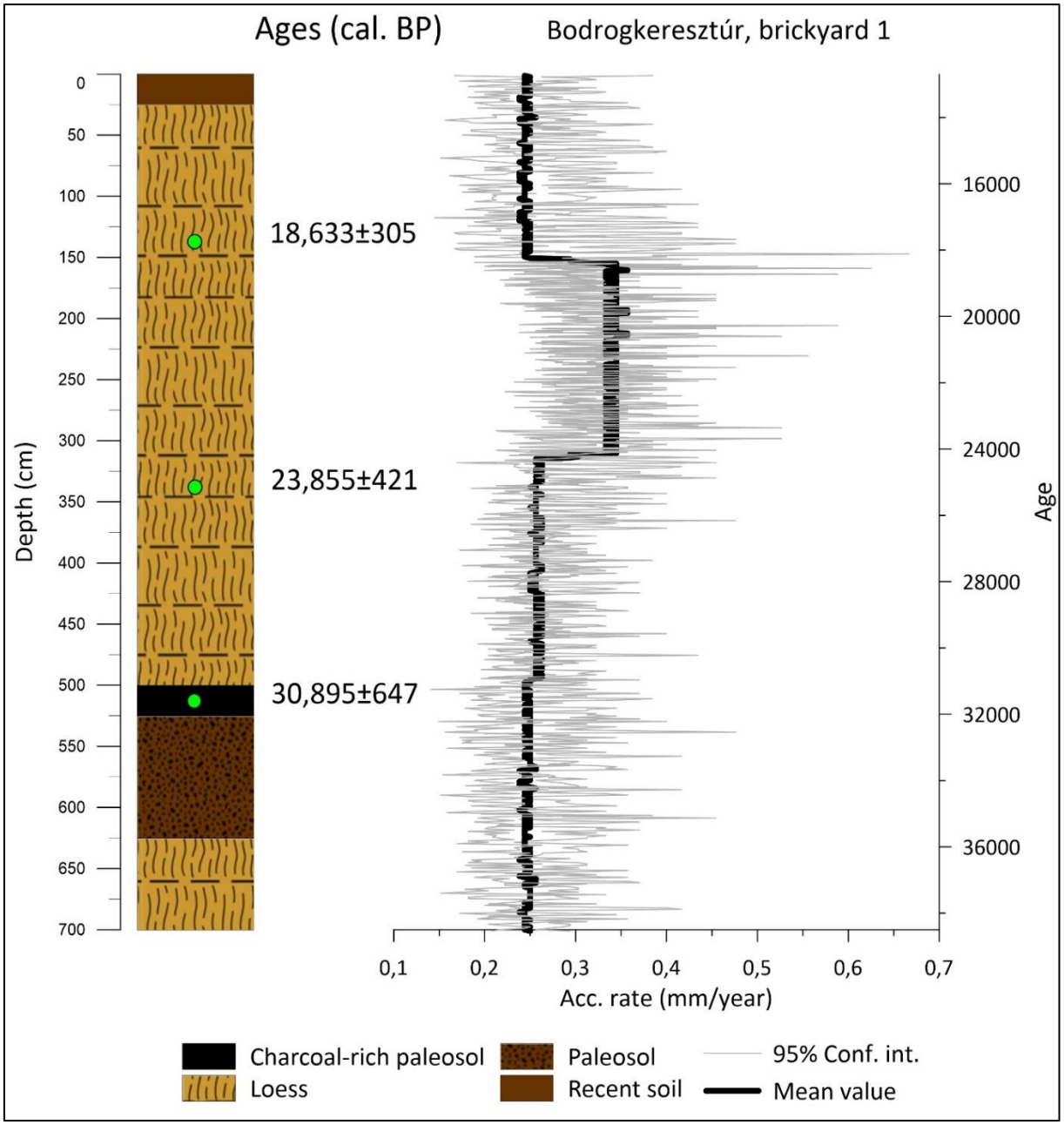

Fig. II. 4. Bodrogkeresztúr, brickyard 1 section with its radiocarbon dates and accumulation rate diagram

II.3.3. MAR values

The MAR values nuances the AR values because, based on the models, we can separate the loess bodies, and we will be able to examine them separately. The MAR table of BKT (Table II.2) was compiled from the OSL data, where we can see the same high accumulation results as in Figure II.3. In the upper loess body, we can see a similarity between the AR and MAR values, but there is still a difference. The AR rates here between 0.45-0.56 mm/year, which means 671-843 g m^{-2} a^{-1} dust accumulation. In the lower part a 0.49 mm/year accumulation can be seen, which meanss 738 g m^{-2} a^{-1} dust.

Table II. 2. MAR results of the BKT section

Age (yr BP)	Depth (cm)	SR (cm/year)	ρ (g/cm^3)	*f*eol	MAR (g/m^2*age)
25744	70 (bottom of recent soil)	-	-	-	-
28000	169	0.045	1.5	1	671
29797	270 (bottom of the upper loess)	0.056	1.5	1	843
29500	290	-	-	-	-
31219	340 (top of the lower loess)	-	1.5	1	-
32439	400 (bottom of the lower loess)	0.049	1.5	1	738
33500	427	-	-	-	-

Table 3 shows the MAR of the Bodrogkeresztúr, brickyard 1, the ages for which were obtained from radiocarbon measurement. Here we have two ages from the upper loess body and one from the charcoal rich paleosol (Fig. II.4.), in absence of any age data, there is no information about the lower loess body. From the bottom to the top, we can see an increase in the middle of the loess body, but here the maximum AR is reaching the 0.38 mm/year, which means 571 g m-2 a-1 what is still lower than the lowest amount of dust in BKT (Table II.2). The lower values similar or a little smaller to the AR, between 0.23-0.246 mm/year, which means 345–370 g m-2 a-1 dust accumulation.

Table II. 3. MAR results of the Bodrogkeresztúr, brickyard 1 section

Age (cal. BP)	Depth (cm)	SR (cm/year)	ρ (g/cm^3)	f_{eol}	MAR (g/m^2*age)
13717	25 (bottom of recent soil)	-	-	-	-
18633	138	0.023	1.5	1	345
23885	338	0.0381	1.5	1	571
30461	500 (bottom of the upper loess)	0.0246	1.5	1	370
30895	513	-	-	-	-

II.4. Discussion

The zones, delimited by the grain composition and the LOI examination show a high degree of coincidence, with unusually high clay content and low carbonate content in the entire section compared to loess. The difference between these two factors suggests that the material of the section is slightly weathered, since the fine effect of weathering and the decarbonisation caused by the lower pH increases the proportion of fine particles and decreases the carbonate content (Bohn et al., 1985; Ding et al., 2001; Molnár, 2015). Furthermore, the two studies support the hypothesis that the dark, clayey sediment on the underside of the section may have been of fluvial origin (Bösken et al., 2019), since high clay accumulation and high organic and carbonate content presuppose a fluvial sediment formation environment (Molnár, 2015; Molnár and Sümegi, 2016). The grain composition of this fluvial sediment is also distinct from that of the recurrent soil and the paleosol layers.

The large difference between AR and MAR values is also partly explained by the upland position of the BKT section, which may result in higher accumulation values. Besides, the wind tunnel phenomenon assumed by the research team, may also increase the accumulation. It is also indicated that the Upper Tokaj Fossil Soil Horizon, which is a charcoal rich paleosol containing Gravettian artefacts (Sümegi et al., 2016), does not appear in the surveyed section. Furthermore, 5,000 years of rejuvenation can be observed between the lowest OSL and the deeper radiocarbon values.

Comparing the AR values from the models and the MAR values derived from the ages and the models also, nuances of difference can be seen in both sites. As long as the AR values (Fig. II.3.) totally uniform, the MAR values show changes in the accumulation inside the upper loess body (0.45-0.56 mm/year instead of 0.49), in the case of BKT. In the lower loess body,

there are no further differences in accumulation. In contrast, in the case of Bodrogkeresztúr, brickyard 1, the AR and the MAR values almost the same, an increase in the accumulation can be observed from the bottom to the top. Based on the MAR, higher maximum accumulation value (0.38 mm/year instead of 0.34-0.36) can be seen. In absence of any age data, there is no information about the lower loess body. From the first MAR values of Table 2 and 3 and the ages it can be assumed that the top of the upper loess site is eroded or redeposited.

More accurate conclusions could be obtained by measuring and examining the radiocarbon dates of the profile since OSL / IRSL dates can only be examined with near-linear accumulation due to their high uncertainty. Therefore, the finding that younger sediments are older in OSL age determination than in radiocarbon age (Újvári et al., 2014; Bösken et al., 2019) should be treated with caution, so it is advisable to use ^{14}C for younger sedimentary contexts and use OSL or other luminescence age determination method on older sediments.

II.5. Conclusion

The loess-paleosol profile, developed at Bodrogkeresztúr (Bösken et al., 2019), is the result of the changes in the paleoenvironment at the foot of the Carpathians and allows us a better and more accurate understanding of the setting of the local Gravettian culture in the area. It deals with the analysis of the particle composition of the section, presents and compares the age models based on the OSL and radiocarbon derived from the radiocarbon results and accumulation rates of the section and the nearby Bodrogkeresztúr, brickyard 1. The Upper Tokaj Fossil Horizon appears both at Bodrogkeresztúr, brickyard 1, (30895±647 cal. BP) previously examined by Sümegi (2005) and at Henye Hill (30376±715; Sümegi et al., 2016) section – it contains Gravettian finds –, but not in the BKT profile. This deficiency, as well as the significant accumulation, the smaller average particle size, the almost complete absence of the sand fraction and the increased carbonate content of the whole segment, are the results of sedimentation processes, recarbonization and leaching. The proximity of the sections, the consistency of their composition, and the differences in dating make it possible to study the accuracy and efficiency of dating methods through age-depth models. The accumulation rate diagrams from the data of our models show that the OSL / IRSL correction methods are not suitable for constructing accurate Bayesian-type age-depth models because of their high uncertainty values. To get a better understanding of sediment accumulation, carbon isotopic data would be needed to clarify issues arising from accumulation differences. As radiocarbon analyzes are no longer available at levels above 65,000 years (Stuiver et al., 1998a, b), it is necessary to use OSL assays at these levels for more accurate age determination (Újvári et al.,

2014). However, our section is still at a chronological level measured by the radiocarbon dating method.

CHAPTER III.

SELECTED GRAIN-SIZE AND GEOCHEMICAL ANALYSES OF THE LOESS-PALEOSOL SEQUENCE OF PÉCEL (NORTHERN HUNGARY): AN ATTEMPT TO DETERMINE SEDIMENT ACCUMULATION CONDITIONS AND THE SOURCE AREA LOCATION

László Makó

Department of Geology and Paleontology, University of Szeged, Hungary

makol@geo.u-szeged.hu

Dávid Molnár

Department of Geology and Paleontology, University of Szeged, Hungary

molnard@geo.u-szeged.hu

Boglárka Runa

Department of Geology and Paleontology, University of Szeged, Hungary

runaboglarka@gmail.com

Gábor Bozsó

Department of Mineralogy, Geochemistry and Petrology, University of Szeged, Hungary

bozso.gabor@geo.u-szeged.hu

Péter Cseh

Department of Geology and Paleontology, University of Szeged, Hungary

cspeti94@gmail.com

Balázs Nagy

Department of Geology and Paleontology, University of Szeged, Hungary

nagba88@gmail.com

Pál Sümegi

Department of Geology and Paleontology, University of Szeged, Hungary

sumegi@geo.u-szeged.hu

Quaternary

Volume 4, no. 2, 2021

DOI: 10.3390/quat4020017

Selected Grain-Size and Geochemical Analyses of the Loess-Paleosol Sequence of Pécel (Northern Hungary): An Attempt to Determine Sediment Accumulation Conditions and the Source Area Location

László Makó, Dávid Molnár, Boglárka Runa, Gábor Bozsó, Péter Cseh, Balázs Nagy, Pál Sümegi

Abstract

The loess-paleosol profile near the settlement of Pécel has a notable size among the loess-paleosol sequences of the Northern Carpathian territories. Therefore, comprehensive sedimentological examinations were performed to understand the profile and the information preserved in it. The past periodicity and intensity of winds were showed by particle composition studies (GSI, U-ratio). At least two source areas can be presumed based on geochemical indices (CIA, CIW, Rb/Sr, Zr/Rb). Based on the characteristics of the chemical composition of sulphide minerals (P, S, Pb, Ni, As sulphides), the lower 10 m of the profile was supposed to be transported from the NW direction (Buda Thermal Karst, Börzsöny, Cserhát). Sufficient information is not yet available in order to determine the source area of the upper 10 m. By using the mentioned indexes, major developing and weathering horizons also could be identified.

III.1. Introduction

The complex investigation of loess-paleosol profiles aims at the detection of paleoclimatic and paleoecological changes of the Quaternary period (Kukla, 1997; Ding et al., 2005; Rousseau, 1990; Antoine et al., 2001; Zhou et al., 1990; Sümegi, 2005; Bösken et al., 2018; Marković et al., 2015; Song et al., 2018; Moine et al., 2008; Sümegi et al., 2011, 2015, 2018, 2019, 2020; Molnár et al., 2019). The sedimentological (particle size composition) and geochemical analyses of loess-paleosol sequences can reveal environmental factors like the prevailing wind direction (Újvári et al., 2010, 2016; Bösken et al., 2019), wind intensity (Pye, 1995), precipitation intake (Rousseau et al., 2002) and weathering conditions and parameters (Gallet et al., 1998; Jahn et al., 2001). The high-resolution sampling of the profiles supported by a sufficient amount of age data allows the examination with the resolution of decades and centuries. Our sediment samples cover a relatively short time interval because of the resolution of the sampling (4 cm), which provides the detection of so-called microcycles (Sümegi et al., 2019, 2020; Hupuczi and Sümegi 2010).

The graphical interpretation of grain size distribution could supplement the investigations with relevant information. One of these is the identification of loess and paleosol levels by the analysis of grain size fractions in the diagrams. Since loess predominantly comprises medium and coarse silt (Pye, 1995), a relatively high sand or clay content indicates a change in the accumulation conditions (Pye, 1995). The high clay content could be the result of postgenetic processes, while an increased sand content suggests a change in the energy of the transport medium (in this case, rivers and wind) (Pye, 1995). Weathering has a prominent role in the postgenetic processes, which causes an increase in the proportion of the fine fraction by the disintegration and fragmentation of larger sediment particles (Pye, 1995).

The loess-paleosol section of Pécel is situated in the western area of the Gödöllő Hills. These hills, with an area of 550 km^2, are rich in natural and landscape values. The elevation of the area ranges between 130 and 344, with a gradual decrease towards SE (Marosi and Somogyi, 1990). The dominant geomorphological forms are the two NW-SE lines of Valkói and Úri ridges (remnant ridges) and the Isaszegi Passage, a wind furrow, eroded by deflation (Ruszkiczay-Rüdiger et al., 2007). On the surface of the ridges, loess-paleosol series up to the height of 40 m were developed, while Isaszegi Passage area is covered by sand (sand dunes, sand sheets (Ruszkiczay-Rüdiger et al., 2007)).

Since no previous research has been carried out on the loess-paleosol profile of Pécel, the authors aim to reconstruct the sedimentological conditions, processes during and following the deposition, and assume the degree of the weathering by the preliminary particle composition and geochemical investigations. This section can be a new area available for further paleoenvironmental and paleoclimatic research. Quaternary studies in Hungary can be supplemented with additional information with the 20–30-m-high profile of Pécel. It has a unique location in contrast to the loess-paleosol profiles of lowland (e.g., Sümegi et al., 2015, 2019, 2020; Molnár et al., 2019; Újvári et al., 2014, 2016) and foothill (e.g., Sümegi et al., 2011, 2016; Bösken 2019, Varga et al., 2011) regions of Hungary. Because of it, the North Hungarian Mountains and Buda Hills could play a role in the origin of the sediment of the Pécel profile.

A further aim of the research primarily could be the malacological examinations (Molnár et al., 2021; Krolopp, 1991; Sümegi, 1995; Sümegi and Krolopp, 2002) or the radiocarbon/OSL dating of the profile. Moreover, age-depth models (Sümegi et al., 2020; Molnár et al., 2019; Újvári et al., 2014; Makó et al., 2021) can be constructed, accumulation rate can be calculated (Újvári et al., 2010, 2016; Makó et al., 2021), and paleoenvironmental reconstruction can be carried out (Sümegi et al., 2011, 2015, 2016; Molnár et al., 2019; Sümegi

and Krolopp, 2002) by using these additional pieces of information. Furthermore, our data can be correlated with other profiles (Marković at al., 2015; Jary, 2009; Jary and Ciszek, 2013).

III.2. Materials and Methods

The loess-paleosol profile of Pécel (47°29′47” N and 19°21′12” E (Fig. III.1)) was sampled in 2019. The section with a height of approximately 18.72 m was created by using nine continuous sub-sections. All subsections were sampled with a resolution of 4 cm (468 samples). The preliminary particle composition and geochemical analyses were carried out at the University of Szeged.

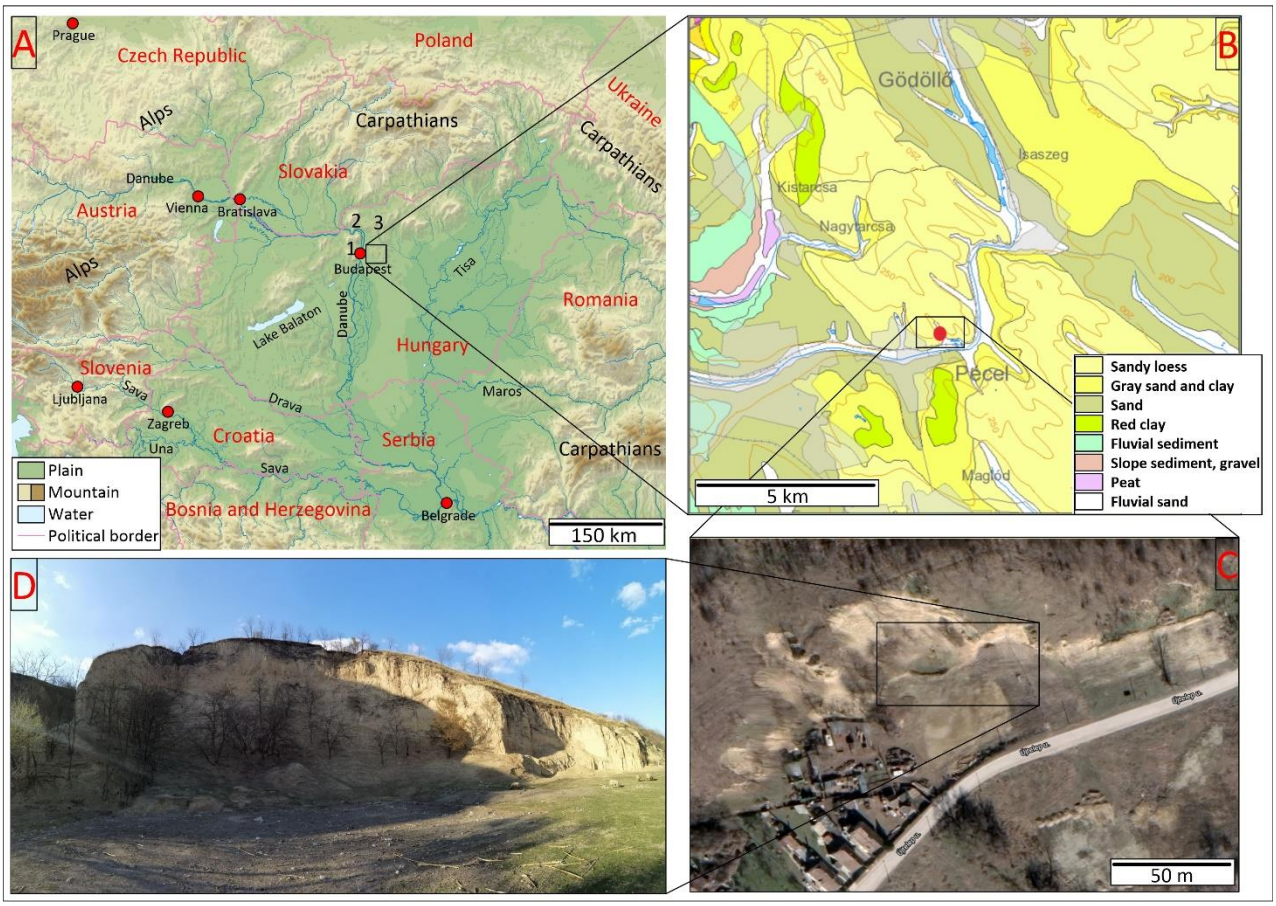

Fig. III. 1. Location of the loess-paleosol sequence of Pécel in the Carpathian Basin ((A) figure: 1. Buda Thermal Karst, 2. Börzsöny, 3. Cserhát (Wikimedia Commons), (B) figure: surface formations (Gyalog and Síkhegyi, 2005), (C) figure: ortophotomap (Google Maps), (D) figure: selfmade site photo)

III.2.1. Grain Size Analysis

The determination of grain size composition was based on Bokhorst et al. (2011). Air dried samples were pre-treated in hydrogen peroxide (30% H_2O_2) and hydrochloric acid (10% HCl) bath to remove organic materials and carbonate from the sediment. Then, 30 mL of Calgon

($Na_2P_6O_{18}$) solution was added to 0.7 g of the sample to separate the individual granules. Immediately before the measurement, the samples were treated in an ultrasonic cleaner for 20 min to prevent the adhesion of the particles. The grain size composition was carried out with an Easysizer 20 laser sedigraph at the Department of Geology and Paleontology, University of Szeged. The source used is a 2 MW of energy, 0.6328 μm wavelength He-Ne laser (Sümegi et al., 2019). The laser sedigraph measured 42 particle size ranges between 0.0001 and 0.5 mm using 54 built-in detectors based on the Mie scattering theory. Frequency and cumulative values were calculated by using the measured values. The results were arranged into particle size ranges based on the Wentworth scale (Wentworth, 1922) and plotted on separated line diagrams.

III.2.2. Grain Size Indices

The U-ratio and GSI values were calculated based on the particle composition results to determine the energy of the transport medium (Vandenberghe et al., 1985, 1997; Vandenberghe and Nugteren, 2001). The U-ratio gives the ratio of coarse silt with medium and fine silt $\frac{16-44\ \mu m}{5.5-16\ \mu m}$. It can be used to distinguish glacial periods with significant aeolian transport (high U-ratio) and high wind speed and warm, wet interglacial periods of weak winds (low U-ratio). This is based on the observation that the predominant particle size of aeolian sedimentation in warmer interglacial periods is <16 μm, while in cold glacial periods it is >16 μmn (Vandenberghe et al., 1997; Nugteren et al., 2004). Clay (<5.5 μm) and fractions <44 μm are not taken into account in the calculation of U-ratio. Thus, information cannot be obtained about clay minerals that formed during secondary, postgenetic processes, as well as fine sand transported by saltation (Vandenberghe et al., 1997; Vandenberghe, 2013). The "Grain Size Index" (GSI), introduced by Rousseau et al. (2002), is quite similar to the U-ratio. The most significant difference between them is that clay fraction is also taken into account in the calculation of GSI $\frac{20-50\ \mu m}{<20\ \mu m}$. GSI values make possible the estimation of sedimentation, sediment transport and accumulation, which are closely related to the changes in wind speed (Rousseau et al., 2007). High GSI values indicate increased frequency and intensity of windstorms in parallel with a higher sedimentation rate (Újvári et al., 2016; Rousseau et al., 2007).

III.2.3. Geochemical Analysis

Samples (44) were chosen representatively and measured with a XRF instrument at the Department of Mineralogy, Geochemistry and Petrology, University of Szeged. After the

homogenization of the selected samples, pellets were formed from 4 g of a sample with the addition of 1.5 g of Cereox adhesive under a pressure of 20 tons. For the evaluation of the measurement results, the data must be corrected with the 1100 °C "loss on ignition" (LOI— Dean, 1974) results of the samples. The following parameters were used: 50 kV excitation voltage, 40 mA anode current, palladium X-ray tube, LiF, PET monochromators, proportional and scintillation detectors, EZ Scan mode, 1200 s measurement time, semi-qualitative analysis in a vacuum. The cooling of the system was allowed by an argon/methane gas mixture.

III.2.4. Geochemical Indices

The examined major and trace elements are presented in percentage and ppm (mg/kg) respectively. Several geochemical indices were used to get information about the weathering conditions of the profile. Most of these are based on the mobility and exchangeability of water-soluble elements (e.g., Varga et al., 2011; Nesbitt et al., 1980; Nesbitt and Young 1982; Liu et al., 1993; Chen et al., 1999; Ding et al., 2001; Mush et al., 2011; Yang et al., 2004; Schellenberger and Veit, 2006; Tan et al., 2006; Jeong et al., 2008, 2011; Bokhorst et al., 2009; Buggle et al., 2011), which are caused by the ionic potential of alkali metals and alkaline earth metals (Railsback, 2003; Reeder et al., 2006). Ca, Mg, and Sr are common alkaline earth metals in silicate minerals that are susceptible to weathering (Nesbitt et al., 1980; Buggle et al., 2011).

The indices used are the following: chemical index of alteration (CIA— Nesbitt and Young, 1982), chemical index of weathering (CIW— Harnois, 1988), Rb/Sr ratio (Ding et al., 2001), Zr/Rb ratio (Chen et al., 2006; Liang et al., 2013). The two major element indices (CIA and CIW) are widespread weather indices in the fields of loess investigations, paleoclimatical, and paleoenvironmental reconstructions (Varga et al., 2011; Nesbitt et al., 1980; Nesbit and Young, 1982; Yang et al., 2004; Jeong et al., 2008, 2011; Buggle et al., 2011). The Zr/Rb ratio has become important because of the extremely high Zr content, which is an excellent indicator of weathering horizons because of its high ionic potential as an insoluble, immobile element (Buggle et al., 2011; Reeder et al., 2006).

III.3. Results

The stratigraphic units and their boundaries were identified during the field sampling, while the lithostratigraphic description and separation were already performed in the laboratory. It includes the determination of the wet and dry color of each sample based on the Munsell color scale. The notations of Chinese loess sections (Ding et al., 2005; Kukla, 1987; Kukla et

al., 1990; Cohen and Gibbard, 2019; Marković, 2008) were used for the description of the lithological horizons.

III.3.1. Grain Size Composition

A well-developed paleosol complex (S3) can be identified between 1784 and 1872 cm (Fig. III.2), which can be divided into two parts. The proportion of the coarser particle size is constantly increasing with the decreasing of the finer ones. The predominant grain size fractions are medium and coarse silt with a high clay content of around 20%.

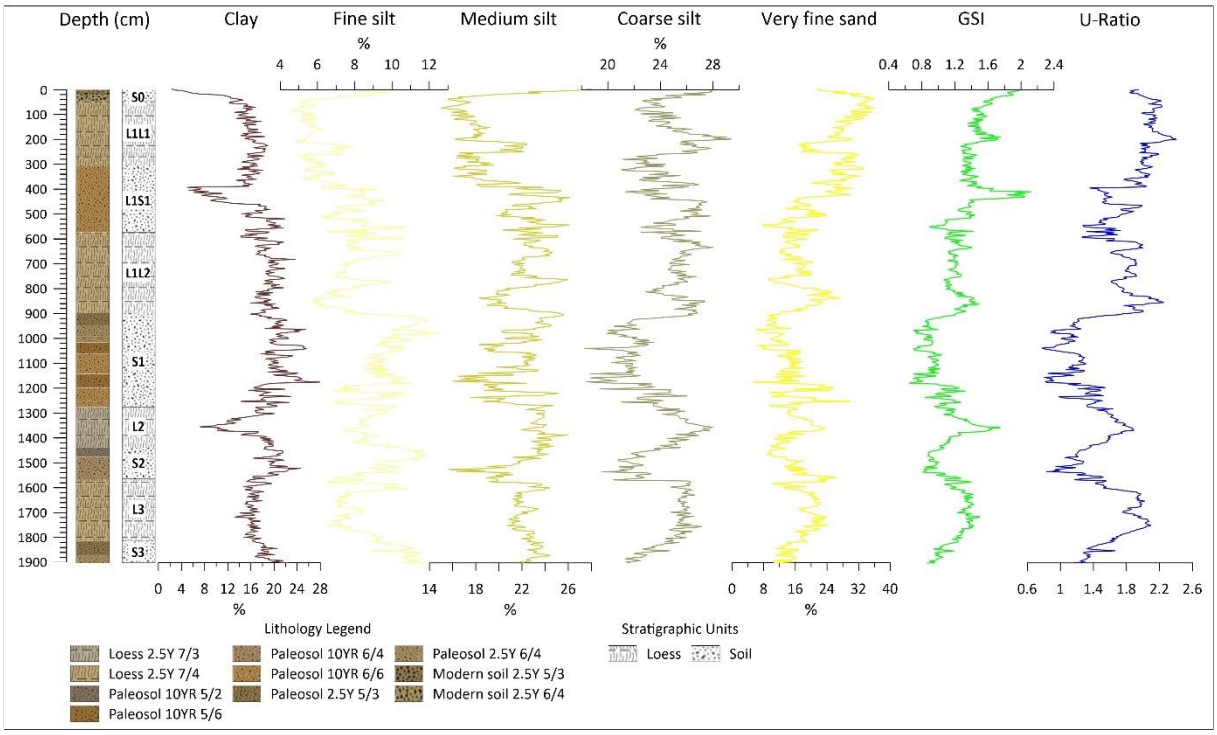

Fig. III. 2. Grain size compositions plotted on separated line diagrams, GSI and U-ratio line diagrams (Sümegi et al., 2015, 2019, 2020; Bösken et al., 2019; Gallet et al., 1998; Ruszkiczay-Rüdiger et al., 2007; Molnár et al., 2019; Újvári et al., 2014, 2016)

A homogeneous loess layer (L3) can be observed between 1540 and 1784 cm with no change in its color. The change in particle size continues from the finer to the coarser fractions, thus coarse silt and very fine sand become predominant. A slight change was detected between 1680–1700 cm, where the proportion of fine and medium silt increases in contrast with the decreasing proportion of very fine sand.

Above the loess layer, between 1416 and 1540 cm, another paleosol layer lies (S2), which was divided into two parts, a lighter part between 1452–1540 cm and a darker between 1416–1452 cm. In the transition zone of the lower part and the L3 loess layer, the amount of very fine sand increases (26%), then decreases upwards. The clay content declines on the

boundary of the lower and upper part (1540 cm) with a slight increase in the proportion of coarse silt and very fine sand.

A well-developed homogeneous loess layer (L2) can be found above S2, between 1256 and 1416 cm, with carbonate concretions between 1350 and 1408 cm. The low proportion of very fine sand (10%) in the S2/L2 transition zone reaches its maximum at 1344 cm with almost 24%. From that point, it decreases back to 10% to the L2/S1 transition. It predominantly comprises coarse (24–28%) and medium (22–26%) silt. The clay content is the opposite of the sand content, shows its minimum (7%) at the maximum of the sand proportion. By the L2/S1 transition, its proportion gradually increases to 20%.

A diverse paleosol layer (S1) can be found between 884 and 1256 cm above the L2 loess layer, which can be divided into 6 parts based on its color. The first part, between 1180 and 1256 cm, is a light-colored section with a rhythmically changing proportion of very fine sand content between 1236 and 1256 cm (increasing from 9 to 30%, then decreasing to 10% again (1216 cm)). In 1200 cm, a minimum can be observed again, then to 1180 cm it increasing to 26%. The clay and very fine silt fraction follow the same trend with an inverse relation. Since outstanding values cannot be observed in geochemical indices, the reasons for this can be the changes of the source area, or the changes in the wind direction, or the drastic relapses in the energy of the transport medium several times. Such a notable trend cannot be observed in the cases of the other fractions. Above, between 1124–1180 cm, a darker part can be found, in which the latter trend continues up to 1160 cm. The proportion of the very fine sand decreases to 5%, while the proportion of clay and very fine silt fractions increase to 28% and 17%. The different grain size fractions in the next part of the paleosol level are characterized by only a few percent of oscillation. Between 1044–1124 cm, the clay, and medium and coarse silt become dominant, but the difference between the minimum and maximum values of each fraction is less than 5%. Between 1000–1044 cm, the trend of the lower parts reappears. The proportion of very fine sand decreases from 17 to 6% (1016 cm) and unlike before, the proportions of fine, medium and coarse silt increase. The presence of a weathering horizon was assumed here, which is also supported by the geochemical indices. Between 932 and 1000 cm, the proportion of fine sand is low, varying between 6–15%. The clay content is between 19–26%, the fine and medium sand are between 20–25% and 20–23%. The uppermost part of the S1 paleosol level can be found at 884–932 cm. The clay content decreases continuously up to a minimum of 16%, the average proportion of medium and coarse silt is 24–24%, with 9–12% of very fine sand. Carbonate concretions can be identified at 1248 cm and between 1188 and 1176 cm.

The next layer between 884–1044 cm consists of two loess layer with a buried paleosol between them. The lower loess layer (L1L2) is between 568–884 cm. The grain composition is gradually fining upwards. A significant change can be observed at 752 cm, where the proportion of fine silt increases, while coarse silt and very fine sand decreases and the clay content stagnates. The refining tendency of the sediment continues upwards. The abovementioned pattern reappears at 652 cm except for the slighter decrease in fine sand and clay content.

The intervening paleosol (L1S1) can be found between 300–564 cm. This part continues to roughen upwards in terms of grain size distribution. A change can be seen between 392 and 456 cm, where the average clay content of 16–20% decreases to 5% as well as coarse silt, meanwhile, all the other fractions increase significantly. The proportion of very fine sand also increases further to the L1S1-L1L1 boundary.

The same color as the L1L2 layer characterizes the uppermost part of the loess body (L1L1) between 44 and 300 cm. The very fine sand fraction in the layer is around 30% but decreases to 20% for 40 cm. Its proportion is constantly increasing from 216 cm and reaches a maximum of 36% at 80 cm. The opposite trend can be observed in the changes of the clay fraction. The proportion of very fine and fine silt ranges between 5–8%. Considering the averages, the very fine sand content becomes predominant with its 28% with 25% coarse silt and 18% medium silt proportions.

The top of the profile is the S0 recent soil layer, which was divided into two parts, a lower (20–44 cm) and an upper (0–20 cm). The clay fraction in the lower part is continuously decreasing from 14% to 6%, and the fine silt fraction increases by 1–2%. The average of the very fine sand proportion is 32%. The dominance of medium and coarse silt (24–28%) and the practically complete absence of clay fraction (2–6%) characterize the upper section. Besides, the proportion of very fine sand drops to 22% from 29%.

III.3.2. GSI/U-Ratio

GSI values (Fig. III.2) increase from 0.87 to 1.14 between 1600–1872 cm, and fall back to 0.9 between 1436–1448 cm. From this point, it rises and reaches 1.75 at 1336 cm. The lowest value of the entire profile is at 1156 cm with 0.69 and remains below 1 up to 904 cm. Below 60 cm, GSI values rise to 1.5, then decrease back below 1 for the next 90 cm. Up to 544 cm, it ranges between 0.9 and 1.4. A significant peak with the highest value (2.12) of the profile can be observed between 364–508 cm. Another peak (1.7) appears at 192–200 cm. Then it continuously decreases to 1.4 at 76 cm, from where it starts to rises again and reaches a value

of 1.97 on the surface. The larger fluctuations in U-ratio can be explained with the consideration of the clay content in the calculation (Vandenberghe et al., 1985, 1997; Vandenberghe and Nugteren, 2001). The movement of the trendlines is uniform, although the L3 layer (1540–1784 cm) indicates a positive protrusion. The most conspicuous ones are between 364–509 cm and 0–75 cm where the values differ from the trend. These anomalies can be explained by the extreme decrease of the clay fraction.

III.3.3. Geochemical Analysis

It can be concluded for the lithological change of S3 level (Fig. III.3), that Mg content gradually ceases and Mn content is quadrupled. The same pattern can be observed in the case of trace elements as Zr, Sr, Rb, Ni. A significant increase is detected in the values of As (from 0 ppm to 48 ppm) at the S3/L3 boundary. In L3, the amount of Ca gradually increase, while Mg, P, S elements show high variability. Pb, Cu and As significantly increase, but the other trace elements show a decreasing trend overall.

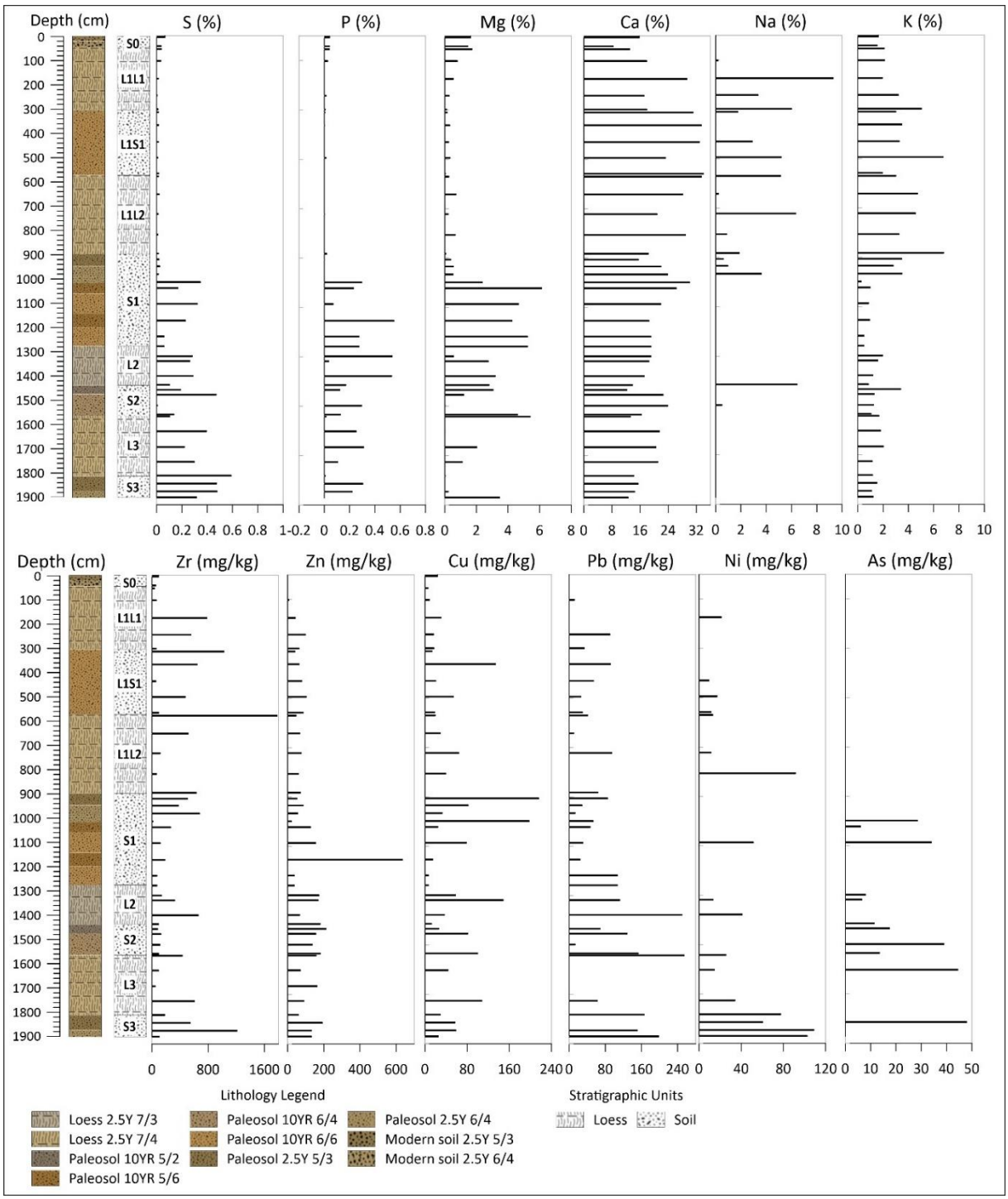

Fig. III. 3. Highlighted geochemical results from XRF (major elements above, trace elements below)

Several changes can be observed in the L2/S2 boundary. The amount of Ca and S halved while Mg increases to 6% from 0. Zr, Pb, Rb and Ni values also increase. Pb reaches its maximum (255 ppm).

S2 can be divided into two lithological layers. At their boundary, the major elements like Fe, Ca, Mg and S and trace elements like Sr, Pb, Cu increase, moreover Rb gradually increases up to S2/L2 boundary, where Na content also rises from 0 to 7%.

The highest p values of the profile were detected (0.5–0.6%) in the L2 loess body and the S1 paleosol layer above where Zr, Pb, Ni values decrease, and in the middle of the loess body Sr, Cu, Rb increase. S1 is divided into six lithological parts, however, it cannot be detected based on the geochemical results. The Fe content gradually decreases up to 1000 cm and reaches a maximum of 27% in the S1/L1L2 boundary zone. Mg, P, S, Zn, Pb, Ni, As is detected with a significant amount up to this zone, from this point Ca, K, Na and Zr elements become predominant. This general change is not significant in the case of Si, except for the decrease from 16% to 4% and the peaks (to 32%) in the upper part of the L1L1 and S0.

Significant changes cannot be seen in the L1L2 loess body except for the smaller peaks of Na, Sr and Ni. The highest Zr content (1781 ppm) is detected in the L1L2/L1S1 boundary. Fe and Ca decrease, while Si and K increase and a slight increase can be observed in Zr and Cu trace elements in the lower part of the L1S1 paleosol (492–496 cm). Rb content continuously increases from 73 to 106 ppm up to the boundary of L1L1, and a peak of Ti is detected (increases from 1–2 ppm to 7.5 ppm).

In the L1L1 loess body, Si, Mg and Al start continuously increase and Fe, Ca, Na (with a maximum of 9.3%) and Mn-and all trace elements- decrease from 172–176 cm. The Al content reaches its maximum at this level: between 0–56 cm ranges between 4.5–5.3%.

III.3.4. Geochemical Indices

The examined geochemical indices suggest a weathering horizon if CIA (Vandenberghe and Nugteren, 2001), CIW (Harnois, 1988) indices and Zr/Rb ratio (Chen et al., 2006; Liang et al., 2013) increase while Rb/Sr ratio (Chen et al., 1999) decreases. These characteristics are caused by the high mobility of Rb, and moderate mobility of Sr and immobility of Zr element (Chen et al, 1999, 2006; Buggle et al., 2011; Liang et al., 2013).

Nine major parts were distinguished within the profile based on the selected geochemical indices. The first layer is between 1780–1862 cm, where a peak of Zr/Rb (1844–1848 cm) and Rb/Sr (1812–1816 cm) can be found. The next level is between 1496–1604 cm, characterized by the positive shift of all examined indices. Above, between 1376–1456 Rb/Sr ratio is doubled, while a slight decrease of Zr/Rb and smaller fluctuation of CIA and CIW indices can be seen. The next level is between 1256–1320 cm, is characterized by a significant Rb/Sr ratio (2–3x value), a minor decrease of Zr/Rb and unchanged CIA, CIW ratios. It is followed by a larger part (804–1088 cm) with varying values of the different indices. The first major change appears between 1020–1024 cm, where the Rb/Sr ratio decreases and Zr/Rb

increases. Then, up 932–936 cm, Rb/Sr ratio more than quadruples (0.89), Zr/Rb ratio decreases to nearly 0 (996–1000 cm) and then ranges between 3–6. CIA, CIW indices slightly drop at 964–968 cm, then increase to 904–908 cm and decrease again, which persists until the next part (556–644 cm). The highest protrusion of the Zr/Rb ratio in the entire profile (19) can be found here caused by the Zr value of 1781 ppm. Between 296–496 cm, CIA and CIW values do not show significant change except for a slight increase. In contrast, high Rb/Sr is associated with a low Zr/Rb ratio at 428–432 cm. In this and the next part, the latter two ratios show the opposite. The Zr/Rb ratio increases because of the presence of over 1000 ppm Zr and the Rb/Sr decreases.

Both CIA and CW indices decrease sharply in the penultimate part between 100–344 cm. Both indices reach their minimum value of 40 and 47, respectively. The Rb/Sr ratio also has a negative peak here, while Zr/Rb ratio increases.

The uppermost part can be observed from 56 cm to the surface (0 cm). At the boundary of L1L1/S0, the CIA and CIW indices reach their maximum within the entire profile (50 and 60, respectively), while the two other indices are at their minimum (0). Following this point, the CIA and CIW slightly decrease, Rb/Sr and Zr/Rb increase from zero to 0.3 and 12, respectively.

A weathering horizon occurs (Fig. III.4) between 1844–1848 cm within the SP3 paleosol layer, which is characterized by high Zr content of 1209 ppm (Fig. III.3). The next weathering horizon is at the transition of L3-S2, where the Rb/Sr ratio moves in a positive direction. Its explanation can be the higher Rb content (115 ppm). The next weathered zone occurs in the upper part of the S2 paleosol. Rb/Sr and Zr/Rb ratios have an opposite trend than the indices because of the high Rb content (Rb: 149 ppm, Sr: 186 ppm, Zr: 92 ppm; Fig. III.3). The high Sr (228–255 ppm) and Zr (325–659 ppm) contents suggest the existence of another weathering horizon between 1316–1380 cm within the L2 loess body. In contrast, based on the grain size composition (Fig. III.2), the high GSI and high U-ratios, the development of a loess body deposited by intensive wind and dust storms are supposed. The proportion of the finer fractions increases again by the weakening of the assumed storms. Rb reaches a maximum of 151 ppm at 1300 cm, which causes a high Rb/Sr ratio. A paleosol developmental stage can be observed within the diverse S1 paleosol layer, which is characterized by a low concentration of Rb (44–58 ppm). Zr also reaches its minimum in the profile (13 ppm). A definite weathering emerges in the upper part of this paleosol between 904–908 cm, yet below the L1L2/S1 boundary.

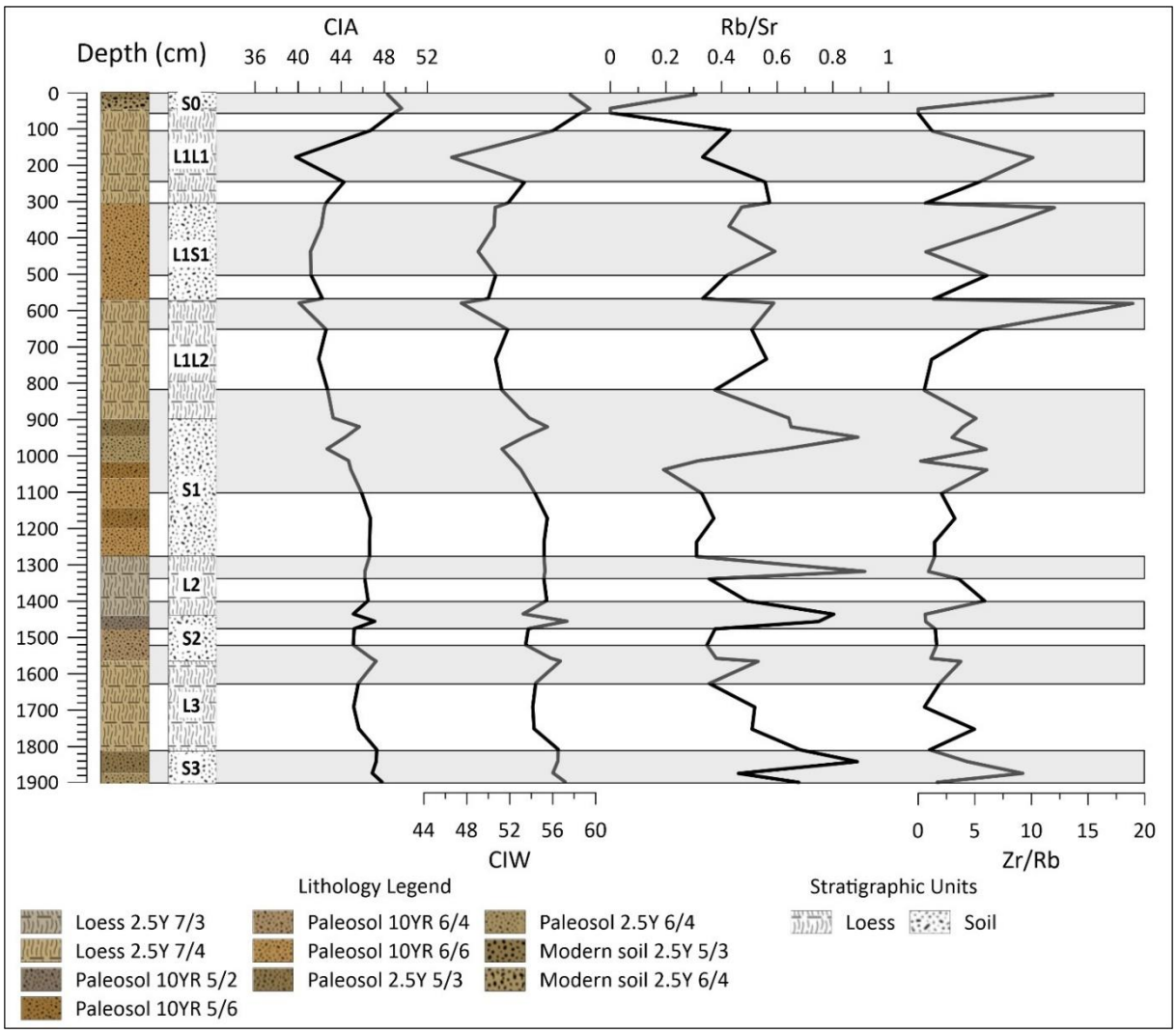

Fig. III. 4. Geochemical indices used to explore weathering in the loess-paleosol sequence

Above a weak weathering horizon in the L1L2 loess body between 640–644 cm, a more significant one also can be observed. However, the highest Zr concentration value (1781 ppm) of the profile occurs at 568–572 cm, the weathering horizon appears only above, at the boundary of L1S1/L1L2 with a moderate Zr (98 ppm). Similar results were obtained in the case of L1L1/L1S1 boundary (296–308 cm) with the Zr values of 1023 ppm and then 60 ppm. Despite the weak weathering within the loess body of L1L1, a more intensive sediment accumulation and the intensified wind is assumed based on the GSI and U-ratio. The complete absence of Rb suggests intense weathering in the L1L1/S0 boundary.

III.4. Discussion

Based on the sedimentological results, it can be noted that the complete section is characterized by a high proportion of very fine sand fraction (5–36%). It indicates increased transport energy (Pye, 1995) or the sediments of the surrounding sand dunes and sand sheets. In consistent with previous studies, among all the examined grain composition indices, U-ratio

is the one, which indicates cold periods and strong winds with higher values in loess bodies, and warmer periods in paleosols (Újvári et al., 2016; Vandenberghe et al., 1997; Nugteren et al., 2004; Vandenberghe, 2013). In addition, the positive peaks of GSI values indicate increased sedimentation rate and frequent powerful dust storms (Újvári et al., 2016; Rousseau et al., 2007). In the case of our profile, two significantly increased and several elongated sections can be observed. The two peaks are detected in the L2 loess body and the L1S1 paleosol. Both parts were characterized by the high proportion of coarser fractions and sharply decreased clay fraction (5%) (Fig. III.2). Non-significant peaks can be observed in the whole L3 loess body, in the initial parts of the S1 and L1L2, and above the weathering horizon in the L1L1 loess body.

A significant change can be observed in the section at the height of 10 m based on the elemental composition and particle size indices. This can be explained by the complete termination of the supply of dust, rich in sulphide minerals. Under 10 m the values of Mg, P and S major elements are relatively common, even if with small percentages (Mg < 6%, P and S < 0.6%). Trace elements as Zn, Pb, Ni, As are significant below 10 m. Considering the mineral composition of the surrounding areas, the origin of the dust, which presumably consists of sulphide minerals and igneous rocks, could have been the Buda Thermal Karst, the Börzsöny or the Cserhát. Thus, NW as the prevailing wind direction can be assumed. However, further research is necessary for the more precise determination of the exact source area of the sediment.

III.5. Conclusions

The foothill/hill-situated loess-paleosol profile of Pécel is located in the Gödöllő Hills in the northern part of the Carpathian Basin. The preliminary sedimentological and geochemical investigations have shown that the profile merits conducting further research, as no significant erosion or intensive weathering could be detected. It carries a wealth of data, which can perfectly complement the results of the surrounding profiles investigated so far and could provide data for the study of the climate changes in the Quaternary. The origin of flying dust and the prevailing winds are also can be examined. The change at about 10 m is an evidence of the change of the source area of the accumulated dust. The seemingly opposite results within the L2 loess body may be explained by the further transport of finer fractions (and a sharp decrease in the proportion of clay) because of the increased transport energy and the deposition of larger particles. Similar fluctuations can be seen in the case of GSI in the L1S1 paleosol layer, where the geochemical indices also indicate soil development. Considering the entire profile, weathering horizons occur at the loess-paleosol transition zones. As this is a preliminary

examination of the profile, further research will be conducted. Radiocarbon and OSL/IRSL data will be suitable for the determination of the actual age of the profile, age-depth models will be built for the estimation of the volume and the rate of sediment accumulation. Besides, malacological examination of the remaining snail shells of the sediment will provide more accurate information about the paleoecological factors. Finally, magnetic susceptibility results will be applied to correlate the paleosol levels and the MIS stages and that will allow us the correlation of the Pécel profile with similar profiles.

CHAPTER IV.

DEVELOPMENT HISTORY OF THE LOESS-PALEOSOL PROFILES OF PÉCEL, KISDOROG AND BONYHÁDVARASD, HUNGARY

László Makó
Department of Geology and Paleontology, University of Szeged, Hungary
makol@geo.u-szeged.hu
Péter Cseh
Department of Geology and Paleontology, University of Szeged, Hungary
cspeti94@gmail.com
Balázs Nagy
Department of Geology and Paleontology, University of Szeged, Hungary
nagba88@gmail.com
Pál Sümegi
Department of Geology and Paleontology, University of Szeged, Hungary
sumegi@geo.u-szeged.hu
Dávid Molnár
Department of Geology and Paleontology, University of Szeged, Hungary
molnard@geo.u-szeged.hu

Quaternary
Volume 6, no. 3, 2023
DOI: 10.3390/quat6030038

Development History of the Loess–Paleosol Profiles of Pécel, Kisdorog and Bonyhádvarasd, Hungary

László Makó, Péter Cseh, Balázs Nagy, Pál Sümegi, Dávid Molnár

Abstract

This study covers the examination of four loess–paleosol profiles in Hungary through grain size composition, organic matter, carbonate content and magnetic susceptibility measurements. One of the profiles (with a thickness of 25.72 m) can be found in the Gödöllő hills, on the border of town Pécel, and the other three profiles (Kisdorog-West—5.60 m, Kisdorog-East—6.40 and Bonyhádvarasd—8.16 m) are located in the Tolna hills of the Transdanubia region. The sections were continuously sampled with an interval of 4 cm. The same interval was also applied to the other three profiles. During the field exploration of the Pécel profile, we were able to study the complete loess wall, which was deposited on the sediment of the nearby Rákos stream. Based on the Ostracod fauna of the clay sediment beneath, the fluvial deposit can be considered as originating from the Upper Miocene. In the case of the Transdanubian sections, a significant change can be observed in the prevailing wind direction based on the grain size analyses. In addition, the results of magnetic susceptibility measurements suggest that the development of the Pécel profile took place during MIS 9–10, while the age of the three Transdanubian sections can be assumed to be the MIS 2–4.

IV.1. Introduction

The four profiles examined in this study can be found in two different geographical regions of Hungary (Fig. IV.1). One of them can be found in the vicinity of the town Pécel in the Gödöllő hills area (Dövényi, 2010) in a foothill location (e.g., Sümegi et al., 2011, 2016; Bösken et al., 2019; Makó et al., 2021; Varga et al., 2011), while the other three profiles are located in the Tolna hills (Dövényi, 2010) in a lowland location (e.g., Sümegi et al, 2015, 2019, 2020, 2021; Molnár et al., 2019, 2021; Újvári et al., 2014, 2016). In addition to the one in Pécel, two of the examined sections are located in Kisdorog and one in Bonyhádvarasd, 130–140 km away from Pécel. In the case of these Transdanubian sections, the direction of the hills in the area is northwest–southeast.

Detailed pieces of information on the loess sequences of the Carpathian Basin are available (e.g., Sümegi et al., 2011, 2015, 2019, 2020; Bösken et al., 2019; Varga et al., 2011; Újvári et al., 2014, 2016; Buggle et al., 2008; Marković et al., 2008, 2015; Galović et al., 2009;

Molnár et al., 2010, 2021), however, the sections we examined have not been studied before, thus, the data extracted from them could provide excellent additional information about the paleoclimate and regional mosaicism of the area. Several profiles have been studied along the River Danube (Sümegi et al., 2011; Újvári et al., 2014, 2016; Marković et al., 2015), the data of which were supplemented by data from southern Hungary (Varga et al., 2011; Sümegi et al., 2015, 2019, 2020, 2021; Molnár et al., 2019), northern Hungary (Bösken et al., 2019; Sümegi et al., 2016; Makó et al., 2021a, b), Transdanubia (Varga et al., 2011; Molnár et al., 2021; Újvári et al., 2014, 2016), and data derived from drillings (Koloszár and Marsi, 2010; Sümegi et al., 2018).

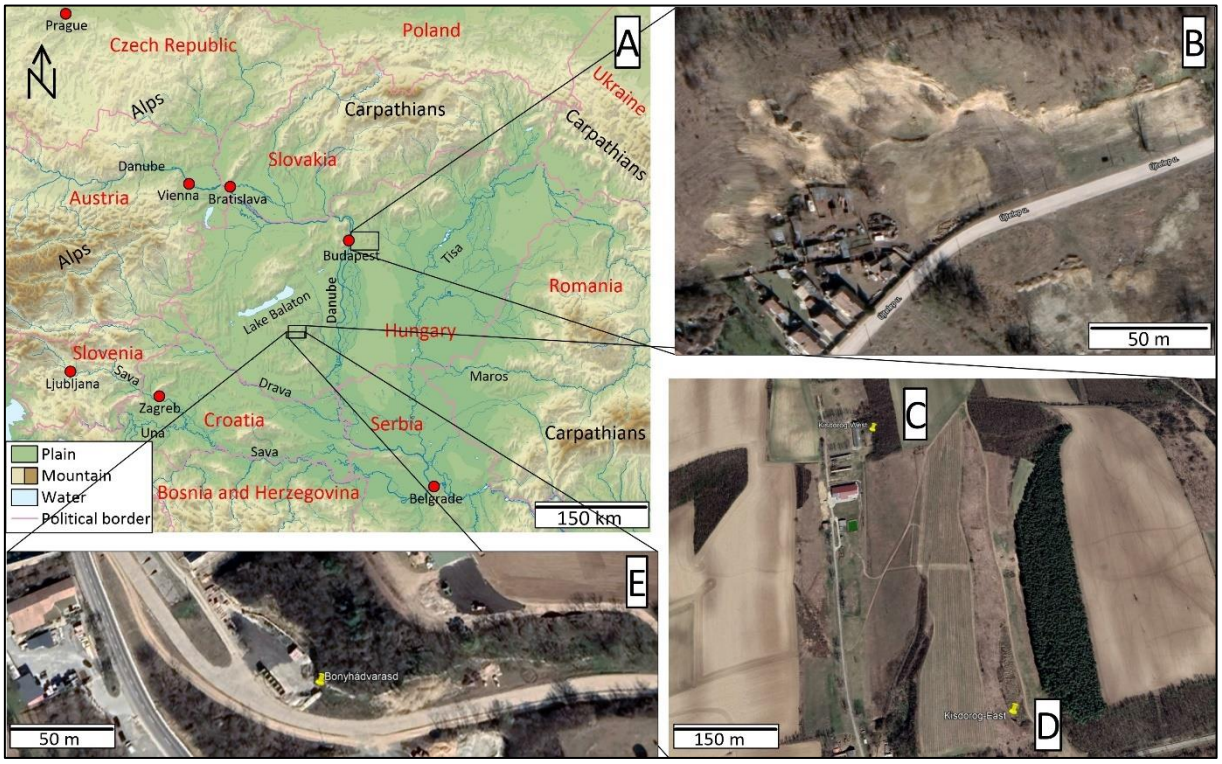

Fig. IV. 1. Location of the loess-paleosol section of Pécel ((B)—ortophotomap), Kisdorog-West ((C)—ortophotomap), Kisdorog-East ((D)—ortophotomap) and Bonyhádvarasd ((E)—ortophotomap) in the Carpathian Basin (A, Wikimedia Commons)

The excavation of the loess–paleosol profile of Pécel was completed in 2022. Prior to this, its preliminary results were reported in 2021 (Makó et al., 2021). The total height of this section is 25.72 m, of which the actual loess deposit was 24.56 m. The sediments (thickness: 51 cm) below this loess section can be considered as the sediments of the former Rákos stream, which recently can be found 300–350 m south of the loess wall. This further deepening of the profile was considered irrelevant since the main purpose of this research is the reconstruction of the development of the loess wall itself. Regardless, the development of the former riverbed below the loess wall could also be clearly reconstructed by the analysis of its sediments. The

bottom 65 cm of it consists of clay, while sand with massive, cross-layered and laminated features can be described in the upper 51 cm. Based on the experiences of previous research on loess bodies and similar sediment depositions, the higher resolution of sampling enables a higher resolution of examination (e.g., Sümegi et al. 2015, 2019, 2020, 2021; Molnár et al. 2021). We have therefore sought to achieve the highest possible resolution—of course within reasonable limits. Thus, a sampling interval of 4 cm was applied, which can result in the resolution of decades-to-centuries if it is supplemented with well-designed radiocarbon age data (e.g., Sümegi and Hertelendi, 1998; Sümegi et al. 2015, 2016, 2019, 2020, 2021; Molnár et al. 2021). The loess–paleosol profiles near Kisdorog (Fig. IV.1) are located in the midwest region of Hungary at 46°23′54″ N and 18°29′47″ E (Kisdorog-West) and 46°23′34″ N and 18°30′01″ E (Kisdorog-East). The two profiles can be found on the opposite slopes of a hill, approximately 700 m from each other. The Kisdorog-West section can be characterized by a height of 5.6 m. One single paleosol layer of about 1 m thickness can be found in it, which can be divided further into 3 sublayers. The Kisdorog-East section can be characterized by a height of 6.4 m, within which a single paleosol layer can be separated similar to the western section. This paleosol layer of 3 m can also be separated into 3 sublayers. The fourth section can be found in Bonyhádvarasd, which is located 3.5 km away from Kisdorog. The coordinates of the Bonyhádvarasd section of 8.16 m height are 46°21′52″ N and 18°29′17″ E. Similar to the Kisdorog sections, it can also be divided into lower and upper loess bodies separated by a paleosol complex.

IV.2. Materials and Methods

The Pécel section (Fig. IV.1) (47°29′47″ N and 19°21′12″ E) was supplemented by a 10th subsection (with a height of 700 cm). This section was also sampled for grain size distribution and LOI analysis by applying the previously used 4 cm sample size.

IV.2.1. Color

During the field studies, following the cleaning of the entire wall surface, the visible layers and their boundaries were registered and their colors were defined according to the Munsell color chart (Munsell, 2010). These macroscopic observations were the basis of the delimitation of the different layers. In the case of the Pécel profile, the paleosols (Nettleton et al., 1998; Kraus, 1999; Krasilnikov and García Calderón, 2006) ranged from brown to reddish-brown, while in the case of the Kisdorog and Bonyhádvarasd profiles, the paleosols showed three different colors, ranging from chestnut brown to dark brown, indicating significant soil

development. In addition, the color of the loess also differed (whitish–pale yellow) in the case of the Bonyhádvarasd profile. Our research was primarily focused on the study of the loess material, thus, detailed pedological examination of the paleosol layers has not been carried out.

IV.2.2. LOI

Dean's Loss on Ignition method (Dean, 1974) was used to determine the organic matter and carbonate content of the samples. This method is based on the measurement of the loss on ignition weight of the powdered sediment samples. The previously air-dried samples are first ignited at 550 °C, at which temperature the organic matter is being burnt, and then, at 900 °C, in order to detect the carbonate content. The 900 °C temperature value was chosen based on the study of Heiri et al. (2001). Regardless, the heating of the samples was performed at both 900 and 1000 °C, resulting in two different series of measurements. The average weight loss was plus 0.0007 g at 1000 °C. This difference can be explained by water present in clay minerals, as well as in crystalline bonds, in which water content is likely to escape from the system at this applied temperature. These measurements were carried out by using a furnace at the Department of Geology and Paleontology of the University of Szeged.

IV.2.3. Grain Size Distribution

For the analysis of the grain size composition, the samples were prepared according to the method of Bokhorst et al. (2011). Air-dry samples were pre-treated in a 30% H_2O_2 and then a 10% HCl bath to remove organic matter and carbonates before further analysis. Subsequently, 30 mL of 5% Calgon ($Na_2P_6O_{18}$) was added to 0.7 g of the sample in order to separate the particles. Right before the measurements, the samples were treated in an ultrasonic cleaner for 10 min to prevent the coagulation of the particles. The grain size composition measurements were carried out by using an OMEC EasySizer 20 laser sedigraph at the Department of Geology and Paleontology, University of Szeged. The source was a He-Ne laser with an energy of 2 MW and a wavelength of 0.6328 μm. The Laser Sedigraph uses 54 built-in detectors for measuring a range of 42 grain size fractions between 0.0001 and 0.5 mm. The approach is based on the theory of Mie laser light scattering. Following the measurements, the system calculates cumulative values by using the measurement results. The values obtained were organized into grain size fractions according to the Wentworth scale (Wentworth, 1922).

IV.2.4. Grain Size Indices

The average particle size (MGS) was calculated from the values of D10-D50-D75 and plotted with a line diagram. The U-ratios and the GSI values were calculated by using the grain size composition results in order to determine the energy of the transport medium (Vandenberghe et al., 1985, 1997; Vandenberghe and Nugteren, 2001).

The U-ratio defines the ratio of the coarse silt and the medium + fine silt fractions. This ratio can be applied to distinguish the cold, dry glacial periods with significant eolian transport and high wind velocity (high U-ratio), and the warm, wet interglacial periods with weak wind intensity (low U-ratio). This distinction approach is based on the observation that the predominant grain size fraction of eolic sedimentation is <16 μm in warmer interglacial periods, while it is >16 μm in colder glacial periods (Vandenberghe et al., 1997; Nugteren et al., 2004). Clay fraction (<5.5 μm) and grain size fractions coarser than 44 μm are not taken into account for the calculation of the U-ratio, thus, no information can be obtained about clay minerals formed by secondary pedogenetic processes or about fine sand particles transported in saltation (Vandenberghe et al., 1997; Vandenberghe, 2013).

The Grain Size Index (GSI) introduced by Rousseau et al. (2002) is similar to the U-ratio. The most significant difference is that the clay fraction is also taken into account for its calculation. Based on this index, the efficiency of sedimentation, transport and accumulation processes can be determined which are closely related to the changes in wind velocity (Rousseau et al., 2002). High GSI values indicate an increased frequency and intensity of dust storms, as well as a higher sedimentation rate (Rousseau et al., 2002, 2007).

IV.2.5. Magnetic Susceptibility

The magnetic susceptibility (Zhou et al., 1990; An et al., 1991; Rousseau and Kukla, 1994; Dearing et al., 1996; Sun and Liu, 2000; Zhu et al., 2004; Hlavatskyi and Bakhmutov, 2021; Chen et al., 2006) measurements were carried out by using a Bartington MS2K surface sensor instrument at the Department of Geology and Paleontology, University of Szeged. The air-dried, powdered samples were measured three times in different directions.

IV.3. Results

IV.3.1. Profiles

IV.3.1.1. Pécel

The notations of Chinese loess sections (Marković et al., 2015; Kukla, 1987; Kukla and An, 1989; Kukla et al., 1990) were used for the description of the lithological horizons. The lowest 65 cm of the section (between 25.07–25.72 m) is clay sediment, which is followed by 51 cm of sand sediment above it (between 24.56 and 25.07 m). Above this, the development of loess (between 0 and 24.56 m) starts with a hiatus in some places. The lowest stratum denoted as L6, is located between 23.48 and 24.56 m and is characterized by a Munsell color of 7.5YR 7/4. Above it, 28 cm of paleosol (S5, between 23.20 and 23.48 m) can be found with 10YR 5/6 color. The loess body L5 is located between 19.36 and 23.20 m and its color is 7.5YR 7/3. The S4 paleosol between 19.08 and 19.36 m has a 10YR 5/6 color, similar to the S5. The L4 stratum between 18.72 and 19.08 m is a 7.5YR 7/3 colored loess again. Above the L4 loess body, the S3 paleosol layer can be found, which consists of two parts, the lower one (between 18.44 and 18.72 m) with 2.5Y 6/4 color, the upper one (between 17.84 and 18.44 m) with 2.5Y 5/3 color. The loess body above this (L3) can be found between 15.40 and 17.84 m and can be characterized by 2.5Y 7/4 color. The S2 paleosol also consists of two parts, the lower one (between 14.52 and 15.40 m) with 10YR 6/4 color, and the upper one (between 14.16 and 14.52 m.) with 10YR 5/2 color. The loess body L2 is located between 12.56 and 14.16 m and has a color of 2.5Y 7/3. The S1 paleosol can be divided into 6 different parts based on its color: 10YR 6/6 (11.80–12.6 m); 10YR 5/6 (11.24–11.80 m); 10YR 6/6 (10.44–11.24 m); 10YR 5/6 (10.00–10.41 m); 2.5Y 6/4 (9.32–10.00 m) and 2.5Y 5/3 (8.84–9.32 m) The overlying sedimentary layer was described as a well-observable loess body with a layer of paleosol in it. L1L2, which can be characterized by 2.5Y 7/4 color, is located between 5.64 and 8.84 m. The paleosol layer in-between denoted as L1S1 (color: 10YR 6/6) can be found between 3.00 and 5.64 m. Above it, the uppermost loess layer (L1L1) between 0.44 and 3.00 m can be characterized with 2.5Y 7/4 color again. The uppermost stratum of the entire sequence is the recent soil layer with a thickness of 44 cm which can be described with 2.5Y 6/4 color between 0.20 and 0.44, and 2.5Y 5/3 between the surface and 0.20 m.

IV.3.1.2. Kisdorog-West

This profile is between 3.84 and 5.6 m of a loess wall of 5.6 m total height, with large carbonate concretions I from the depth of 5.5 m. A notable paleosol horizon can be found

between 2.32 and 3.84 m. The lower part (between 3.28 and 3.84 m) of this paleosol can be characterized by chestnut brown color (7.5YR 3/6), while the middle part of it (2.52–3.28 m) is dark brown (2.5Y 2/2). Several carbonate concretions can be found in these two lower layers between 3 and 3.9 m. The uppermost part of the paleosol layer between 2.32 and 2.52 can be characterized by light brown color (2.5Y 3/2). The upper loess body of the profile (0.4–2.32 m) can be found above the paleosol layer. Above, the uppermost 0.4 m is the recent soil horizon. In these two uppermost layers, several rhizoliths can be observed between 0 and 1.3 m.

IV.3.1.3. Kisdorog-East

The lowermost 0.20 m of this profile with a height of 6.4 m is a loess layer (between 6.2 and 6.4 m). A notable paleosol horizon can be found between 2.72 and 6.2 m, which can be divided further into sublayers. The following sublayers can be distinguished based on their colors: chestnut brown (7.5YR 3/6) between 5.84 and 6.2 m, dark brown (2.5Y 2/2) between 4.6 and 5.84 m, light brown (2.5Y 3/2) between 4.2 and 4.6 m, and dark brown again between 3.16 and 4.2 m with crotovines between 3.24 and 3.3 m. The uppermost paleosol layer can be found between 2.72 and 3.16 m and can be characterized by light brown color. The upper loess layer can be found between 0.36 and 2.72 m, which is followed by the recent surface soil (0 and 0.36 m).

IV.3.1.4. Bonyhádvarasd

This profile of 8.16 m total height can be described with the presence of a loess layer in the lower position (6.08–8.16 m) and a paleosol layer between 3.76 and 6.08 m, which latter can also be divided into further sublayers. These certain sublayers were defined by their colors, which are the followings: chestnut brown (7.5YR 3/6, between 5.52 and 6.08 m), dark brown (2.5Y 2/2, between 5.2 and 5.4 m), light brown with lime spots (2.5Y 3/2, between 4.84 and 4.96 m), dark brown (2.5Y 2/2, between 3.76 and 4.36 m) and chestnut brown with rhizoliths (7.5YR 3/6, between 3.76 and 4.36 m). The upper loess layer can be found above the paleosol horizon (between 0.15 and 3.76 m) with carbonate concretions in its lower parts. The uppermost 0.15 m of the section can be described as another paleosol horizon.

IV.3.2. LOI

IV.3.2.1. Pécel

The upper 18.72 m of the loess–paleosol profile of Pécel was previously studied and published (Makó et al, 2021), thus, only the newly obtained results are presented in this paper (Fig. IV.2).

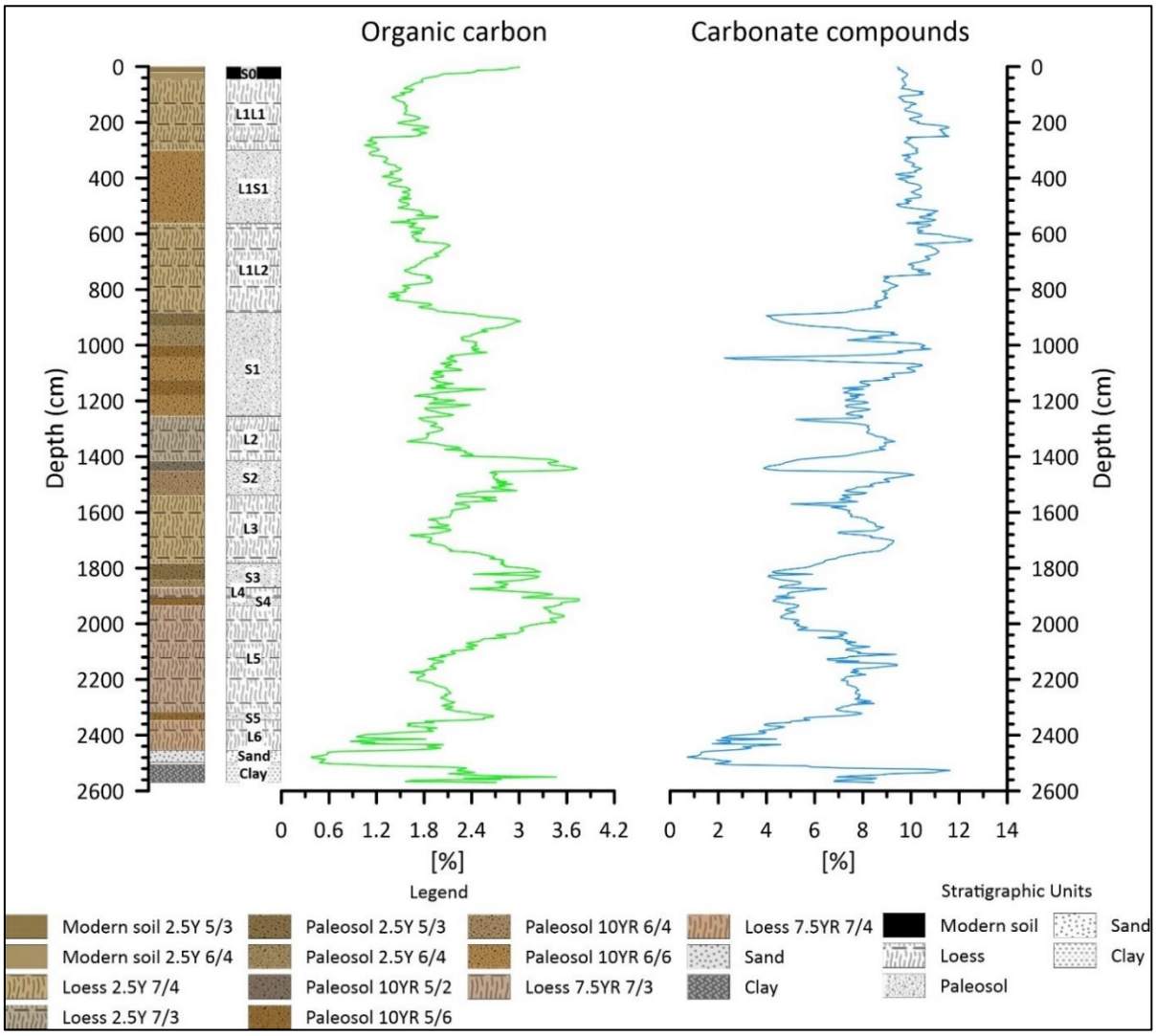

Fig. IV. 2. LOI results (Organic carbon: 550 °C, carbonate: 900 °C) of the Pécel section

Greyish-brown clay sediment can be found in the range 25.07–25.72 m where the organic matter content varies in the range 1.2–2.7%. The carbonate content gradually increases towards the sand layer deposited on the top of the clay (~7 to 11% to 2.5%).

The lowest organic matter (0.4–1%) and carbonate (0.7–2.5%) content values can be detected in this sand body in the range 24.56–25.07 m. Subsequently, the lowermost loess body (L6) is located in the range 23.48–24.56 m, in which organic matter (1–2%) and carbonate (1.7–5%) show relatively constant values. Both organic matter and carbonate content values constantly increase up to the level of the next paleosol horizon above this loess layer.

A thinner paleosol layer (S5) can be found in the range 23.20–23.48 m, in which the organic matter varies in the range 2.3–2.7%, while the carbonate content shows a more significant increase and rises from 5.8 to ~8 %. The increased values of the latter persist in the overlying loess.

A thicker loess layer (L5) lies in the range 19.36–23.20 m, in which, the organic matter content decreases to 1.71% up to 21.92 m, while the carbonate content varies in the range 7.2–8.5%. Despite this variability, these values can still be considered stable compared to the layers below. Subsequently, organic matter content starts a significant increase from 21.92 m and reaches 3.5%. At the same time, carbonate content decreases with smaller and larger fluctuations, reaching 3.7%.

A thinner paleosol layer (S4) can be found again in the range 19.08–19.36 m. Within this paleosol, the proportion of organic matter content increases and the carbonate content decreases slightly upwards.

The uppermost loess (L4) layer examined within this study is located in the range 18.72–19.08 m. Herein, the organic matter content continuously increases from 3% to 3.4% and then decreases to 2.4% up to the paleosol horizon above it. In contrast, the carbonate content decreases from 5.2 to 4.4% and then increases to 6.5% by the boundary of the paleosol layer.

IV.3.2.2. Kisdorog-West

The significant changes that were observed in the case of the Pécel profile cannot be detected here (Fig. IV.3). The carbonate content constantly increases in the lower part of the lower loess layer (from 12% to 16% in the range 5.6–4 m). This value drops extremely at the depth of 4 m and reaches 2% up to 3.5 m. In contrast, it starts to increase up to the depth of 3 m by ~8% within the paleosol layer. Then, it starts to decrease again back to 4% between 3 and 2.5 m (the boundary of the paleosol and the upper loess layer), then increases to 10% up to the depth of 2 m. Subsequently, it decreases to 6% up to the depth of 1.6 m and then increases to 12% up to the horizon of the recent surface soil.

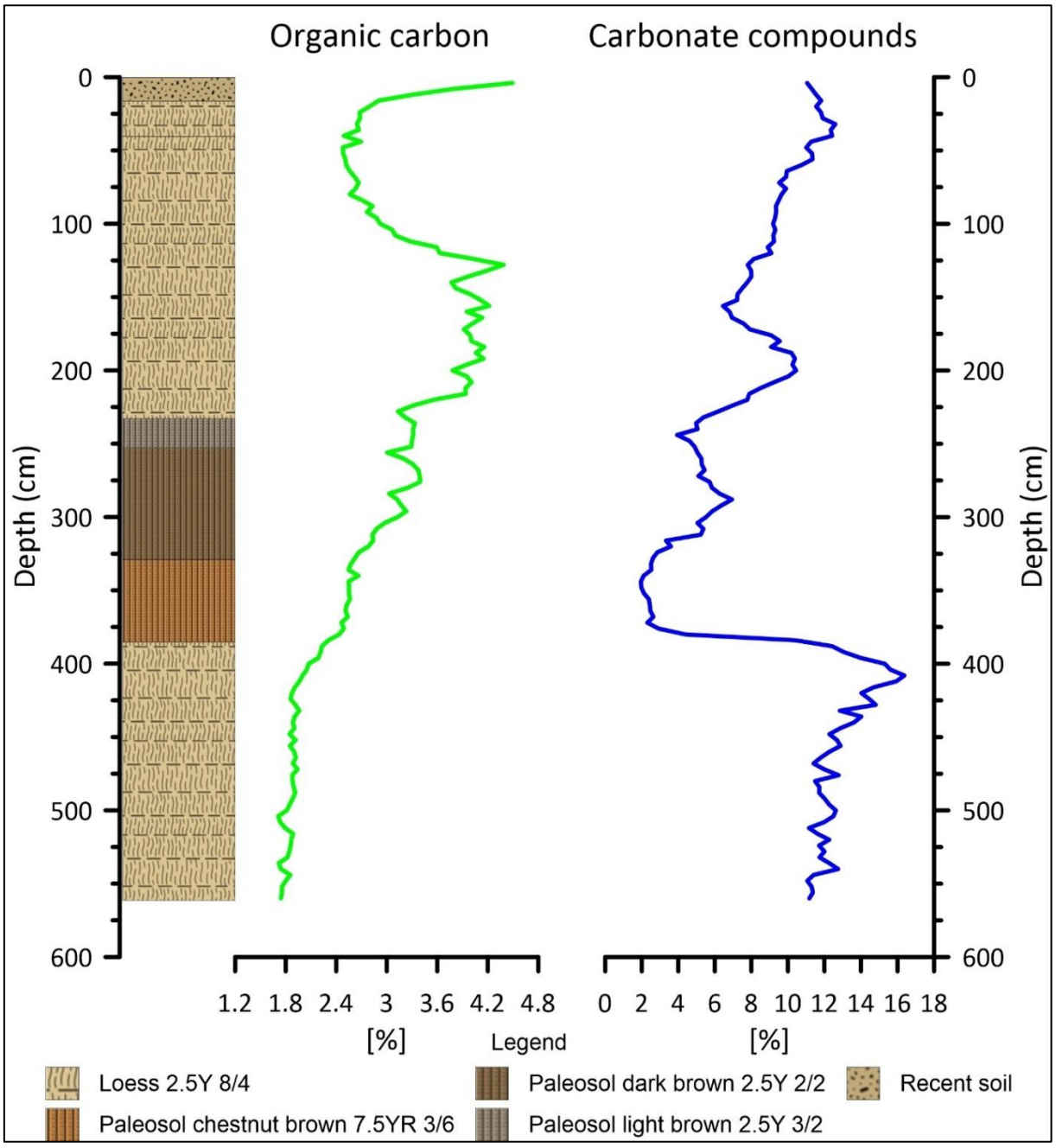

Fig. IV. 3. LOI results (Organic carbon: 550 °C, carbonate: 900 °C) of the Kisdorog-West section

The changes in organic matter content show even less variability. It increases continuously from ~1.8% to ~4.2% with smaller fluctuations between 5.6 and 1.5 m (the upper boundary of the loess). Above it, the value falls back to 2–2.4% and then reaches its maximum of ~4.4% in the recent surface soil level.

IV.3.2.3. Kisdorog-East

This section, with its ~6.5-m height, contains a significant paleosol complex of nearly 3.5 m. However, as the Figure IV.4 shows, the organic matter content within this layer is still low (varying in the range 2–5%). The peak value of the organic matter can be observed within

the recent soil layer with a value of almost 9%. At the same time, this value is constant ~2% on average within the loess bodies. The carbonate content is higher (around 8–10%) in the paleosol levels characterized by chestnut (7.5YR 3/6) and dark brown (2.5Y 2/2) color. A significant decrease to 4% is observed in the middle-positioned, light brown-colored (2.5Y 3/2) layer. In contrast to the paleosol layer, high carbonate contents (10–16%) were measured in both the lower and upper loess bodies.

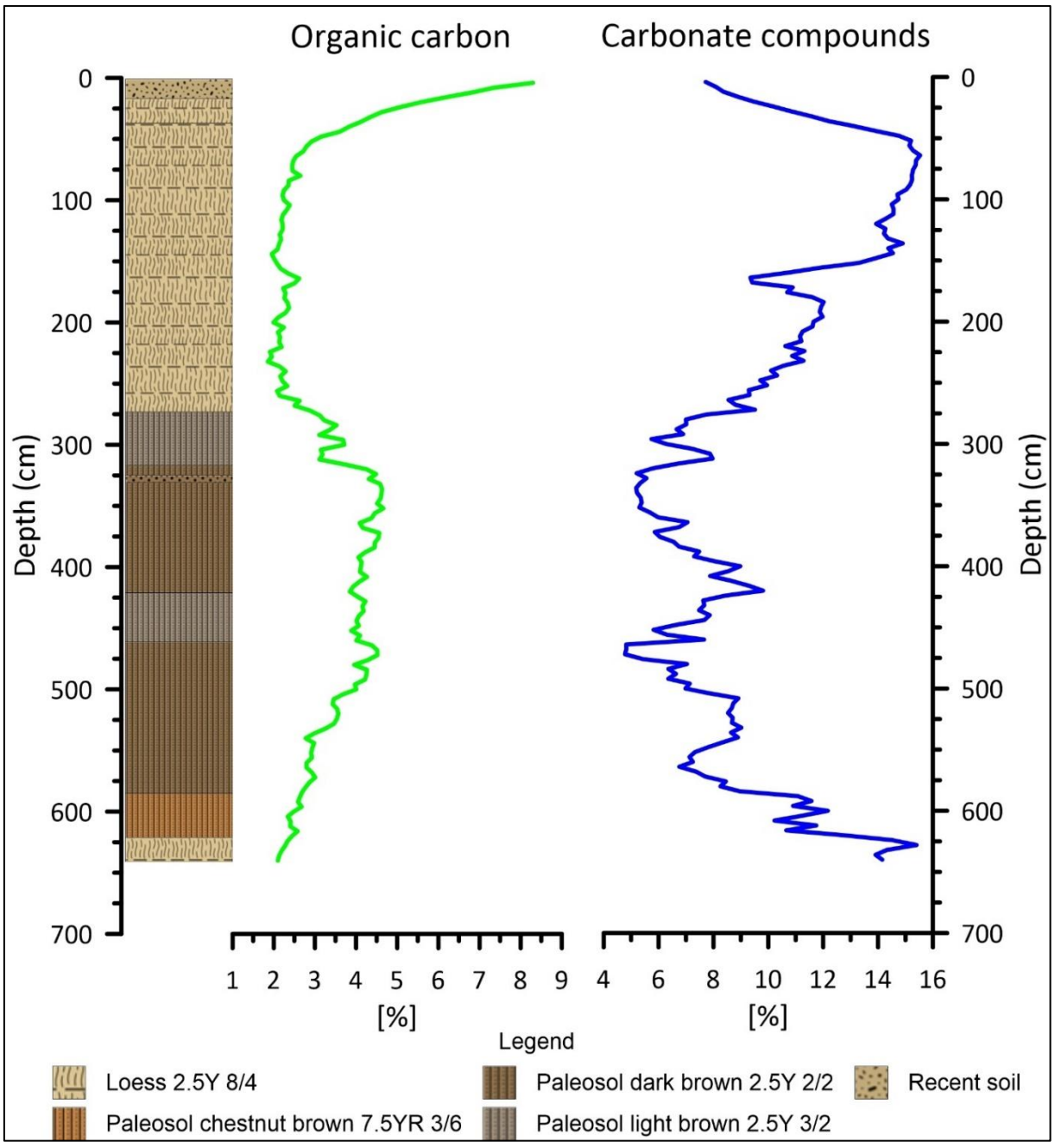

Fig. IV. 4. LOI results (Organic carbon: 550 °C, carbonate: 900 °C) of the Kisdorog-East section

IV.3.2.4. Bonyhádvarasd

In the case of this profile, the organic matter content continuously increases in the lower loess body towards the paleosol complex (from 1.8% to 3%, Fig. IV.5). A significant decrease (~2.2%) in the organic matter content can be observed in the lower, light brown layer of the paleosol, which is followed by an increase (to 3%) towards the chestnut-colored layer. Subsequently, it falls below 2% in the lower parts of the upper loess body, then starts to increase again upwards, and reaches its maximum of 4%.

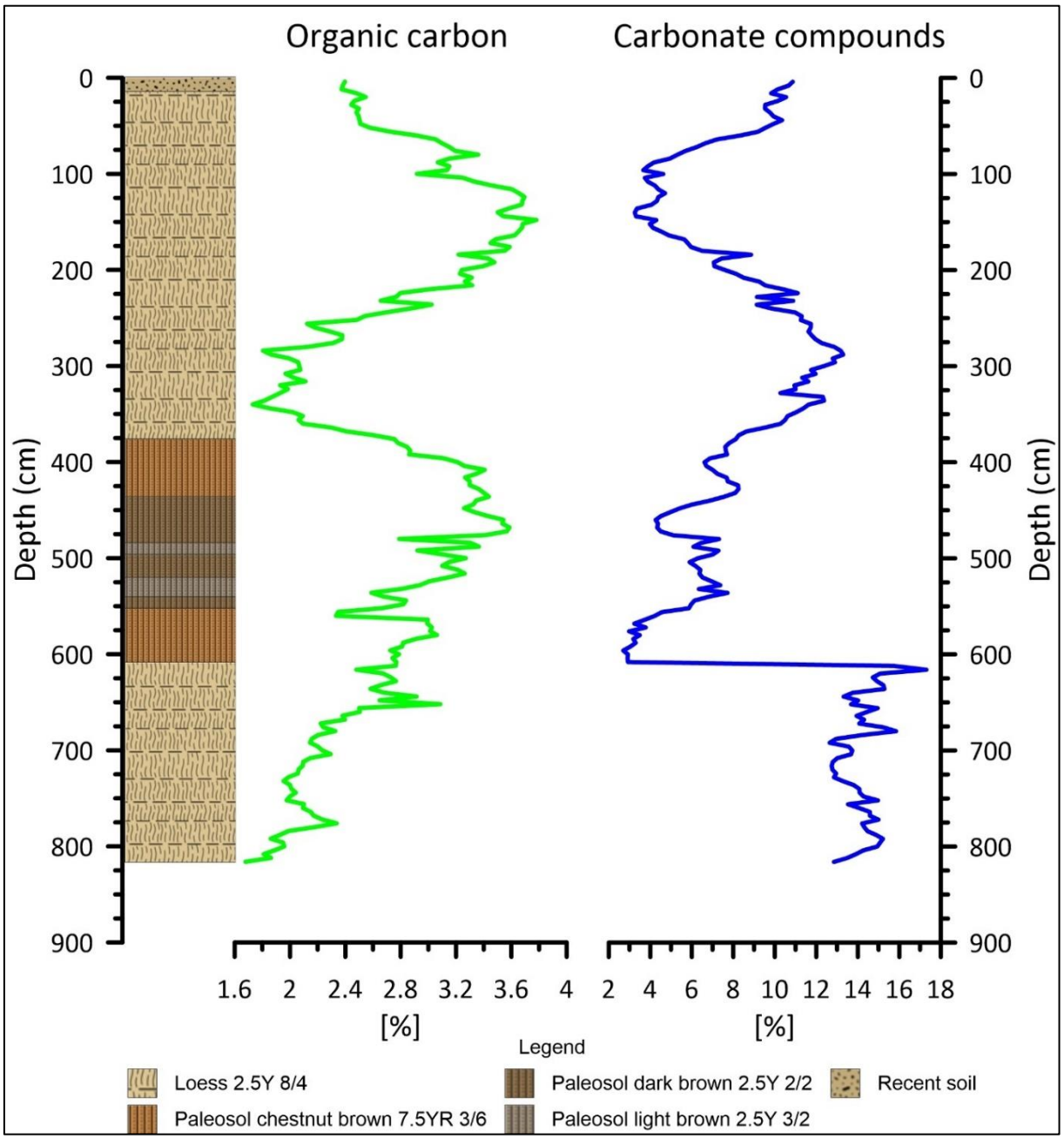

Fig. IV. 5. LOI results (Organic carbon: 550 °C, carbonate: 900 °C) of the Bonyhádvarasd section

The carbonate content increases upward from 13% to 18% within the lower loess body. At the depth of 6.08 m, where the loess–paleosol boundary is located, it drops drastically to ~2%. Its value reaches 8% in the paleosol complex; however, it falls back under 4% in the upper light brown (2.5Y 3/2) paleosol layer. Within the upper loess body, its value varies in the range 4–13%. The lowest carbonate content values are measured whereas the organic matter values are the highest. The recent soil cannot be detected clearly on the basis of these values only.

IV.3.3. Grain Size Distribution

The profile of Pécel was the only examined one among the four where grain size fractions larger than very fine sand were detected. The main reason for this can be the sand deposits found below the loess body as well as the slight (more than 1%) fine sand content of the L1S1 paleosol horizon.

IV.3.3.1. Pécel

It can be generally concluded that the proportion of very fine sand is significantly high (10%) in the entire section (Fig. IV.6). Despite this fact, coarser sand fractions can be detected only in the fluvial sand layers at the bottom of the loess wall and do not reach 1% in the loess sediments above. In parallel with the general characteristics of loess walls (Pye, 1995), the two dominant grain size fractions are the medium (21.6%) and the coarse silt (30.6%).

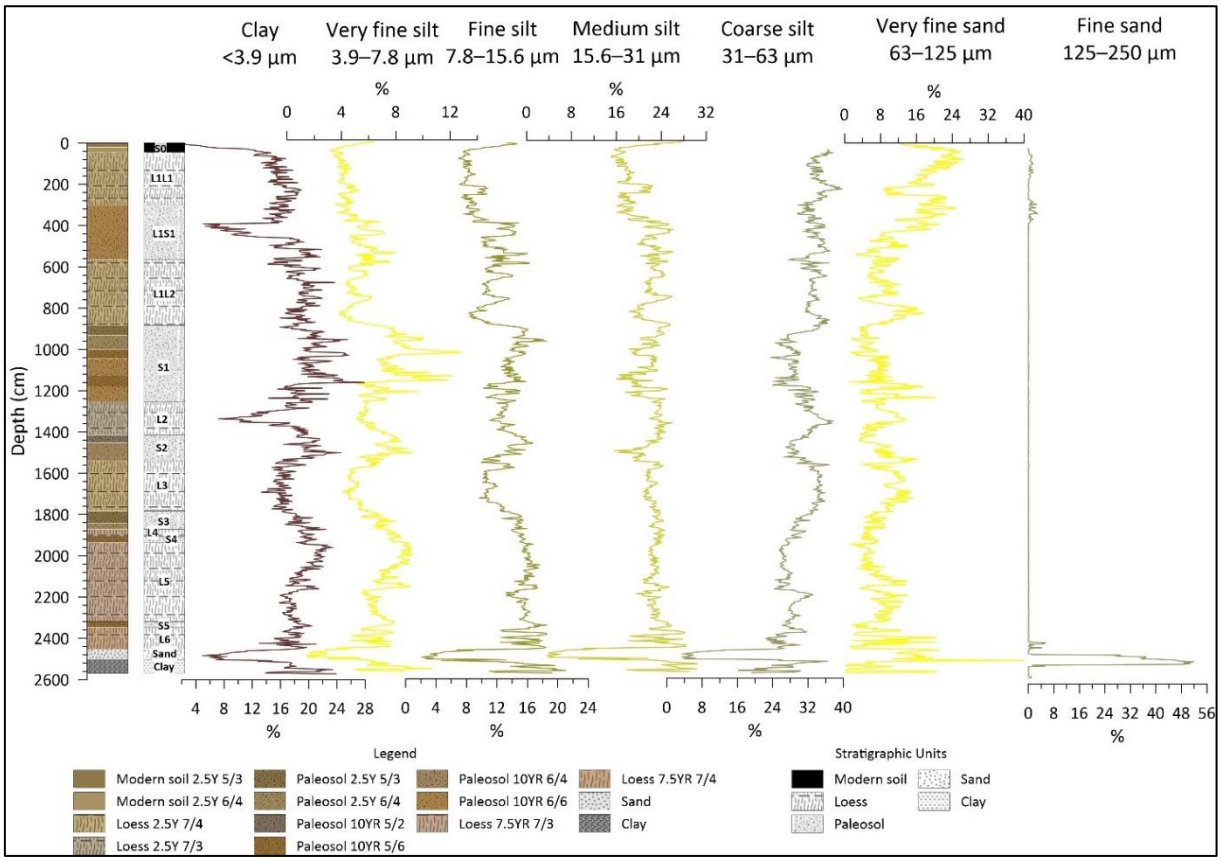

Fig. IV. 6. Grain size distribution of the Pécel section without medium and corase sand

Finer fractions become predominant in the range 25.07–25.72 m: 18.1% clay, 24.5% medium silt, and 26.4% coarse silt. In addition, an unusually high very fine sand ratio (8%) can be detected here as well.

The grain size composition of the sand body in the range 24.56–25.07 m is predominated by sand fractions. The proportion of the fine sand and larger fractions exceeds 1% only in this part within the entire section. However, the 15.5% proportion of very fine sand is combined with 35.8% fine sand and 10.3% medium sand here. An average ratio of 2.7% coarse sand can be detected as well.

Between 23.48 and 24.56 m, a loess body (L6) can be found. It can be characterized by a clay content of 17.5% and predominantly consists of medium (24.6%) and coarse (26.6%) silt. In addition, 8% of very fine sand can also be detected.

The S5 paleosol layer is located in the range 23.20–23.48 m. In this layer, a clay content of 19% can be detected, while the medium (24.6%) and coarse (27.4%) silt fractions are dominant here, with an additional 4.3% of very fine sand ratio.

Between 19.36 and 23.20 m, the proportion of medium silt (22.6%) decreases while the very fine sand (7.5%) increases compared to the paleosol below the L5 loess.

The paleosol layer (S4) in the range 19.08–19.36 m shows the highest clay content (19.9%) within the entire section. In addition, 23.6% of medium silt (close to the average) and 27.4% of coarse silt fractions can be detected as well. The proportion of very fine sand decreases to 5.8% here.

The L4 loess (in the range 18.72–19.08 m) is a thinner layer between 2 paleosol horizons, where the second highest clay (19.6%) content was measured. In this layer, the proportion of medium silt is similar to that in the paleosol below it. At the same time, the coarse silt increases to 29.7%, and the proportion of very fine sand decreases to 5%.

IV.3.3.2. Kisdorog-West

The dominant grain size fractions in the lower loess body (3.84–5.6 m) of this profile (Fig. IV.7) are the coarse (35–39%) and medium (20–26%) silt. The proportion of the coarser fractions continuously decreases upwards against the finer fractions. At the same time, a relatively constant proportion of clay fraction was measured here (ranging between 16% and 24%). The proportion of the very fine sand fraction gradually decreases from its maximum of about 15% upwards to the paleosol complex (to 3.84 m), in which it almost completely disappears.

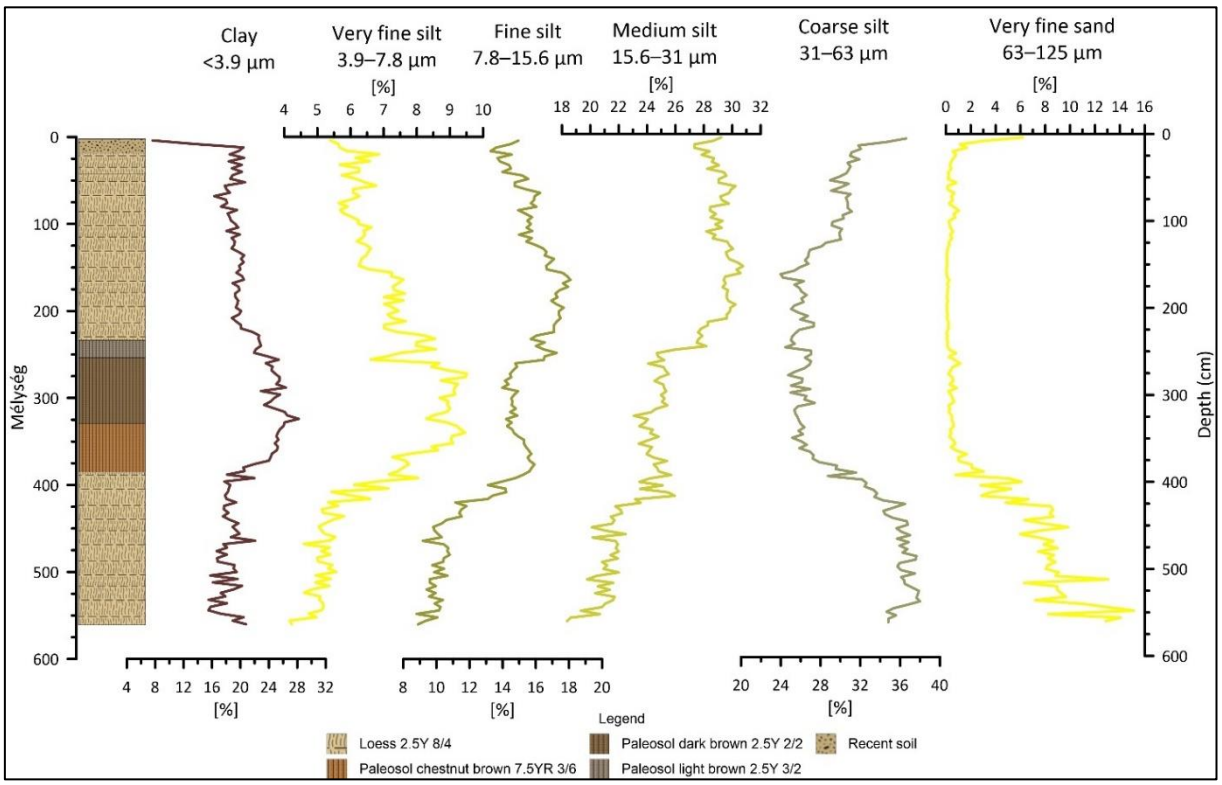

Fig. IV. 7. Grain size distribution of the Kisdorog-West section

The grain size distribution of the paleosol complex (2.32–3.84 m) is dominated by finer fractions like clay and very fine silt that reach their maximum here (~28% and ~10%, respectively). At the boundary of the dark brown (2.5Y 2/2) and light brown (2.5Y 3/2) paleosol layers (2.52–2.76 m), the very fine silt fraction decreases from 10% to 6%.

Subsequently, the upper loess body (0.40–2.32 m) is dominated by medium and coarse silt; however, their proportions continuously decrease in parallel with the clay and very fine silt. A slight peak was detected in the proportion of very fine sand in the range 0.56–0.88 m, although it still does not exceed 1%.

The clay fraction decreases below 8% in the recent soil levels (0–0.4 m), which is the smallest value in the entire section. At the same time, this layer is also dominated by coarser fractions like coarse silt and even the proportion of the very fine sand increases and reaches 6%.

IV.3.3.3. Kisdorog-East

Unlike the Western profile, the lower loess body (6.20-6.40 m) of the Eastern one (Fig. IV.8) is dominated by medium silt (30–35%), as well as fine and coarse silt (22–28%). The proportion of the clay fraction decreases from 20% to 8% towards the boundary of the paleosol complex (6.20 m). Although the very fine sand fraction still can be detected here, its proportion is significantly less (maximum 4%).

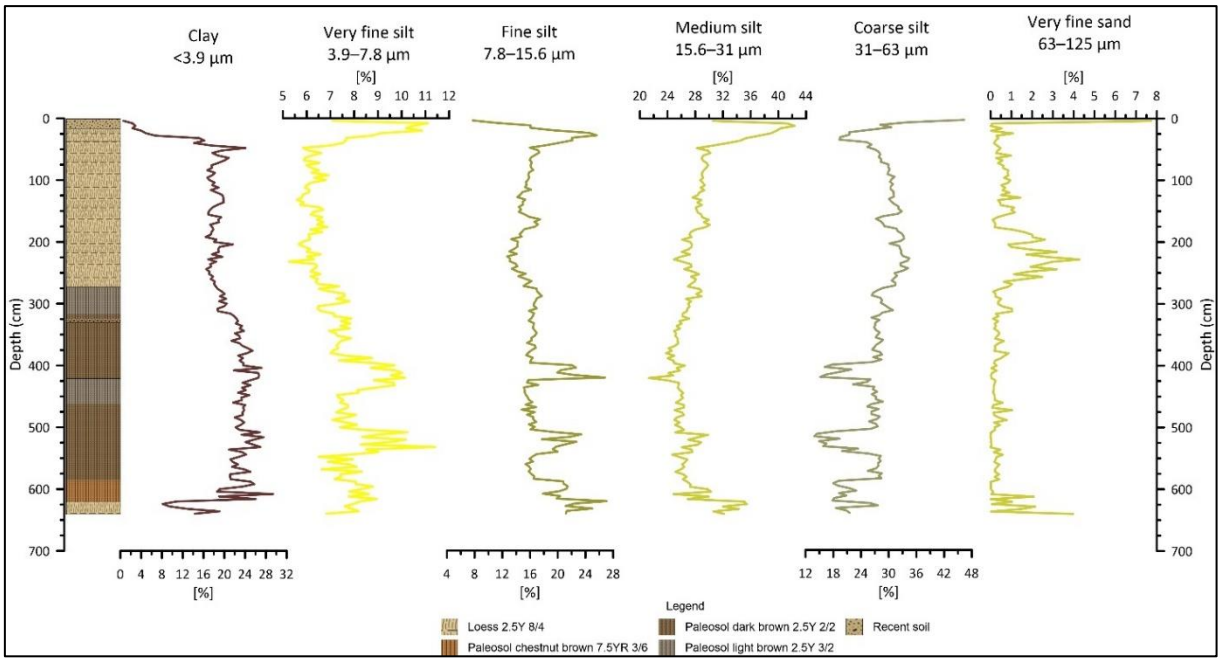

Fig. IV. 8. Grain size distribution of the Kisdorog-East section

The chestnut-brown-colored (7.5YR 3/6) layer (5.84–6.20 m) of the paleosol complex (in the range 2.72–6.20 m) is dominated by clay and medium silt (20–28%). Above it, the dark brown (2.5Y 2/2) layer (4.60–5.84 m) can be found, with a remarkable part between 5–5.50 m, where the proportion of the smaller fractions significantly increases against the coarse silt. At the boundary of the middle light brown (2.5Y 3/2, 4.10–4.60 m) and the upper dark brown (2.5Y 2/2, 2.16–4.20 m) paleosol layers, the proportion of the very fine and fine silt increases–-similar to the lower dark brown (2.5Y 2/2) layer; however, the proportion of the medium and coarse silt decreases. At the same time, the proportion of the clay and very fine silt decreases at the lower boundary of the upper light brown (2.5Y 3/2) layer.

At the lower levels of the upper loess body (0.36–2.72 m), in the range 1.80–2.60 m, the proportion of the very fine sand increases to even 4% in some places. The proportion of the silt fractions continuously increases upwards the recent soil horizon, where they fall back in parallel with the increase of the very fine sand (up to ~8%).

IV.3.3.4. Bonyhádvarasd

The dominant grain size fraction of the lower loess body (6.08–8.16 m) of this profile (Fig. IV.9) is medium silt with values varying in the range 22–33%. Concurrently, the proportion of clay fraction is also significant; the clay peak of the entire profile is detected here with a value of ~34%. In the upper part of the lower loess body, the proportion of fine silt increases by more than 10% against the coarse silt.

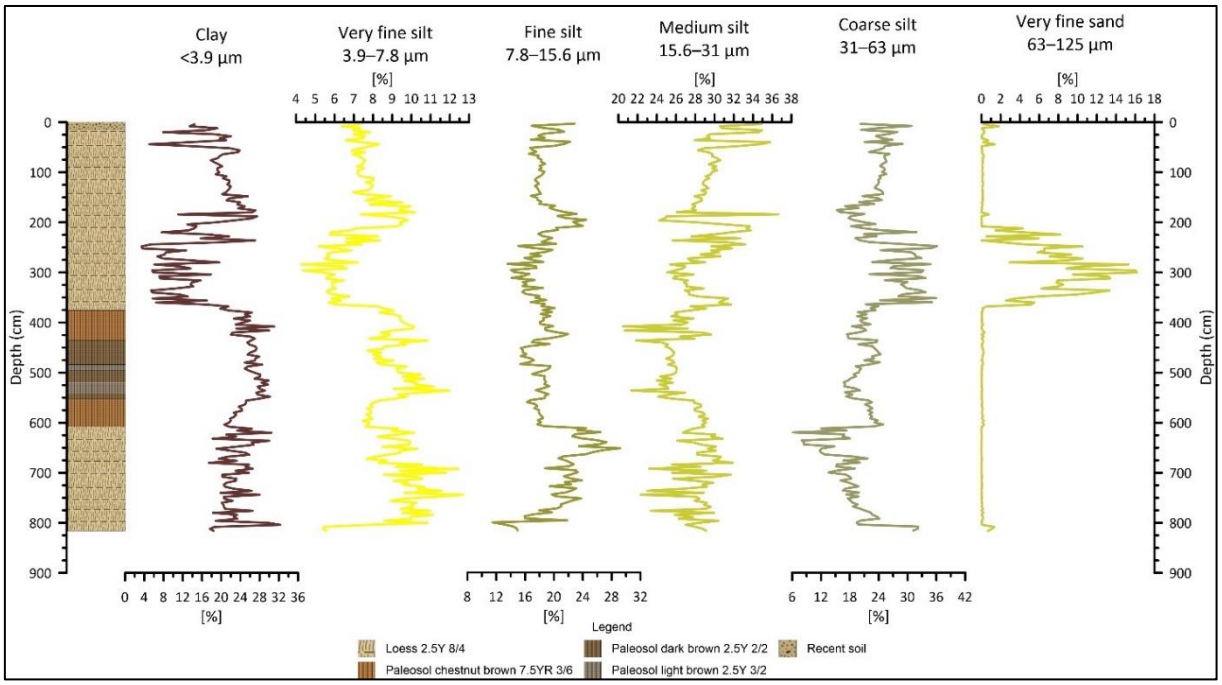

Fig. IV. 9. Grain size distribution of the Bonyhádvarasd section

A contrary change can be detected at the boundary of the paleosol complex (3.76–6.08 m) and the lower loess body, where the coarse silt becomes dominant in addition to the medium silt. The shift of the middle light brown (2.5Y 3/2) and dark brown (2.5Y 2/2) layers (4.84–5.52) is hardly observable; however, the slight dominance of finer fractions can be detected. This trend reverses again in the upper dark brown (2.5Y 2/2) paleosol layer (4.36–4.84 m). These proportions fluctuate intensively within the upper chestnut-brown-colored (7.5YR 3/6) layer (3.76–4.36 m).

The following layer is the upper loess body (0.15–3.76 m). The lower parts of this level can be characterized by coarser fractions. In addition to the dominance of coarse silt, the clay fraction falls below an average of 10%, while an average of 8% of very fine sand can be detected with a maximum value of ~16%. The upper loess body is almost identical to the lower one in terms of grain composition.

IV.3.4. Grain Size Indices

IV.3.4.1. Pécel

The MGS value provides relatively less information in the case of the Pécel profile (Fig. IV.10) due to the presence of the sandy sediment at the bottom of the section. The GSI and U-ratio values show a peak within the loess bodies and their trends are similar except for their trends in the L1S1 paleosol layer.

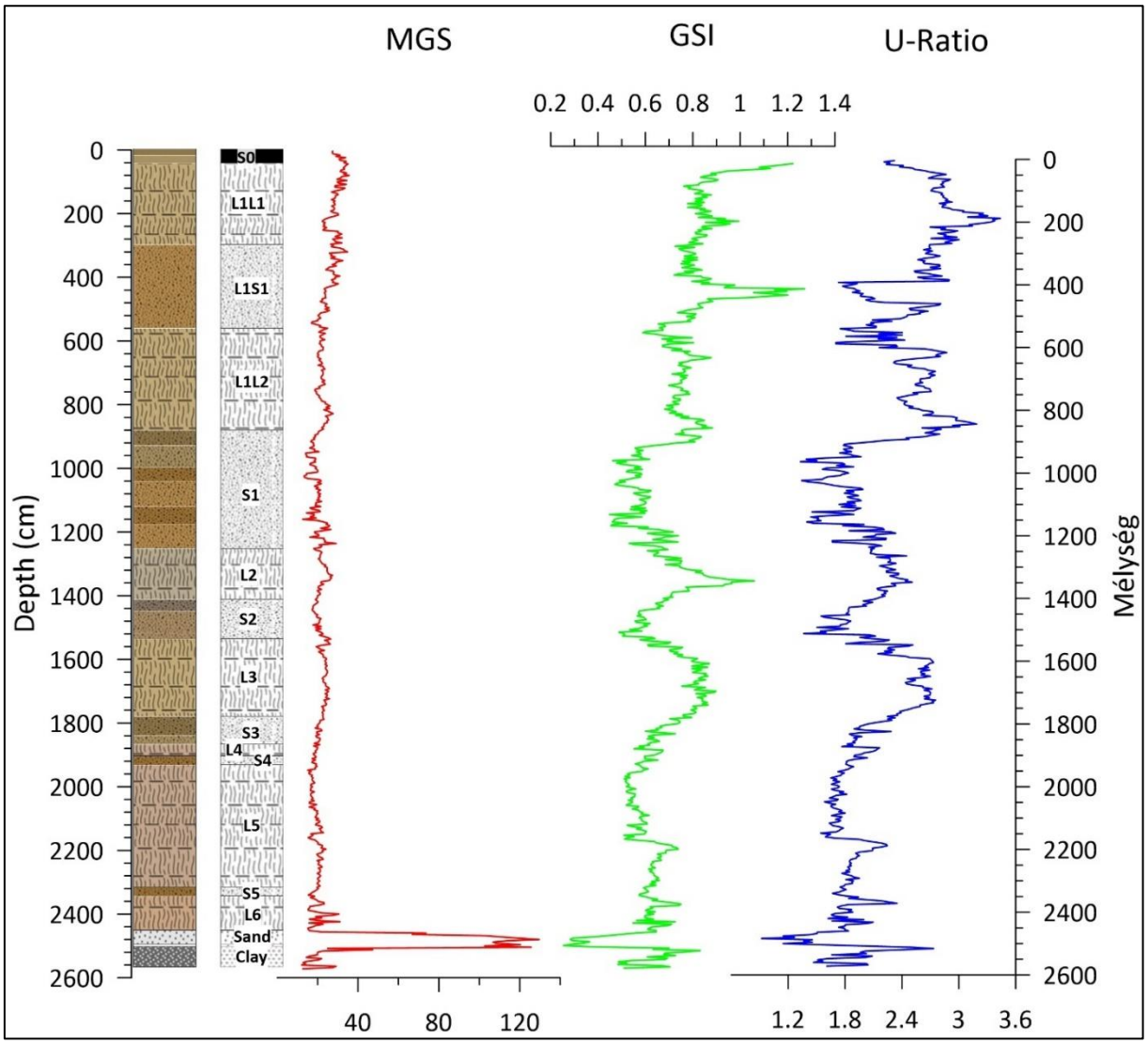

Fig. IV. 10. Mean grain size and grain size indices of the Pécel sequence

IV.3.4.2. Kisdorog-West

In Figure IV.11, we can see that all three indices show higher values within the lower loess body, while the lower values of the paleosol complex start to increase only from the middle of the upper loess body.

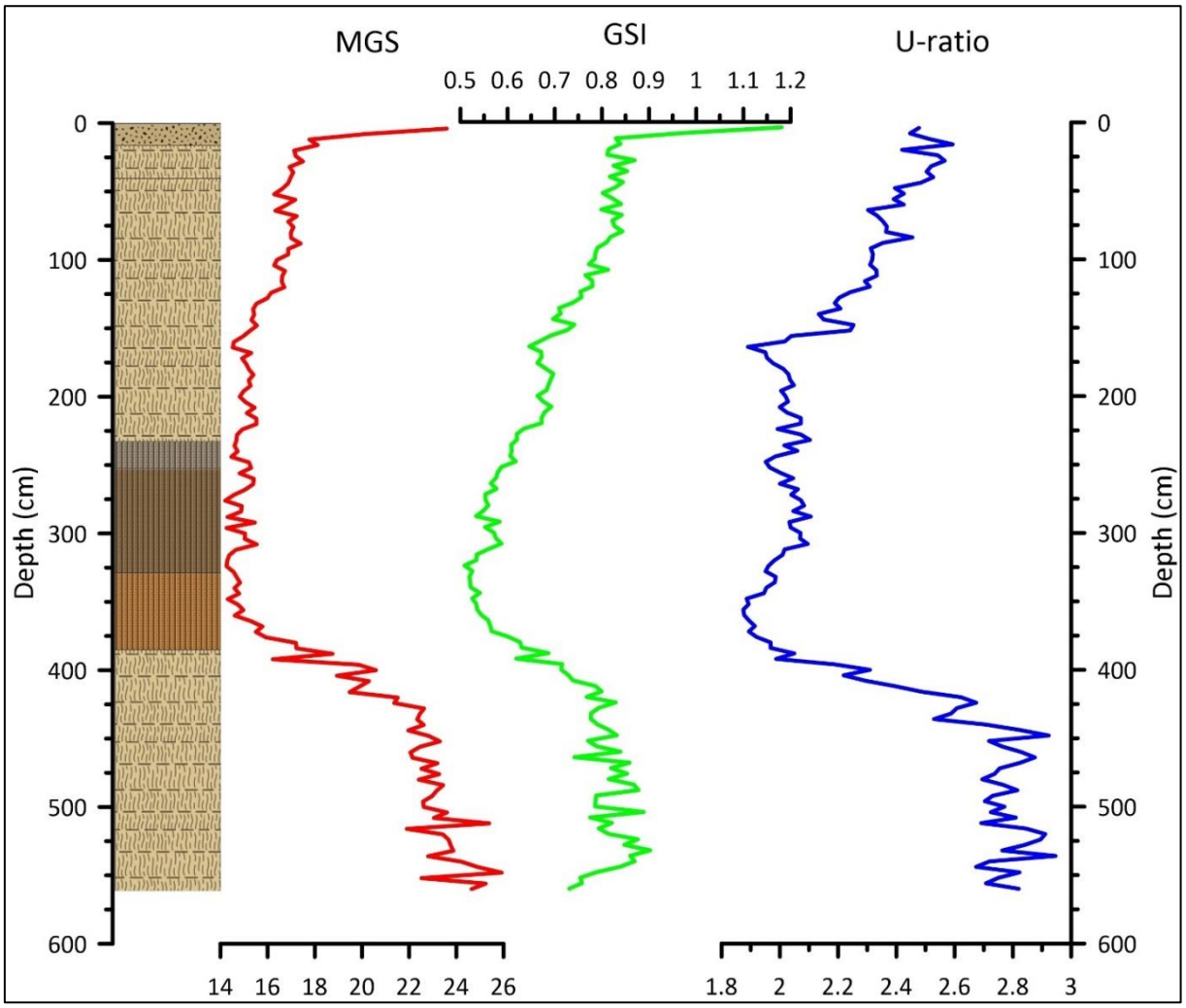

Fig. IV. 11. Mean grain size and grain size indices of the Kisdorog-West sequence

IV.3.4.3. Kisdorog-East

The GSI value is almost stable within the entire profile (Fig. IV.12) except for some minor decreases. At the same time, the MGS and U-ratio values show two notable increases and a similarly significant decrease.

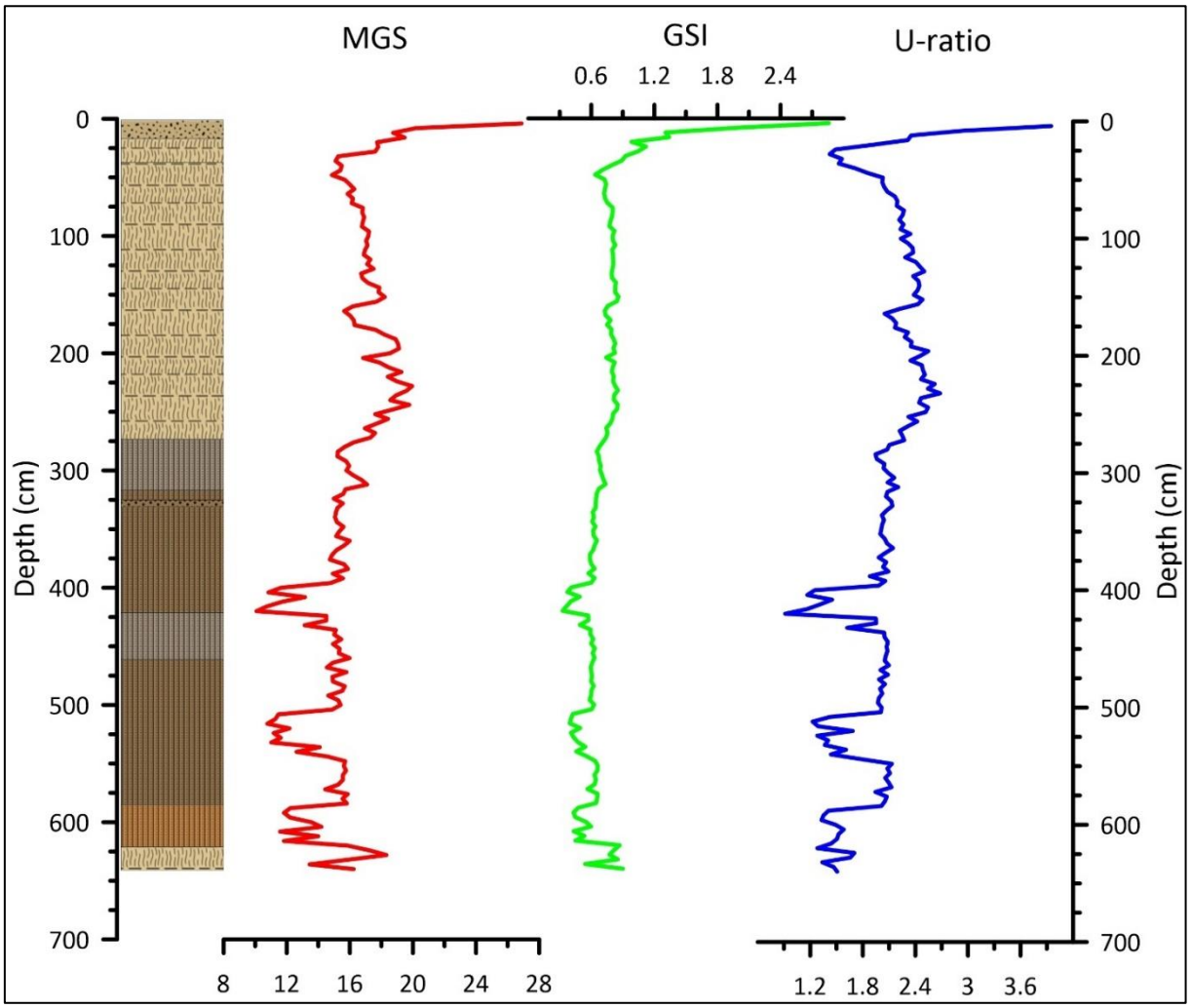

Fig. IV. 12. Mean grain size and grain size indices of the Kisdorog-East sequence

IIIV.3.4.4. Bonyhádvarasd

In the case of this profile (Fig. IV.13), a significant increase can be observed for all three indices in the lower part of the upper loess body. Two parts with outstanding values of U-ratio can be seen in the paleosol complex.

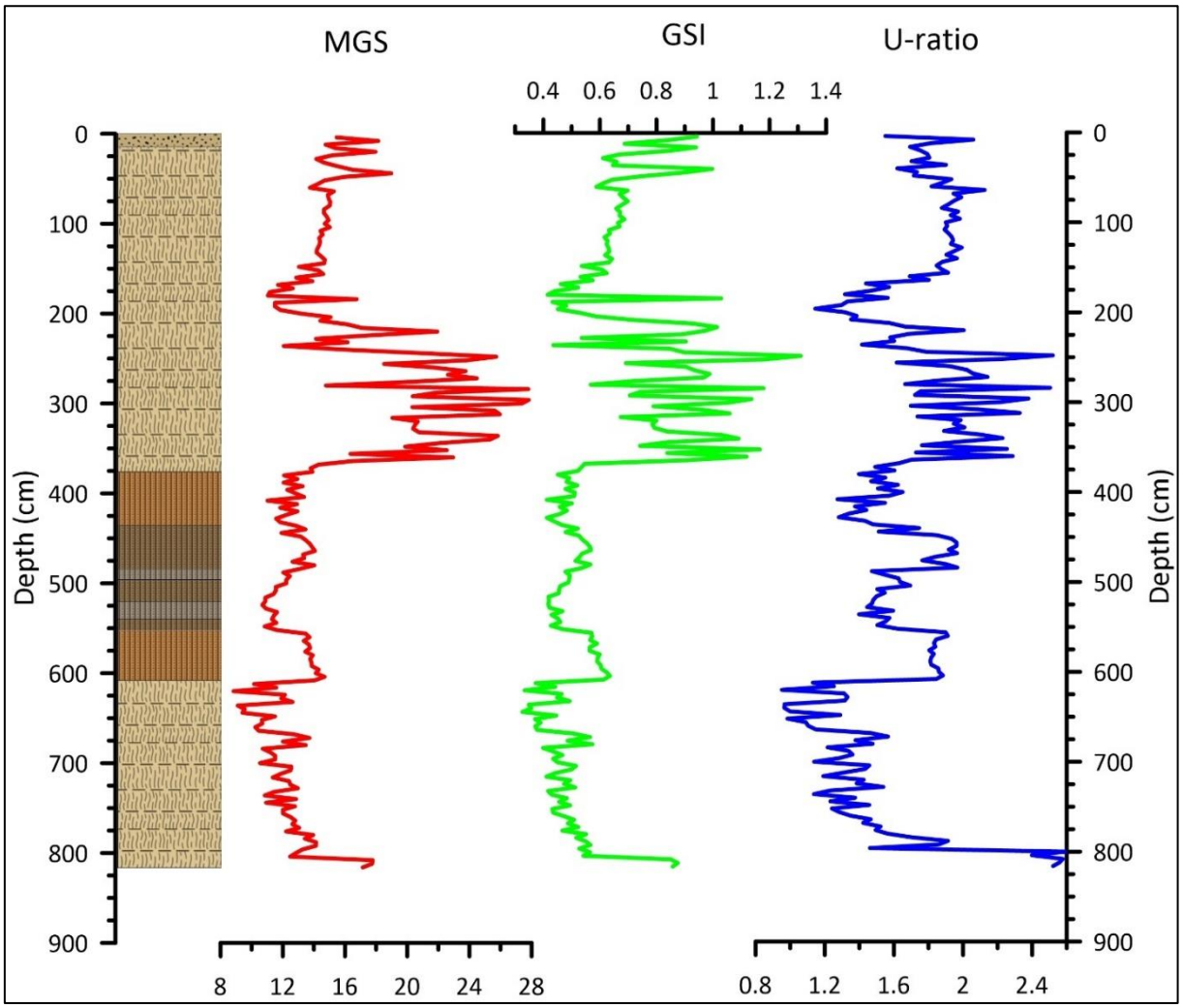

Fig. IV. 13. Mean grain size and grain size indices of the Bonyhádvarasd sequence

IV.3.5. Magnetic Susceptibility

Magnetic susceptibility values measured show high variability in the Pécel profile. The MS peak was detected in the upper part of the upper part of the L5 loess body with values of more than 100. For the rest of the profiles, only paleosol layers can be described with higher MS values. A double peak trend in the MS can be observed in the Transdanubian profiles; however, the upper peak can be observed in the upper loess body in the case of the Kisdorog-West section.

IV.4. Discussion

IV.4.1. Pécel

The periodical and permanent water cover characteristics of the fluvial areas suggest that intensive element mobilization may have occurred during the deposition of the fluvial sediments beneath the loess wall. The first stratum of these fluvial sediments is a clay layer. This is presumably a marsh sediment, the result of this former periodic water cover. A noticeable part of this section can be found in the range 25.20–25.40 m. At this depth, more than 10% carbonate content was measured.

The upper boundary of this red sand is a sand layer with a thickness of 51 cm. It contains massive, cross-layered, and laminated sand, in this order, from bottom to top. These sediments represent perfectly the development of the former stream's riverbed. Massive sand indicates a crevasse splay formation process, while cross-layered sand indicates turbulent, and laminated sand indicates laminar flow during the deposition of this sediment. The uppermost 7 cm of this sand layer is red-colored sand.

The L6 loess above, which was deposited on the fluvial sediment (with hiatus in some places), can be characterized by varying grain size composition and LOI values. In addition, fine sand can also be found in the lower parts of it. It can be assumed that the accumulation of the dust started in a period of temporary existing water coverage which may have mixed with the sand sediment underneath. The S5 layer above is a small paleosol horizon with a thickness of 28 cm.

Subsequently, a significant weathering horizon can be detected in the L5 loess body, predominated by finer grain size fractions. Subsequently, continuous soil development can be reconstructed based on the continuously increasing proportion of organic matter content towards the S4 paleosol layer. The outstanding GSI and U-ratio values in the range 21.80–21.92 m indicate an increase in wind velocity. Apart from this, no other significant change can be detected here.

The S4 paleosol layer is a small horizon of 28 cm, which cannot be detected clearly only on the basis of the changes in grain size distribution; however, it is clearly indicated by the shift of the Munsell colors and the LOI values. Above the S4 paleosol, a loess layer of 26 cm can be detected up to 18.72 m, where the paleosol of the previous section ended.

The subsequent L4 loess body is a small layer of only 36 cm; however, it could clearly be separated visually from the paleosols below and above it. The decrease in LOI values—a typical feature of loess sediments—can also be observed here.

The increase in both GSI and U-ratio values within the L3 loess body indicates an increase in wind and dust storm activities.

In the upper part of the S2 paleosol, the organic matter content increases significantly while the carbonate content values decrease, presumably due to leaching activity. Here, the grain size composition is dominated by finer fractions, and particle indices have declined significantly, indicating warming and a decrease in wind energy.

Above, clay fraction decreases significantly within the L2 loess body, while the proportion of the coarser fractions slightly increases in parallel with the increase of GSI values, indicating a significant increase in the transport energy.

In the S1 paleosol, horizons with significant decreases in carbonate content can be observed, which layers can be considered as leaching horizons. The grain size composition is dominated by finer fractions; thus, the particle indices are low, indicating low transport energy.

In the L1 complex, the L1L2 and L1L1 loess bodies are dominated by coarser fractions and higher particle indices, assuming a high wind activity during the accumulation of these layers. A significant decrease in clay proportion can be observed within the L1S1 paleosol. This is in parallel with the increase of the GSI values and the decrease of U-ratios. The formation of the paleosol layer indicates warming, which was interrupted by a cold period of stronger winds.

IV.4.2. Kisdorog-West

This profile is divided into two loess bodies with a paleosol complex of three sublayers in between. The grain size composition results combined with the color analysis of the samples clearly indicate the paleosol layers. The lower loess body can be characterized by a high proportion of coarse silt and very fine sand. In addition, its carbonate content is low and MS values were measured in the range 10–20.

Among the three parameters gained from the LOI measurements, the low carbonate content is the one that clearly indicates the presence of the paleosol complex. Clay and very fine silt are the dominant grain size fractions here. High MS values can be detected in this section; however, the maximum value is only in the range 70–80.

The lower section of the upper loess body is dominated by fine and medium silt in addition to the extremely high organic matter content and high MS values as well. At the same time, the upper levels of this loess are dominated by coarser fractions with increased carbonate and decreased organic matter content.

The particle indices show increased values within the lower loess body while they decrease significantly up to the paleosol complex before start increase gradually up to the surface.

IV.4.3. Kisdorog-East

This section is located 700 m away from the western one, on the eastern side of the loess hill. Its general structure is similar to the western one; 2 loess bodies with a paleosol layer in between; however, this paleosol can be divided into five sublayers. The lower loess is of small size, where very fine sand can also be observed. It can be characterized by low organic matter and MS values.

Within the dark brown layers of this paleosol complex, 2 notable levels can be observed with high fine silt proportion compared to the coarser fractions. An increase in carbonate content can also be detected within these levels. MS values measured increase up to 150–160.

Very fine sand fraction occurs again in the lower levels of the upper loess body. From the depth of 150 cm upwards, carbonate content notably increases in addition to the shift of the grain size to the finer fractions.

Two notable levels of decrease in the grain size indices can be observed within the paleosol complex.

IV.4.4. Bonyhádvarasd

Although this profile can be found 7 km away from the profiles of Kisdorog, it is quite similar to them in terms of structure. The paleosol complex of this profile can be divided into 7 sublayers with a 1–1 loess body above and below it similar to the ones of Kisdorog. The lower loess body can be characterized by constantly high carbonate as well as continuously increasing organ matter content upwards. The dominant grain size fraction is medium silt; however, the proportion of the clay fraction is also remarkable in this layer.

At the lower boundary of the paleosol complex, a significant decrease in the carbonate constant and a slight increase in the coarse silt fraction can be detected. The MS values are generally high in the paleosol layer and almost reach 160.

The very fine sand fraction appears in the lower levels of the upper loess body and its proportion reaches 16%. At this level, the organic matter decreases below 2% accompanied by 10–12% carbonate content. In its upper section, the particle size is shifted towards the finer fractions. In addition, the highest organic matter content in the entire section (3–4%) was also measured here.

Similar to the Kisdorog-East profile, a significant decrease and then increase of the particle indices can be observed within the paleosol complex, although the highest values here were measured in the lower parts of the upper loess body.

IV.5. Conclusion

The relative ages of the profiles could be determined by the comparison of the MS values measured here to the values obtained from the study of the Chinese Loess Plateau (Figures IV.14 and IV.15). Due to its size, among other factors, more information can be extracted by the examination of the profile of Pécel than from the three other ones studied in this paper. By comparing the MS values with the one measured in the case of the Chinese Loess Plateau, this profile can be traced back to the MIS 9–10 stages. The deposition of the other three (Transdanubian) profiles can presumably be dated back to the MIS 2–4; moreover, they can be parallelized with the L1L1-L1S1-L1L2 strata of the Pécel profile.

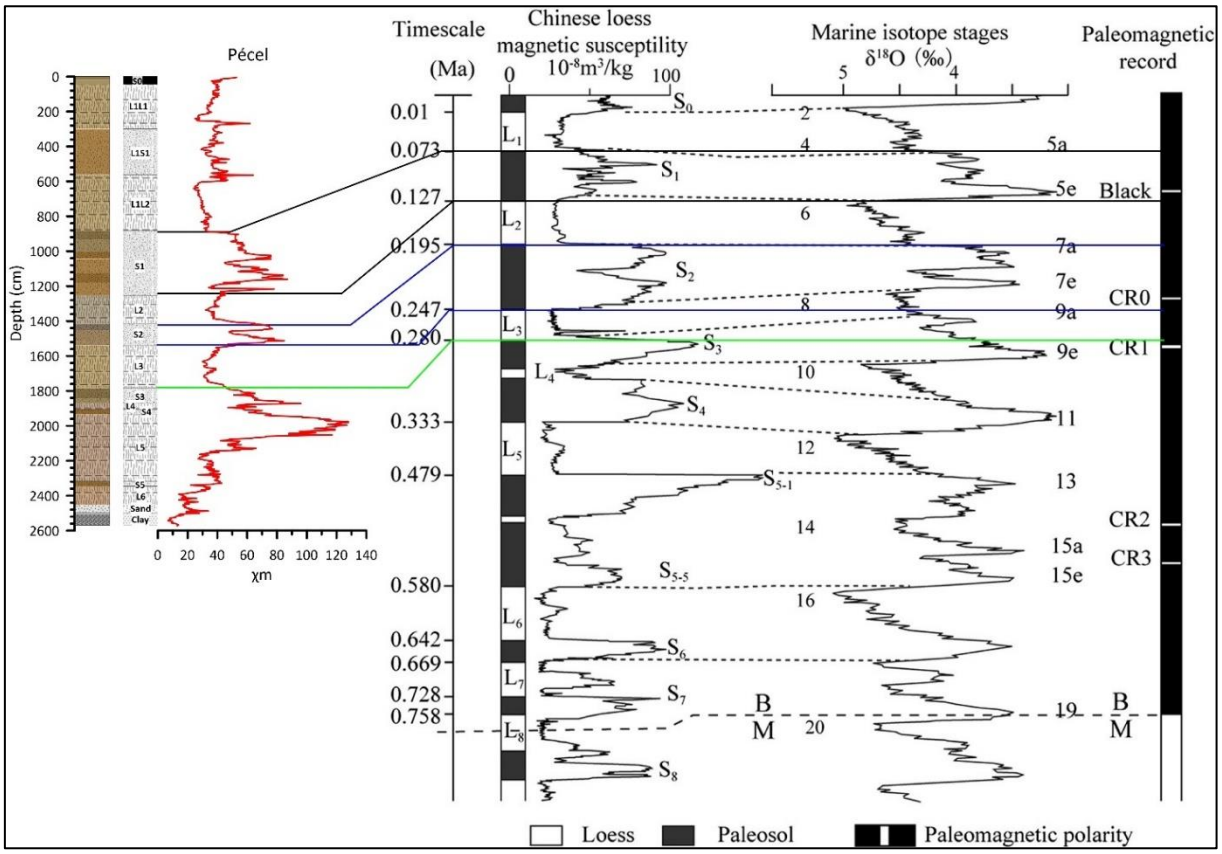

Fig. IV. 14. MS comparisons between the Pécel sections and the Chinese Loess Plateau (Ren et al., 2014). The black lines describe the S1 paleosol, the blue ones the S2, and the green line is the beginning of the S3 paleosol of the Chinese loess sequence

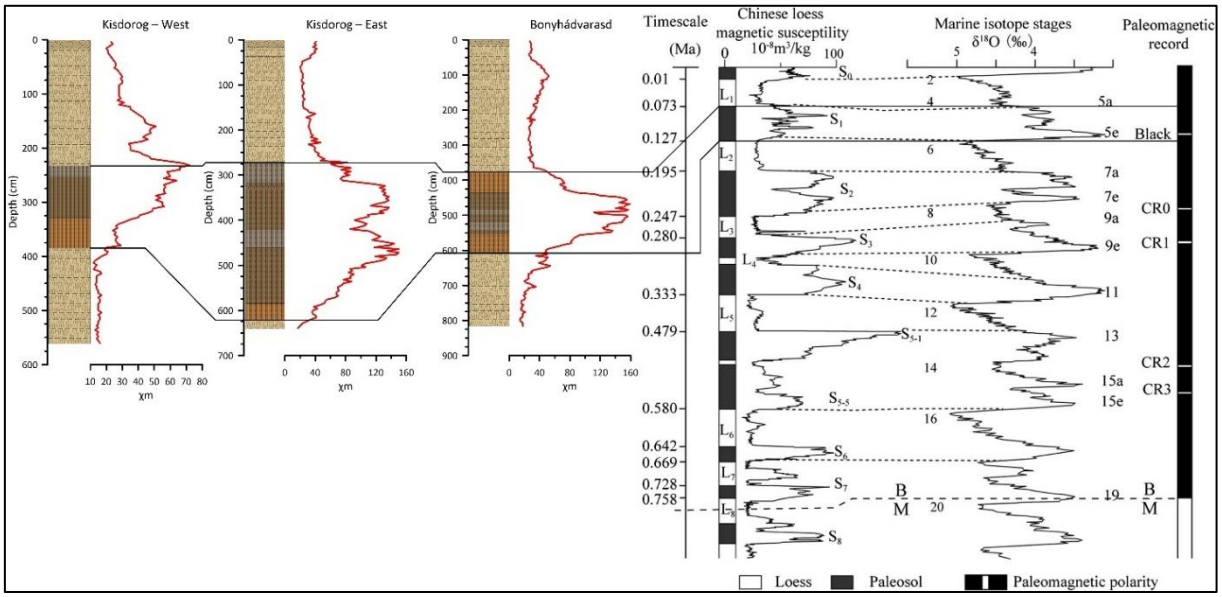

Fig. IV. 15. MS comparisons between the Transdanubian sections and the Chinese Loess Plateau (Ren et al., 2014)

IV.5.1. Pécel

The development of the loess wall and the deposition of its sediments began with the southward movement of the stream. The variable sand content indicates a periodically increasing wind energy and velocity of which traces can be detected in the different layers deposited. However, only smaller periods of time can be characterized by this high wind velocity.

Ostracods were found in the clay sediment at the bottom of the section, suggesting an Upper Miocene age of the sediment. Based on the presence of this Upper Miocene stratum, the erosion of the lowermost part of the profile can be assumed and the deposition of the loess sediment began after the termination of the fluvial sediment.

IV.5.2. Transdanubian Profiles

In the case of the three Transdanubian profiles, significant differences can be observed compared to the Pécel one. The topography of the hill area in the surroundings of the examined profiles can be characterized by northwest–southeast-oriented hills. Based on the grain size analysis, very fine sand fraction can be detected in the lower loess body of Kisdorog-West and Kisdorog-East and in the upper loess body of the Bonyhádvarasd profiles. This suggests that the prevailing wind direction was north–northwest during the deposition of the lower layers and south–southeast during the deposition of the upper layers. The significant changes observed in the particle indices also support this assumption for the paleosol complexes. In addition, it can be concluded that the eastern-oriented profile includes less-developed paleosol horizons. In its case, only three sublayers could be distinguished and the MS values barely reached 80, while they increased to 150–160 in the cases of the other two profiles.

CHAPTER V.

DEVELOPMENT HISTORY OF A MIS 2/3 LOESS-PALEOSOL SEQUENCE SUPPORTED BY A RADIOCARBON-BASED ADE-DEPTH MODEL, PÉCEL, HUNGARY

László Makó

Department of Geology and Paleontology, University of Szeged, Hungary

makol@geo.u-szeged.hu

Péter Cseh

Department of Geology and Paleontology, University of Szeged, Hungary

cspeti94@gmail.com

Balázs Nagy

Department of Geology and Paleontology, University of Szeged, Hungary

nagba88@gmail.com

Pál Sümegi

Department of Geology and Paleontology, University of Szeged, Hungary

sumegi@geo.u-szeged.hu

Dávid Molnár

Department of Geology and Paleontology, University of Szeged, Hungary

molnard@geo.u-szeged.hu

Quaternary Research

Under review

Development History a MIS 2/3 loess-paleosol sequence supported by a radiocarbon-based age-depth model, Pécel, Hungary

László Makó, Péter Cseh, Balázs Nagy, Pál Sümegi, Dávid Molnár

Abstract

The loess-paleosol profile of Pécel is an approximately 26-meter-high well-preserved sequence in the Northern part of the Carpathian Basin, Hungary which was sampled in high resolution. The research team found the nearby Rákos stream's river sediment beneath the sequence of which the forming and movement of the riverbank can be traced. The loessy sediment was deposited on that sediment with an erosion horizon presumably due to water flow. There were 20 radiocarbon measurements carried out from the samples of the upper 8 meters. Based on these, and the magnetic susceptibility measurement results, the developing progress of the loess wall can be traced from this river sediment to the recent surface. Sedimentological analysis and geochemical indices were used to determine the rate of weathering. The previous research showed that at about 10 meters, based on the trace elements' changes it is an alteration of the dust transport's direction. We assumed that the uppermost, weakly-developed paleosol layer could be redeposited, which is also proved by radiocarbon dates, and sedimentological and magnetic susceptibility data. Further research will be based on malacological investigations, geophysical measurements or probably OSL/IRSL measurements to get to know the exact age of the sequence.

V.1. Introduction

The study of loess-paleosol sequences has an essential role in the research of the Quaternary Period (e.g., Pye, 1995; Krolopp and Sümegi, 1995; Gallet et al. 1996; Marković et al. 2015, 2018; Újvári et al. 2010, 2014, 2016). By using basic analytical approaches such as particle composition, organic matter and carbonate content analysis, identification of the Mollusca fauna, moreover age data, and the age-depth models obtained from them, changes in the paleoenvironment and paleoclimate can be examined in high resolution (e.g., Sümegi et al. 2015, 2019, 2020, 2022; Molnár et al. 2021).

The examined loess-paleosol section of Pécel is located in the Carpathian Basin, in Hungary (Fig. V.1), in the area of the Gödöllő Hills (Dövényi, 2010), 47°29.797'N and 19°21.235'E (WGS 84). A southern exposed, mountain-footed (e.g., Varga et al., 2011; Sümegi

et al.; 2011, 2016; Bösken et al., 2019; Makó et al. 2021a) wall, which was sampled in 2019 and 2021 (Makó et al., 2021b, 2023), by using 10 subsections.

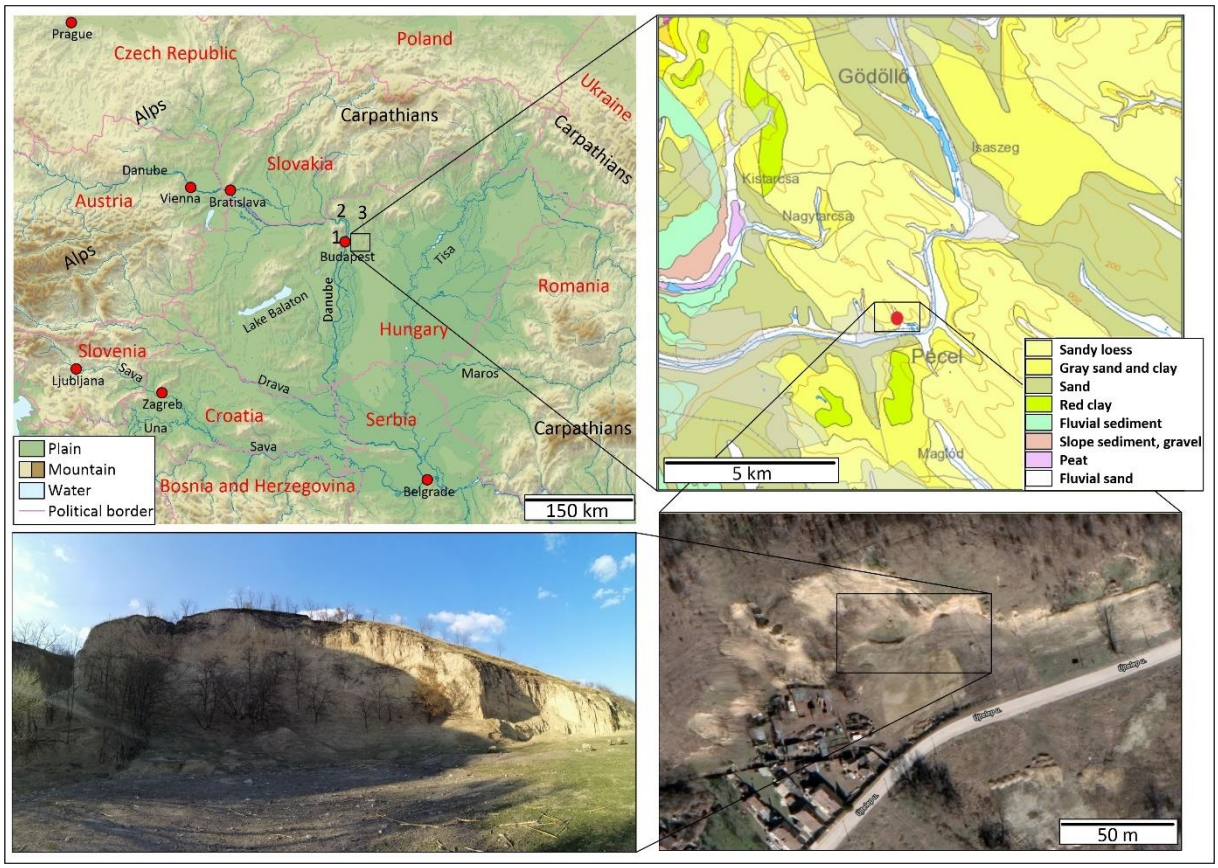

Fig. V. 1. Location of the loess-paleosol sequence of Pécel in the Carpathian Basin ((A) figure: 1. Buda Thermal Karst, 2. Börzsöny, 3. Cserhát (Wikimedia Commons), (B) figure: surface formations (Gyalog and Síkhegyi, 2005), (C) figure: ortophotomap (Google Maps), (D) figure: selfmade site photo); Makó et al. 2021

V.2. Methods

The loess wall with a height of 25.72 m was sampled with an interval of 4 cm for the laboratory measurements and with an interval of 12 cm (5-5 kg) for obtaining a sufficient amount of Mollusca material. The mollusc content of the sediment was extracted by wet sieving followed by H_2O_2 preparation. Subsequently, the extracted material was sorted and identified, moreover, a part of it from certain depths was selected for radiocarbon measurements.

V.2.1. Grain size analysis

The grain size composition measurements were carried out at the Department of Geology and Paleontology, University of Szeged by using an OMEC EasySizer 20 device, in which 42 lasers scan the particle sizes between 0.1-500 micrometers (Sümegi et al., 2019; Makó et al., 2021, 2023). During the preparation of the samples, the method of Bokhorst et al. (2011)

was used, and the obtained results were plotted with line diagrams according to the intervals of the Wentworth scale (Wentworth, 1922). Mean Grain Size (MGS) values were also calculated from D10, D50, and D75 values.

V.2.2. Magnetic susceptibility

The magnetic susceptibility test (e.g., Zhou et al. 1990; An et al. 1991; Rousseau and Kukla, 1994; Dearing et al. 1996; Sun and Liu 2000; Zhu et al. 2004; Hlavatskyi and Bakhmutov 2021) took place at the Department of Geology and Paleontology of the University of Szeged by using a Bartington MS2 K (Makó et al. 2023) instrument. The air-dried, powdered samples were measured three times in different directions.

V.2.3. Absolute dating

20 radiocarbon measurements were carried out in the Isotoptech laboratory in Debrecen (Molnár et al. 2013a, b) by using the extracted snail shells. The obtained BP data were calibrated with the IntCal20 calibration curve (Reimer et al. 2020) using the Calib 8.2 software (Stuiver and Reimer, 1993).

V.2.4. Age-depth model, AR, MAR

20 uncalibrated age data were selected for the age-depth model. After several attempts with Bacon software (Blaauw and Christen, 2011), 17 of them were selected as suitable for creating the model. The depth of the model was set between 0.44 and 8.84 meters, which covers the entire L1 section of the profile. 82% of the data provided falls within the 95% confidence interval. The model was created with an interval of 12 cm (according to the sampling), based on 16.28 million iterations from 72 sections, from which the accumulation values per centimeter, the ages and the accumulation rate, were plotted. The Accumulation Rate (AR) specifies the possible minimum, mean and maximum ages for a given depth, depending on its dimension (m a^{-1}). From the AR value, the Mass Accumulation Rate (MAR, Újvári et al., 2010) can be calculated, which is a value multiplied by the density of the dry powder material (1.5 – Újvári et al., 2010) and the mass concentration of the loess (1 – Kohfeld and Harrison, 2001; Újvári et al. 2010), with a dimension of g m^{-2} a^{-1}.

V.3. Results

The description and analysis of the entire profile are presented in two papers (Makó et al., 2021, 2023), so those results are described that are relevant for this paper. For the separation

of the loess-paleosol layers, the nomenclature used in the case of the Chinese Loess Plateau was used (e.g., Kukla, 1987; Harnois, 1988; Kukla, et al., 1990; Ding et al., 2005; Chen et al., 2006; Liang et al., 2013).

V.3.1. Grain size analysis

Since the age-depth model was made from the upper 8.84 meters of the loess body, the grain size composition results (Fig. V.2) are shown up to the fine sand fraction in this paper, because larger fractions did not occur in this depth. It can be observed that the L1L2 loess body (between 5.64-8.84 m) is predominated by finer fractions, medium and coarse silt. Subsequently, a protrusion can be observed in the L1S1 (3.00-5.64 m) layer between 3.92-4.56 m, where the clay fraction decreases from 16% to 5% and the ratio of very fine sand doubles, from 10 to 21%. In the L1 (0.44-8.84 m) loess layer fine sand fraction appears, however, its maximum value is only 3%. On the other hand, the L1L1 (0.44-3.00 m) loess body is clearly predominated by coarser fractions. A significant spike can be observed in the case of fine and medium silt between 2.16-2.56 m, with values above 10% for the former and 20% for the latter, in parallel with the decrease of the fine sand fraction under 10%. Fine sand fraction appears between 1.08-1.24 m, however, its maximum value is only 1.6%.

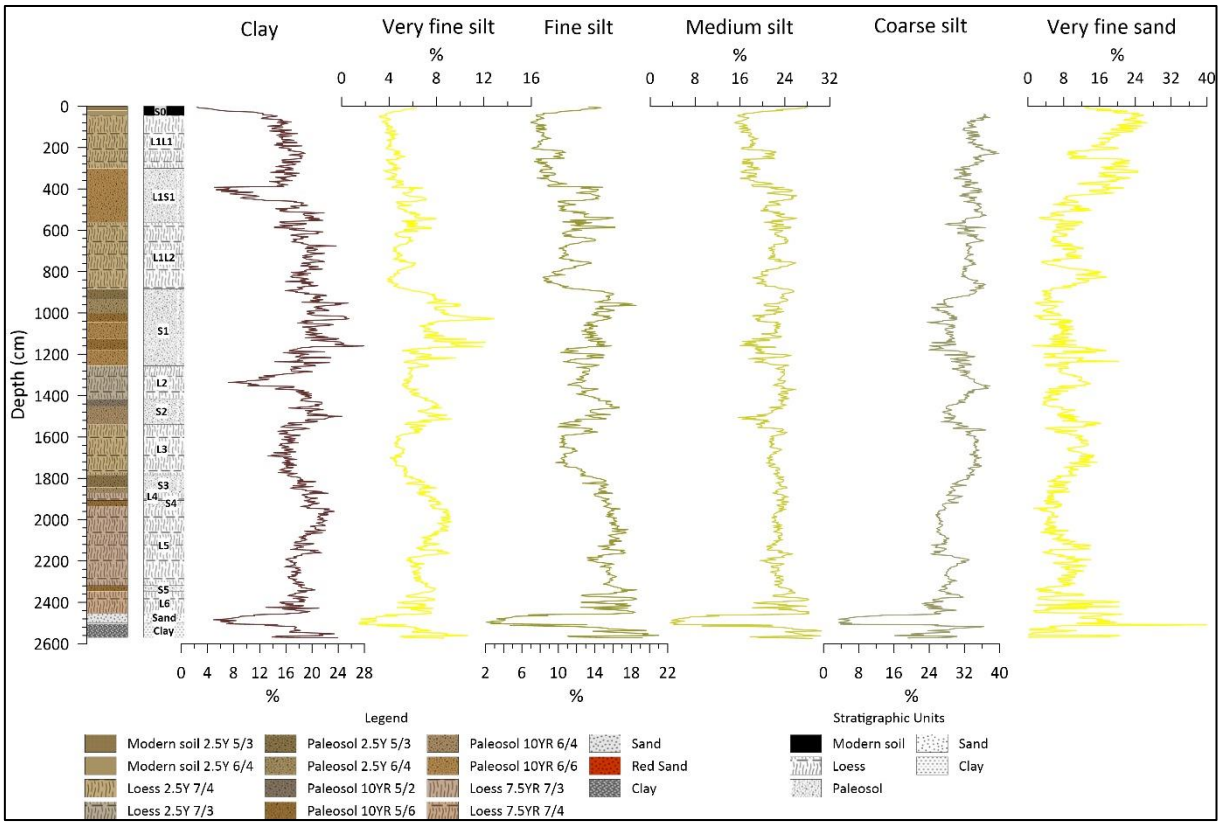

Fig. V. 2. Grain size composition of the loess-paleosol profile of Pécel (modified, Makó et al. 2021)

V.3.2. Magnetic susceptibility

The MS curve (Fig. V.3) shows that the L1L2 (5.64-8.84 m) can be characterized by low values throughout the entire loess body, with an average value of 31. Subsequently, generally low values can be observed also in the case of the L1S1 (3.00-5.64 m) paleosol layer compared to the average paleosols. It can be characterized by higher and lower fluctuations, however, the average values do not exceed 38. The L1L1 (0.44-3.00 m) loess body shows continuously increasing values in the direction of the recent surface soil, with an average value of 36.

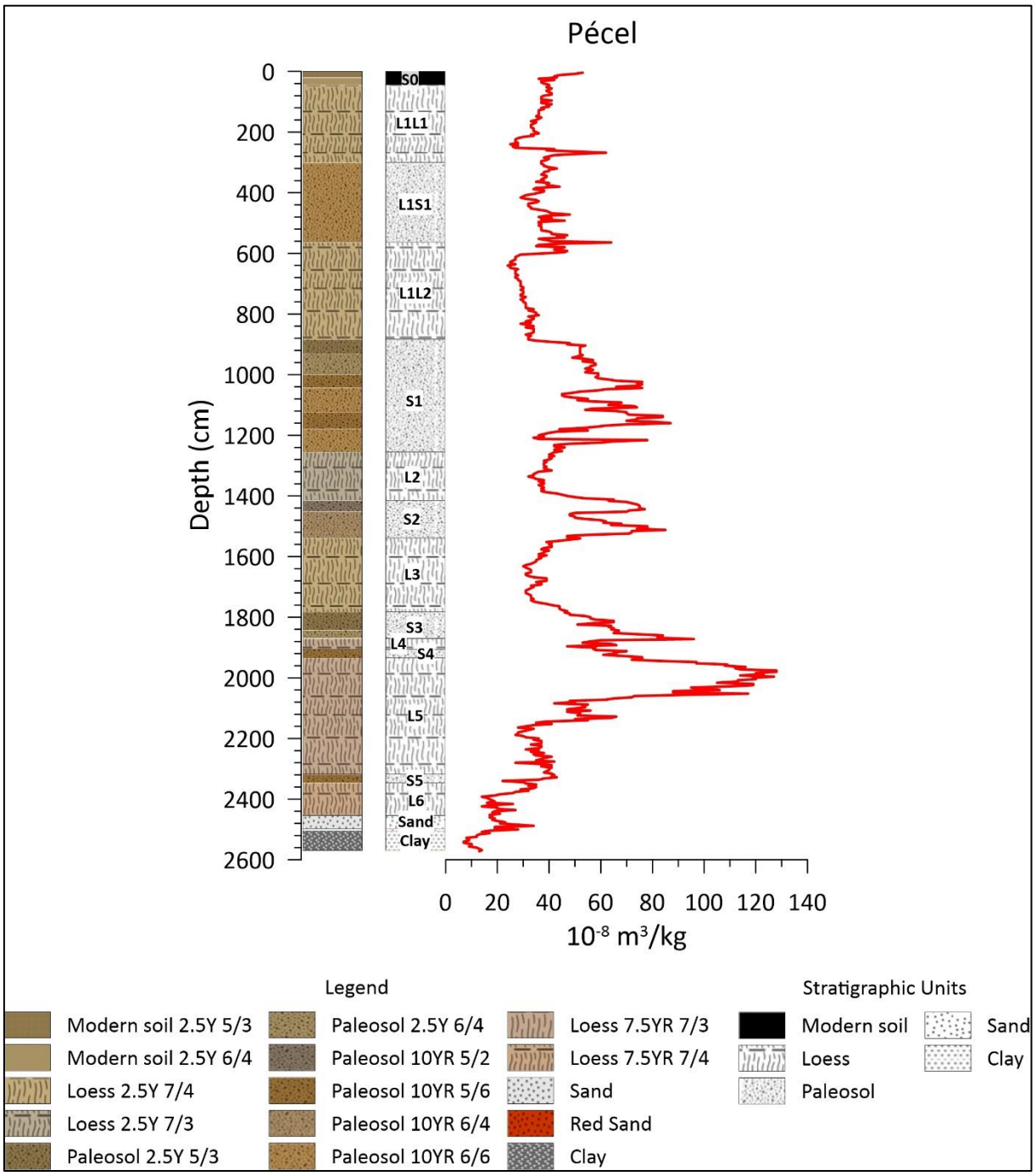

Fig. V. 3. Magnetic susceptibility results of the loess-paleosol profile of Pécel

V.3.3. Absolute dating, AR, MAR

Table V.1 shows the 20 measured age data, of which 17 were used for the modelling. Data not used are marked with underlining. The first one of these unused data originated from the recent soil, moreover 1-1 from the paleosol and the lower loess body. In these cases, the values of these outliers can be considered as measurement anomalies or the pollution of the samples.

Table V. 1. Radiocarbon ages from the Pécel sequence. The crossed ones was not used in the model

Lab code	Depth (cm)	Uncal. BP	σ	cal. BP	σ
~~DeA-34288~~	~~12-24~~	~~1381~~	~~21~~	~~1297~~	~~16~~
DeA-34278	108-120	18105	58	22062	159
DeA-34289	132-144	19698	63	23781	74
DeA-34279	264-276	20135	68	24119	235
DeA-34290	276-288	20361	69	24442	240
DeA-34280	300-312	20004	67	24022	184
DeA-34291	336-348	20556	66	24773	261
DeA-34281	360-372	20634	71	24862	244
DeA-34282	408-420	20775	72	25043	220
DeA-34292	432-444	20902	70	25183	188
DeA-34283	468-480	21113	70	25546	124
DeA-34293	480-492	20541	67	24751	256
~~DeA-34284~~	~~516-528~~	~~34640~~	~~206~~	~~39937~~	~~593~~
DeA-34294	540-552	21266	73	25568	245
DeA-34285	552-564	21008	73	25385	232
~~DeA-34295~~	~~576-588~~	~~20141~~	~~66~~	~~24126~~	~~233~~
DeA-34296	624-636	35214	214	40349	519
DeA-34286	648-660	38904	325	42607	277
DeA-34287	744-756	39385	334	42803	343
DeA-34297	756-768	38639	290	42508	248

The accumulation rate (Fig. V.4) for L1L2 (5.64-8.84 m) indicates a slow accumulation of 0.3-0.5 cm/year. In the case of the L1S1 (3.00-5.64 m) paleosol layer above it, these values are between 1.5-2.0 cm/year, however, soil development is the predominant process against the dust fall activity. Higher (around 1 cm/year) accumulation rates can be observed in the lower parts of the L1L1 (0.44-3.00 m) loess body, while it decreases to 0.2-0.3 cm/year towards to recent soil surface.

Since the MAR value aims to determine the falling dust, the section of the paleosol layer is covered with a grey rectangle. The average value of MAR within the L1L2 loess body (5.64-8.84 m) is 391, while in the L1L1 (0.44-3.00 m) is 1098. The latter average was increased by high values near the boundary of the loess and paleosol layers.

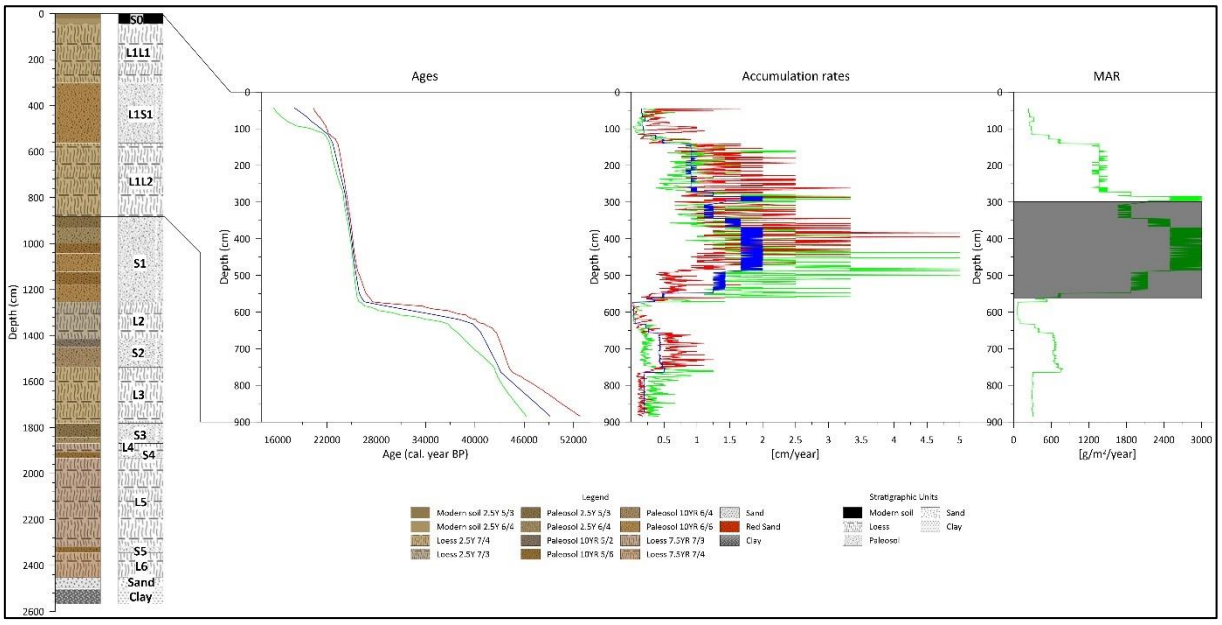

Fig. V. 4. Accumulation rate and MAR values of the Pécel sequence, highlighted the paleosol layer.

V.4. Discussion

The finer particle sizes dominate the L1L2 loess body (5.64-8.84 m) with an MGS value of 22.41. The MS values are relatively low in parallel with the fact that loess sediments generally can be characterized by low MS values. The average value is 31. Both the AR and MAR values are low, indicating a slow accumulation, with some smaller (although not so significant) outstanding values between 6.50-7.50 m.

The averages shift towards coarser grain size fractions in the L1S1 paleosol layer (3.00-5.64 m) with the appearance of fine sand with a maximum of 3%. Moreover, a significant change can also be observed between 3.92-4.56 m within this layer, where clay fraction decreases to 5% from 16% and the value of the MGS reaches 25.46. The MS values are relatively low here compared to a general paleosol layer. Although smaller and greater fluctuations can be observed, its average value is around 38. The high AR values indicate an accumulation rate of 1.5-2 cm/year, however, the soil development processes should be treated separately from dust fall processes. MAR results are not taken into account here, as their values provide information about the mass accumulation of falling dust.

The L1L1 (0.44-3.00 m) loess body is characterized by coarser grain sizes upwards and an MGS value of 29.01. Fine sand fraction can also be detected here, however, it is less significant, with a maximum value of 1.6%. MS values here show a steady increase towards the recent soil, although the mean value is low (due to the fact this is a loess sediment), and can

be characterized by a value of 36. AR and MAR values are continuously decreasing from the boundary of the loess and paleosol layer towards the recent soil.

V.5. Conclusion

The age of the entire profile can be dated back to the MIS9/10 (Makó et al., 2023) stages based on the comparison of the MS curves with the curves of the Chinese Loess Plateau and the Marine Isotope Stages (Ren et al., 2014; Fig. V.5). Based on the absolute ages it can be stated that the L1L1-L1S1-L1L2 loess layers assumed to be parallel with MIS 3-4 stages before, now can clearly be correlated with these levels. By extending the relative ages, considering the shape of the MS curves and the separation of the different layers, it can be concluded that the profile can be traced back to the MIS 12-14 stages (the first loess body above the fluvial sediment at the bottom). However, the MS curves clearly indicate that the L1S1 paleosol layer is a weakly developed or redeposited paleosol layer, which shows paleosol characteristics in its color and grain size distribution. The accumulation of the loess body was presumably interrupted by a stadial stage. The appearance of fine sand and the increasing AR and MAR values certainly indicate the increase in transport energy, moreover, make possible the determination of the prevailing wind direction. In addition to the recent research approaches carried out in this paper, OSL studies could clarify the actual age of the profile. Furthermore, this research could be supplemented with the study of the malacofauna, which could provide information on the decadal-centennial changes in the paleoenvironment in the Pécel area to provide additional information on the environmental changes of the Carpathian Basin in the past.

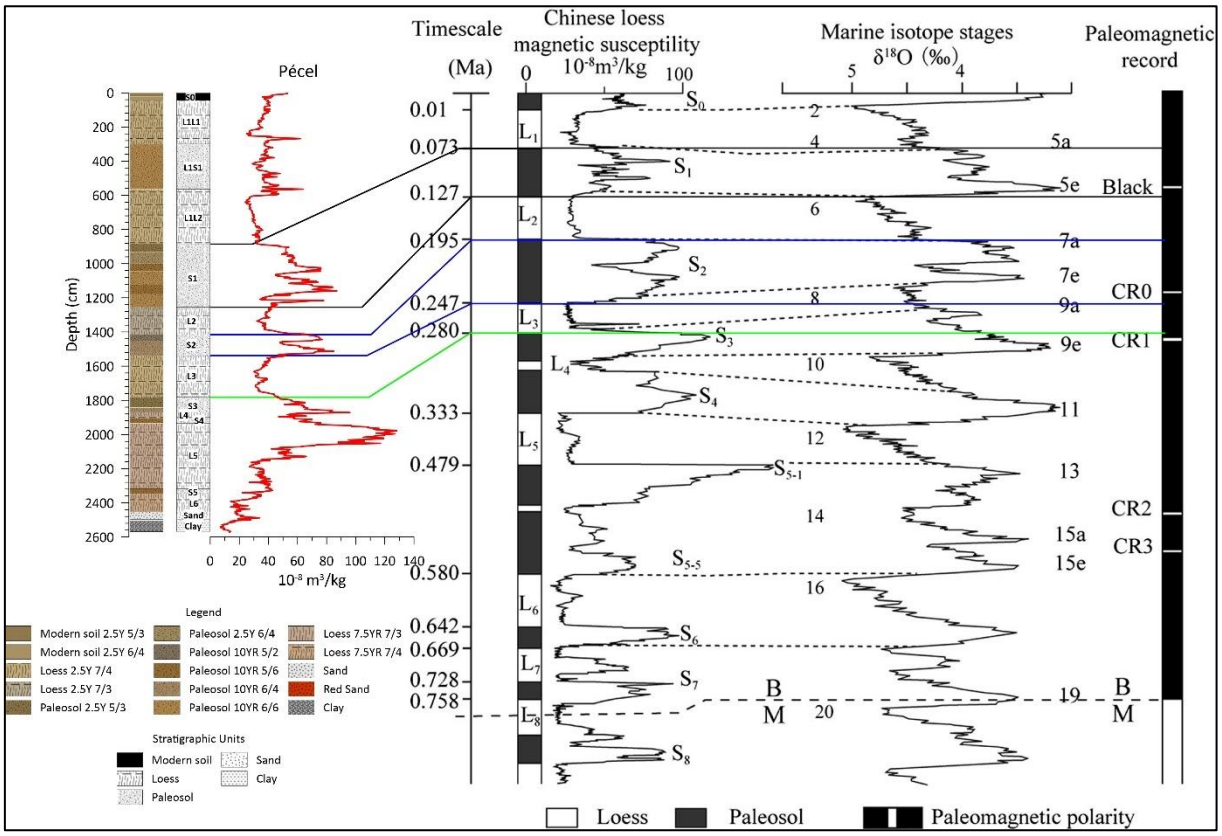

Fig. V. 5. Magnetic susceptibility results compared to the Chinese Loess Plateau data (Ren et al., 2014)

CHAPTER VI.

Conclusion

This study primarily focuses on the examination and research of the loess-paleosol sequence of Pécel. The first direction of the research was the comparison between different chronometric methods usability for age-depth models. This part was discussed in Chapter II. The results showed that in younger ages (between 0-70 ka.) the radiocarbon method is far more reliable with the lower uncertainty, because the more accurate the age, the more accurate the model. However, at older ages, the luminescence methods are also acceptable. In the case of large sequences, the two methods can be used together, with appropriate model parameters.

In addition to the Pécel sequence, three Transdanubian sequence were investigated also, for the reason that they provide a basis for comparison in the investigated parameters locally and regionally. It concluded in the 5 sequences, that there must be a change in the dominant wind direction, both the grain size composition results and the geochemical element changes in Pécel support this.

Bodrogkeresztúr

The loess-paleosol profile, developed at Bodrogkeresztúr (Bösken et al., 2019), is the result of the changes in the paleoenvironment at the foot of the Carpathians and allows us a better and more accurate understanding of the setting of the local Gravettian culture in the area. It deals with the analysis of the particle composition of the section, presents and compares the age models based on the OSL and radiocarbon derived from the radiocarbon results and accumulation rates of the section and the nearby Bodrogkeresztúr, brickyard 1. The Upper Tokaj Fossil Horizon appears both at Bodrogkeresztúr, brickyard 1, (30895±647 cal. BP) previously examined by Sümegi (2005) and at Henye Hill (30376±715; Sümegi et al., 2016) section – it contains Gravettian finds –, but not in the BKT profile. This deficiency, as well as the significant accumulation, the smaller average particle size, the almost complete absence of the sand fraction and the increased carbonate content of the whole segment, are the results of sedimentation processes, recarbonization and leaching. The proximity of the sections, the consistency of their composition, and the differences in dating make it possible to study the accuracy and efficiency of dating methods through age-depth models. The accumulation rate diagrams from the data of our models show that the OSL / IRSL correction methods are not suitable for constructing accurate Bayesian-type age-depth models because of their high uncertainty values. To get a better understanding of sediment accumulation, carbon isotopic

data would be needed to clarify issues arising from accumulation differences. As radiocarbon analyzes are no longer available at levels above 65,000 years (Stuiver et al., 1998a, b), it is necessary to use OSL assays at these levels for more accurate age determination (Újvári et al., 2014). However, our section is still at a chronological level measured by the radiocarbon dating method.

Pécel

The foothill/hill-situated loess-paleosol profile of Pécel is located in the Gödöllő Hills in the northern part of the Carpathian Basin. The preliminary sedimentological and geochemical investigations have shown that the profile merits conducting further research, as no significant erosion or intensive weathering could be detected. It carries a wealth of data, which can perfectly complement the results of the surrounding profiles investigated so far and could provide data for the study of the climate changes in the Quaternary. The origin of flying dust and the prevailing winds are also can be examined. The change at about 10 m is an evidence of the change of the source area of the accumulated dust. The seemingly opposite results within the L2 loess body may be explained by the further transport of finer fractions (and a sharp decrease in the proportion of clay) because of the increased transport energy and the deposition of larger particles. Similar fluctuations can be seen in the case of GSI in the L1S1 paleosol layer, where the geochemical indices also indicate soil development. Considering the entire profile, weathering horizons occur at the loess-paleosol transition zones. Besides, malacological examination of the remaining snail shells of the sediment will provide more accurate information about the paleoecological factors.

The development of the loess wall and the deposition of its sediments began with the southward movement of the stream. The variable sand content indicates a periodically increasing wind energy and velocity of which traces can be detected in the different layers deposited. However, only smaller periods of time can be characterized by this high wind velocity.

Ostracods were found in the clay sediment at the bottom of the section, suggesting an Upper Miocene age of the sediment. Based on the presence of this Upper Miocene stratum, the erosion of the lowermost part of the profile can be assumed and the deposition of the loess sediment began after the termination of the fluvial sediment.

The age of the entire profile can be dated back to the MIS9/10 (Makó et al., 2023) stages based on the comparison of the MS curves with the curves of the Chinese Loess Plateau and

the Marine Isotope Stages (Ren et al., 2014; Fig. V.5). Based on the absolute ages it can be stated that the L1L1-L1S1-L1L2 loess layers assumed to be parallel with MIS 3-4 stages before, now can clearly be correlated with these levels. By extending the relative ages, considering the shape of the MS curves and the separation of the different layers, it can be concluded that the profile can be traced back to the MIS 12-14 stages (the first loess body above the fluvial sediment at the bottom). However, the MS curves clearly indicate that the L1S1 paleosol layer is a weakly developed or redeposited paleosol layer, which shows paleosol characteristics in its color and grain size distribution. The accumulation of the loess body was presumably interrupted by a stadial stage. The appearance of fine sand and the increasing AR and MAR values certainly indicate the increase in transport energy, moreover, make possible the determination of the prevailing wind direction. In addition to the recent research approaches carried out in this paper, OSL studies could clarify the actual age of the profile. Furthermore, this research could be supplemented with the study of the malacofauna, which could provide information on the decadal-centennial changes in the paleoenvironment in the Pécel area to provide additional information on the environmental changes of the Carpathian Basin in the past.

Transdanubian sequences

In the case of the three Transdanubian profiles, significant differences can be observed compared to the Pécel one. The topography of the hill area in the surroundings of the examined profiles can be characterized by northwest–southeast-oriented hills. Based on the grain size analysis, very fine sand fraction can be detected in the lower loess body of Kisdorog-West and Kisdorog-East and in the upper loess body of the Bonyhádvarasd profiles. This suggests that the prevailing wind direction was north–northwest during the deposition of the lower layers and south–southeast during the deposition of the upper layers. The significant changes observed in the particle indices also support this assumption for the paleosol complexes. In addition, it can be concluded that the eastern-oriented profile includes less-developed paleosol horizons. In its case, only three sublayers could be distinguished and the MS values barely reached 80, while they increased to 150–160 in the cases of the other two profiles.

SUMMARY

The primary goal of this research was the complete investigation of the loess-paleosol sequence of Pécel, located in the Gödöllő hills. During several sampling sessions, a 25.72-meter-high section was constructed, the upper 24.56 meters of which is a series of loess-paleosols, 0.51 meters of fluvial sand sediments are located below it, and the lower 0.65 meters, the Ostracoda fauna found in it based on, clay sediment of Pannonian age. During the investigations, 6 loess and 5 paleosol layers were isolated. From the layer thicknesses of the sand sediment, we can conclude that it may be the sediment of the former bed of the Rákos stream, which flows a few hundred meters from the section.

The entire research covers the examination of 5 loess-paleosol sequences, with different locations: foothill (Bodrogkeresztúr, Pécel) and lowland (Kisdorog-kelet, Kisdorog-west, Bonyhádvarasd). With the exception of the Bodrogkeresztúr section, all the other newly excavated sections, whose results are compared with each other, contain a lot of information.

The primary investigations were the determination of the organic matter and carbonate content based on mass loss on ignition (LOI - Dean, 1974), as well as the grain composition. After the accurate separation of the loess and paleosol layers on the basis of the field description and the above results, the composition and degree of weathering of the dust sediment that forms the material of the section was determined with geochemical (XRF) results and the geochemical indices obtained from them. In the following, a relative age to the profile with a magnetic susceptibility (MS) test, and an absolute age with 20 radiocarbon ages were assigned. Using the radiocarbon data, an age-depth model was created, from which the rate of sediment accumulation was calculated, in order to reveal the intensity of the fall of dust. The oldest available age from a depth of 7.56-7.68 meters is 42508 cal. BP, which, when compared with the relative age data, supports the assumed age of the section to be 300-400,000 years old, so the accumulation on the fluvial sediments began at the MIS 9/10 level.

The usability of age data for age-depth models was discussed in the publication in Chapter II. on the Bodrogkeresztúr section, where radiocarbon and optically stimulated luminescence (OSL) data from a section were also available. The results show that, due to their small uncertainty, radiocarbon age data produce more reliable models compared to the results obtained from luminescence tests. However, the measurement limit of the radiocarbon test is low (0-70 thousand years), so it can only be used uniformly in very young layers or in archaeological research. In the case of large, older sections, the mixed use of dating methods is

unavoidable, however, when creating age-depth models, it is important to accurately determine the input parameters.

In addition to Péceli, 3 Transdanubian sections were formed, Kisdorog-East (6.40 meters), Kisdorog-West (5.60 meters) and Bonyhádvarasd (8.16 meters). All three sections are in plain locations and are located in the Tolna Hill area. The Kisdorog sections are located 500 meters apart, on the east and west sides of a hill. This double sampling enabled a local and regional comparison of the development of the loess-paleosol profiles. In the case of both sections, only one, however, very developed paleosol layer was excavated. The Bonyhádvarasd section, located 4 km from Kisdorog, has a southern position and also has a well-developed paleosol layer.

From the grain size composition results of the three southern (Bodrogkeresztúr, Pécel, Bonyhádvarasd), one eastern (Kisdorog-East) and one western (Kisdorog-West) sections, a dominant wind direction change (North-Northwest - South-Southeast change) emerges. The change in the prevailing dust load is also supported by the geochemical results in Pécel, where a change in element content can be seen at a depth of 10 meters.

The processing of the Mollusca fauna extracted from the sections will give a more accurate picture in the future, both in terms of climatic and vegetation changes.

ÖSSZEGZÉS

Kutatásom elsődleges célja a Gödöllői-dombság területén elhelyezkedő péceli lösz-paleotalaj szelvény teljes megkutatása volt. Több mintázási alkalom során egy 25,72 méter magas szelvény került kiakalításra, melynek a fölső 24,56 métere egy lösz-paleotalaj sorozat, alatta 0,51 méternyi folyóvízi homoküledék helyezkedik el, az alsó 0,65 méter pedig, a benne talált Ostracoda fauna alapján, Pannon korú agyagüledék. A vizsgálatok során 6 lösz és 5 paleotalaj réteg került elkülönítésre. A homoküledék rétegvastagságaiból arra következtethetünk, hogy az a szelvénytől párszáz méterre folyó Rákos patak egykori medrének üledéke lehet.

A teljes kutatás 5 lösz-paleotalaj szelvény vizsgálatát fedi le, különböző, hegylábi (Bodrogkeresztúr, Pécel), valamint síksági (Kisdorog-kelet, Kisdorog-nyugat, Bonyhádvarasd) fekvéssel. A bodrogkeresztúri szelvény kivételével az összes többi újonnan feltárt szelvény, melyek eredményeinek egymással való összehasonlítása számos információt hordoz magában.

Az elsődleges vizsgálatok az izzításos tömegveszteségen alapuló szervesanyag-, és karbonáttartalom (LOI - Dean, 1974), valamint a szemcseösszetétel meghatározás voltak. Miután a terepi leírás és a fenti eredmények alapján pontosan elkülönítettem a lösz és paleotalaj rétegeket, geokémiai (XRF) eredményekkel és az azokból nyert geokémiai indexekkel a szelvény anyagát adó porüledék összetételét és mállottsági foka került meghatározásra. A továbbiakban mágneses szuszceptibilitás (MS) vizsgálattal relatív-, 20 radiokarbon koradattal pedig abszolút kort rendeltem a szelvényhez. A radiokarbon adatok felhasználásával kor-mélység modell készült, melyből üledékfelhalmozódási ráta került számításra, a poranyag hullás intenzitásának feltárása érdekében. A legidősebb rendelkezésre álló koradat 7.56-7.68 méter mélységből 42.508 cal. BP, mely a relatív koradatokkal összevetve alátámasztja a szelvény feltételezhető 300-400.000 éves korát, tehát MIS 9/10 szintben kezdődött meg a felhalmozódás a folyóvízi üledékre.

A kor-mélység modellekhez a koradatok felhasználhatóságát a 2. fejezetben található publikációban dolgoztam fel a bodrogkeresztúri szelvényen, ahol rendelkezésre állt egy szelvényből radiokarbon és optikailag stimulált lumineszcens (OSL) adat is. Az eredményekből kirajzolódik, hogy a radiokarbon koradatok a kis bizonytalanságuk miatt megbízhatóbb modelleket produkálnak a lumineszcens vizsgálatokból nyert eredményekkel szemben. A radiokarbon vizsgálat mérési határa azonban alacsony (0-70 ezer év), így csak nagyon fiatal rétegekben, vagy régészeti kutatásokban használható egyöntetűen. Nagy kiterjedésű, idősebb

szelvények esetében a korolási módszerek vegyes használata elkerülhetetlen, azonban a kormélység modellek készítsekor a bevitt paraméterek pontos meghatározása fontos.

A péceli mellett 3 dunántúli szelvény került kialakításra, Kisdorog-kelet (6,40 méter), Kisdorog-nyugat (5,60 méter) és Bonyhádvarasd (8,16 méter). Mindhárom szelvény síksági helyzetű, a Tolnai-dombvidék területén helyezkedik el. A kisdorogi szelvények egymástól 500 méterre helyezkednek el, egy domb keleti, valamint nyugati oldalán. Ez a kettős mintázás lehetővé tette a lösz-paleotalaj szelvények fejlődésének lokális és regionális összehasonlítását. Mindkét szelvény esetében csupán egy, azonban nagyon fejlett paleotalaj réteg került feltárásra. A bonyhádvarasdi, egy Kisdorogtól 4 km-re elhelyezkedő, déli fekvésű, szintén jól fejlett paleotalaj réteggel rendelkező szelvény.

A három déli (Bodrogkeresztúr, Pécel, Bonyhádvarasd), egy keleti (Kisdorog-kelet) és egy nyugati (Kisdorog-nyugat) szelvények szemcseösszetételi eredményeiből kirajzolódik egy uralkodó szélirány változás (Észak-Északnyugati - Dél-Délkeleti változás). Az uralkodó porhordás változását a péceli geokémiai eredmények is alátámasztják, ahol 10 méteres mélységben elemtartalom változás rajzolódik ki.

A szelvényekből kinyert Mollusca fauna feldolgozása a jövőben pontosabb képet fog adni, mind a klimatikus, mind a vegetációs változások tekintében.

ACKNOWLEDGEMENTS

First, I am very grateful to my supervisor, ***Dr. Dávid Molnár***, who had supported me during my university years. His guidance and reminders of deadlines were always there for me when I got stuck.

I am also grateful to my colleagues, ***Péter Cseh***, ***Balázs Nagy***, ***Balázs Turuczki***, ***Gábor Gubucz***, ***Kata Csányi***, ***Ágoston Brüggeman*** and ***Gábor Radnai***, who helped me during the fieldworks.

I would like to thank to ***Gedeon Rajcsinec***, who is the owner of the Pécel site, to let the teams work in his "garden" and for being very helpful to us. Special thanks to the ***Illés Vinery***, to my friends, ***Bettina Barna-Illés*** and ***János Barna*** and also to ***Pál Illés*** to the accommodation, food and the tasty wines during the samplings.

I would also thanks to all my colleagues in the Department of Geology and Paleontology, ***Réka Benyó-Korcsmáros***, ***Péter Cseh***, ***Balázs Nagy***, ***Zoltán Patocskai*** and ***Máté Petróczy***, who were my second family over these years.

Naturally, I am very grateful to my family, who supported me from the beginning and never stopped to ask "when will it be ready?".

Last, but not least, I would like to thank to my love ***Nóra Pintér***, who supported me and helped a lot during my works. Thank you very much for your patience when anything else was more important than this progress.

REFERENCES

An, Z.; Kukla, G.J.; Porter, S.C.; Xiao, J. 1991. Magnetic Susceptibility Evidence of Monsoon Variation on the Loess Plateau of Central China during the last 130,000 Years. Quaternary Research, 36, pp. 29–36.

Antoine, P.; Rousseau, D.-D.; Zöller, L.; Lang, A.; Munaut, A.-V.; Hatté, C.; Fontugne, M. 2001. High-resolution record of the last Interglacial-glacial cycle in the Nussloch loess-palaeosol sequences, Upper Rhine Area, Germany. Quaternary International, 76–77, pp. 211–229.

Bennett, K.D. 1994. Confidence intervals for age estimates and deposition times in late-Quaternary sediment sequences. The Holocene 4, pp. 337-348.

Blaauw, M.; Christen, A.J. 2011. Flexible paleoclimate age-depth models using an autoregressive gamma process. Bayesian Analysis 6(3), pp. 457-474.

Bohn, H.L.; McNeal, B.L.; O'Connor, G.A. 1985. Talajkémia, Mezőgazdasági Kiadó – Gondolat Kiadó, Budapest, 363 p.

Bokhorst, M.P.; Vandenberghe, J.; Sümegi, P.; Łanczont, M.; Gerasimeno, N.P.; Matviishina, Z.N.; Marković, S.B.; Frechen, M. 2011. Atmospheric circulation patterns in central and eastern Europe during the Weichselian Pleniglacial inferred from loess grain-size records, Quarternary International 234, pp. 62-74.

Bokhorst, M.P.; Beets, C.J.; Marković, S.B.; Gerasimenko, N.P.; Matviishina, Z.N.; Frenchen, M. 2009. Pedo-chemical climate proxies in Late Pleistocene Serbian-Ukrainian loess sequences. Quaternary International, 198, pp. 113–123.

Bösken, J.; Obreht, I.; Zeeden, C.; Klasen, N.; Hambach, U.; Sümegi, P.; Lehmkuhl, F. 2019. High-resolution paleoclimatic proxy data from the MIS3/2 transition recorded in northeastern Hungarian loess, Quaternary International 502, pp. 95-107.

Bösken, J.; Sümegi, P.; Zeeden, C.; Klasen, N.; Gulyás, S.; Lehmkuhl, F. 2018. Investigating the last glacial Gravettian site 'Ságvár Lyukas Hill' (Hungary) and its paleoenvironmental and geochronological context using a multi-proxy approach. Palaeogeography, Palaeoclimatology, Palaeoecology, 509, pp. 77–90.

Bronk Ramsey, C.; Lee, S. 2013. Recent and Planned Developments of the Program OxCal. Radiocarbon, 55(2-3), pp. 720-730.

Buggle, B.; Glaser, B.; Hambach, U.; Gerasimenko, N.; Marković, S.B. 2011. An evaluation of geochemical weathering indices in loess-paleosol studies. Quaternary International, 240, pp. 12–21.

Buggle, B.; Glaser, B.; Zöller, L.; Hambach, U.; Marković, S.B.; Glaser, I.; Gerasimenko, N. 2008. Geochemical characterization and origin of Southeastern and Eastern European loesses (Serbia, Romania, Ukraine). Quaternary Science Reviews, 27, pp. 1058–1075.

Chen, J.; An, Z.; Head, J. 1999. Variation of Rb/Sr Ratios in the Loess-Paleosol Sequences of Central China during the Last 130,000 Years and Their Implications for Monsoon Paleoclimatology. Quaternary Research, 51, pp. 215–219.

Chen, J.; Chen, Y.; Liu, L.; Ji, J.; Balsam, W.; Sun, Y.; Lu, H. 2006. Zr/Rb ratio in the Chinese loess sequences and its implication for changes in the East Asian winter monsoon strength. Geochimica et Cosmochimica Acta, 70, pp. 1471–1482.

Cohen, K.; Gibbard, P. 2019. Global chronostratigraphical correlation table for the last 2.7 million years, version 2019 QI-500. Quaternary International, 500, pp. 20–31.

Dean, W.E. 1974. Determination of carbonate and organic matter in calcareous sediments and sedimentary rocks by loss on ignition: comparison with other methods, Journal of Sedimentary Petrology, 44, pp. 242-248.

Dearing, J.A.; Hay, K.L.; Baban, S.M.J.; Huddleston, A.S.; Wellington, E.M.H.; Loveland, P.J. 1996. Magnetic susceptibility of soil: An evaluation of conflicting theories using a national data set. Geophysical Journal International, 127, pp. 728–734.

Ding, Z.; Derbyshire, E.; Yang, S.; Sun, J.; Liu, T. 2005. Stepwise expansion of desert environment across northern China in the past 3.5 Ma and implications for monsoon evolution. Earth Planetary Science Letters, 237, pp. 45–55.

Ding, Z.L.; Sun, J.M.; Yang, S.L.; Liu, T.S. 2001. Geochemistry of the Pliocene red clay formation in the Chinese Loess Plateau and implications for its origin, source provenance and paleoclimate change, Acta Geochimica et Cosmochimica 65, pp. 901-913.

Dokuchaev, V.V. 1879. Chernozem (black earth) of European Russia, Societé Imperiale Libre Économique Trenke & Fusnot, St. Petersburg, p. 66.

Dövényi, Z. 2010. Cserhát-Vidék in Magyarország Kistájainak Katasztere, 2nd ed.; MTA Földrajztudományi Kutatóintézet, Budapest, Hungary, pp. 705–708.

Dövényi, Z. 2010. Mecsek és Tolna-Baranyai-Dombvidék in Magyarország Kistájainak Katasztere, 2nd ed.; MTA Földrajztudományi Kutatóintézet, Budapest, Hungary, pp. 500–503.

Gallet, S.; Jahn, B.-M.; Lanoë, B.V.V.; Dia, A.; Rossello, E. 1998. Loess geochemistry and its implications for particle origin and composition of the upper continental crust. Earth Planetary Science Letters, 156, pp. 157–172.

Gallet, S.; Jahn, B.; Torii, M. 1996. Geochemical characterization of the Louchan loess-paleosol sequence, China and paleoclimatic implications. Chemical Geology, 133, pp. 67-88.

Galović, L.; Frechen, M.; Halamić, J.; Durn, G.; Romić, M. 2009. Loess chronostratigraphy in Eastern Croatia—A luminescence dating approach. Quaternary International, 198, pp. 85–97.

Google Maps. Available online: https://goo.gl/maps/n5twBG8njBKdCgSR9. (accessed on 15 May 2021)

Gyalog, L.; Síkhegyi, F. 2005. Magyarország földtani térképe, M=1:100 000. A Magyar Állami Földtani Intézet kiadványa: Budapest, Hungary.

Harnois, L. 1988. The CIW index: A new chemical index of weathering. Sedimentary Geology, 55, pp. 319–322.

Heiri, O.; Lotter, A.F.; Lemcke, G. 2001. Loss on ignition as a method for estimating organic and carbonate content in sediments: Reproducibility and comparability of results. Journal of Paleolimnology, 25, pp. 101–110.

Hlavatskyi, D.; Bakhmutov, V. 2021. Early-Middle Pleistocene Magnetostratigraphic and Rock Magnetic Records of the Dolynske Section (Lower Danube, Ukraine) and Their Applications to the Correlation of Loess-Palaeosol Sequences in Eastern and South-Eastern Europe. Quaternary, 4, 43.

Huntley, D.J.; Godfrey-Smith, D.I.; Thewalt, M.L.W. 1985. Optical dating of sediments. Nature 313 (5998), pp. 105-107.

Hupuczi, J.; Sümegi, P. 2010. The late pleistocene paleoenvironment and paleoclimate of the madaras section (South Hungary), based on preliminary records from mollusks. Open Geosciences, 2, pp. 64–70.

Jahn, B.-M.; Gallet, S.; Han, J. 2001. Geochemistry of the Xining, Xifeng and Jixian sections, Loess Plateau of China: Eolian dust provenance and paleosol evolution during the last 140 ka. Chemical Geology, 178, pp. 71–94.

Jary, Z. 2009. Periglacial markers within the Late Pleistocene loess–palaeosol sequences in Poland and Western Ukraine. Quaternary International, 198, pp. 124–135.

Jary, Z.; Ciszek, D. 2013. Late Pleistocene loess–palaeosol sequences in Poland and western Ukraine. Quaternary International, 296, pp. 37–50.

Jeong, G.Y.; Hillier, S.; Kemp, R.A. 2011. Changes in mineralogy of loess–paleosol sections across the Chinese Loess Plateau. Quaternary Research, 75, pp. 245–255.

Jeong, G.Y.; Hillier, S.; Kemp, R.A. 2008. Quantitive bulk and single particle mineralogy of a thick Chinese loess-plaeosol section: implications for loess provenance and weathering. Quaternary Science Reviews, 27, pp. 1271–1287.

Kohfeld, K.E.; Harrison, S.P. 2001. DIRTMAP: the geological record of dust. Earth-Science Reviews, 54, pp. 81-114.

Koloszár, L.; Marsi, I. 2010. The thickest and the most complete loess sequence in the Carpathian Basin: The section of the borehole Udvari-2A and its significance in the Quaternary stratigraphy (in Hungarian). Földtani Közlöny, 140, pp. 251–262.

Krasilnikov, P.; García Calderón, N.E. 2006. A WRB-based buried paleosol classification. Quaternary International, pp. 156–157, 176–188.

Kraus, M.J. 1999. Paleosols in clastic sedimentary rocks: Their geologic applications. Earth-Science Reviews, 47, pp. 41–70.

Krolopp, E. 1991. Malacological analysis of the loess from the archaeological site at Esztergom-Gyurgyalag. Acta Archaeologica, 43, pp. 257–259.

Krolopp, E.; Sümegi, P. 1995. Palaeoecological Reconstruction of the Late Pleistocene, Based on Loess Malacofauna in Hungary. GeoJournal 36 (2-3), pp. 213-222.

Kukla, G. 1987. Loess stratigraphy in central China. Quaternary Science Reviews, 6, pp. 191–219.

Kukla, G. 1977. Pleistocene land-sea correlations. Earth-Science Reviews, 13, pp. 307–374.

Kukla, G.; An, Z. 1989. Loess stratigraphy in Central China. Palaeogeography, Palaeoclimatology, Palaeoecology, 72, pp. 203–225.

Kukla, G.; An, Z.S.; Melice, J.L.; Gavin, J.; Xiao, J.L. 1990. Magnetic susceptibility record of Chinese Loess. Transactions of the Royal Society of Edinburgh: Earth Sciences 81, pp. 263-288.

Liang, L.; Sun, Y.; Beets, C.J.; Prins, M.; Wu, F.; Vandenberghe, J. 2013. Impacts of grain size sorting and chemical weathering on the geochemistry of Jingyuan loess in the northwestern Chinese Loess Plateau. J. Asian Earth Sciences, 69, pp. 177–184.

Liu, C.-Q.; Masuda, A.; Okada, A.; Yabuki, S.; Zhang, J.; Fan, Z.-L. A geochemical study of loess and desert sand in northern China: Implications for continental crust weathering and composition. Chem. Geol. 1993, 106, pp. 359–374.

Makó, L.; Molnár, D.; Cseh, P.; Nagy, B.; Sümegi, P. 2023. Development history of the loess-paleosol profiles of Pécel, Kisdorog and Bonyhádvarasd, Hungary. Quaternary, 6(3), 38.

Makó, L.; Molnár, D.; Cseh, P.; Sümegi, P. 2021. MAR comparisons between different chronometric methods for two profiles in the Bodrogkeresztúr area. Studia Quaternaria, 38, pp. 67–73.

Makó, L.; Molnár, D.; Runa, B.; Bozsó, G.; Cseh, P.; Nagy, B.; Sümegi, P. 2021. Selected Grain-Size and Geochemical Analyses of the Loess-Paleosol Sequence of Pécel (Northern Hungary): An Attempt to Determine Sediment Accumulation Conditions and the Source Area Location. Quaternary, 4(2), 17.

Marković, S.B.; Bokhorst, M.P.; Vandenberghe, J.; McCoy, W.D.; Oches, E.A.; Hambach, U.; Gaudenyi, T.; Jovanović, M.; Zöller, L.; Stevens, T.; Machalett, B. 2008. Late Pleistocene loess-palaeosol sequences in the Vojvodina region, north Serbia. Journal of Quaternary Science, 23, pp. 73–84.

Marković, S.B.; Stevens, T.; Kukla, G.J.; Hambach, U.; Fitzsimmons, K.E.; Gibbard, P.; Buggle, B.; Zech, M.; Guo, Z.; Hao, Q.; Wu, H.; O'Hara-Dhand, K.; Smalley, I.J.; Újvári, G.; Sümegi, P.; Timar-Gabor, A.; Veres, D.; Sirocko, F.; Vasilijević, D.A.; Jary, Z.; Scensson, A.; Jović, V.; Lehmkuhl, F.; Kovács, J.; Svirčev, Z. 2015. Danube loess stratigraphy—Towards a pand-European loess stratigraphic model. Earth-Science Reviews, 148, pp. 228–258.

Marković, S.B.; Stevens, T.; mason, J.; Vandenberghe, J.; Yang, S.; Veres, D.; Újvári, G.; Timar-Gabor, A.; Zeeden, C.; Guo, Z.; Hao, Q.; Obreht, I.; Hambach, U.; Wu, H.; Gavrilov, M.B.; Rolf, C.; Tomić, N.; Lehmkuhl, F. Loess correlations – Between myth and reality. Palaeography, Palaeoclimatology, Palaeoecology 509, pp. 4-23.

Marosi, S.; Somogy, S. 1990. Gödöllői-dombság. In Magyarország Kistájainak Katasztere II Földrajztudományi Kutató Intézet: Budapest, Hungary; pp. 802–807.

Moine, O.; Rousseau, D.-D.; Antoine, P. 2008. The impact of Dansgaard–Oeschger cycles on the loessic environment and mal-acofauna of Nussloch (Germany) during the Upper Weichselian. Quaternary Research, 70, pp. 91–104.

Molnár D. 2015. Dél-dunántúli és kelet-horvátországi lösz-paleotalaj szelvények paleoökológiai rekonstrukciója malakológiai és üledéktani adatok segítségével. Doktori disszertáció, Földtudományok Doktori Iskola, Szeged.

Molnár D.; Sümegi P. 2016. Dél-dunántúli és kelet-horvátországi lösz-paleotalaj szelvények paleoökológiai rekonstrukciója malakológiai és üledéktani adatok segítségével, In: Unger J., Pál-Molnár E. (Eds.): Geoszférák 2015, GeoLitera, Szeged, pp. 185-209.

Molnár, D.; Hupuczi, J.; Galović, L.; Sümegi, P. 2010. Preliminary malacological investigation on the loess profile at Zmajevac, Cro-atia. Open Geosciences, 2, pp. 52–56.

Molnár, D.; Makó, L.; Cseh, P.; Sümegi, P.; Fekete, I.; Galović, L. 2021. Middle and Late Pleistocene loess-palaeosol archives in East Croatia: Multi-proxy palaeoecological studies on Zmajevac and Šarengrad II sequences. Studia Quaternaria, 38, pp. 3–17.

Molnár, D.; Makó, L.; Sümegi, P.; Sümegi, B.P.; Törőcsik, T. 2019. Revisiting the palaeolithic site at Szeged-Öthalom: Attempt for appoint the palaeolithic horizon. Studia Quaternaria, 36, pp. 45–53.

Molnár, D.; Sümegi, P.; Fekete, I.; Makó, L.; Sümegi, B.P. 2019. Radiocarbon dated malacological records of two Late Pleistocene loess-paleosol sequences from SW-Hungary: Paleoecological inferences. Quaternary International, 504, pp. 108–117.

Molnár, D.; Sümegi, P.; Makó, L.; Cseh, P.; Zeeden, C.; Nett, J.; Lehmkuhl, F.; Törőcsik, T.; Sümegi, B.P. 2021. Palaeoecological background of the Upper Palaeolithic site of Ságvár, Hungary: Radiocarbon-dated malacological and sedimentological studies on the Late Pleistocene environment. Journal of Quaternary Sciences, 36, pp. 1353–1363.

Molnár, M.; Janovics, R.; Major, I.; Orsovszki, J.; Gönczi, R.; Veres, M.; Leonard, A.G.; Castle, S.M.; Lange, T.E.; Wacker, L.; Hajdas, I.; Jull, A.J.T. 2013. Status report of the new AMS C-14 preparation lab of the Hertelendi Laboratory of Environmental Studies, Debrecen. Hungary. Radiocarbon 55 (2-3), pp. 665-676.

Molnár, M.; Rinyu, L.; Veres, M.; Seiler, M.; Wacker, L.; Synal, H.A. 2013. EnvironMICADAS: a mini 14C AMS with enhanced Gas Ion Source Interface in the Hertelendi Laboratory of Environmental Studies (HEKAL), Hungary. Radiocarbon 55 (2-3), pp. 338-344.

Muhs, D.R.; Bettis, E.A.; Been, J.; McGeehin, J.P. 2001. Impact of climate and parent material on chemical weathering in loess-derived soils of the Mississippi River valley. Soil Science Society of America Journal, 65, pp. 1761–1777.

Munsell Color (Firm). Munsell Soil Color Charts: With Genuine Munsell Color Chips. Munsell Color: Grand Rapids, MI, USA, 2010.

Nesbitt, H.; Markovics, G.; Price, R. 1980. Chemical processes affecting alkalis and alkaline earths during continental weathering. Geochimica et Cosmochimica Acta, 44, pp. 1659–1666.

Nesbitt, H.W.; Young, G.M. 1982. Early Proterozoic climates and plate motions inferred from major element chemistry of lutites. Nature, 299, pp. 715–717.

Nettleton, W.D.; Brasher, B.R.; Benham, E.C.; Ahrens, R.J. 1998. A classification system for buried paleosols. Quaternary International, 51–52, pp. 175–183.

Nugteren, G.; Vandenberghe, J.; van Huissteden, K.; An, Z.S. 2004. A Quaternary climate record based on grain size analysis from the Luochuan loess section on the Central Loess Plateau, China. Global and Planetary Change, 41, pp. 167–183.

Pécsi M. 1993. Negyedkor és löszkutatás. Akadémia kiadó, Budapest, 375 p.

Pye, K., 1995. The nature, origin and accumulation of loess, Quaternary Science Reviews 14, pp. 653-667.

Railsback, L.B. 2003. An earth scientist's periodic table of the elements and their ions. Geology, 31, pp. 737–740.

Reeder, S.; Taylor, H.; Shaw, R.A.; Demetriades, A. 2006. Introduction to the Chemistry and Geochemistry of the Elements. In: Geochemical Atlas of Europe. Part 2. Interpretation of Geochemical Maps, Additional Tables, Figures, Maps, and Related Publications.; Tarvainen, T., de Vos, M. Eds.; Geological Survey of Finland: Espoo, Finland, pp. 48–429.

Reimer, P.J.; Austin, W.E.N.; Bard, E.; Bayliss, A.; Blackwell, P.G.; Bronk Ramsey, C.; Butzin, M.; Cheng, H.; Edwards, R.L.; Friedrich, M.; Grootes, P.M.; Guilderson, T.P.; Hajdas, I.; Heaton, T.J.; Hogg, A.G.; Hughen, K.A.; Kromer, B.; Manning, S.W.; Muscheler, R.; Palmer, J.G.; Pearson, C.; van der Plicht, J.; Reimer, R.W.; Richards, D.A.; Scott, E.M.; Southon, J.R.; Turney, C.S.M.; Wacker, L.; Adolphi, F.; Büntgen, U.; Capano, M.; Fahrni, S.M.; Fogtmann-Schulz, A.; Friedrich, R.; Köhler, P.; Kudsk, S.; Miyake, F.; Olsen, J.; Reinig, F.; Sakamoto, M.; Sookdeo, A.; Talamo, S. 2020. The IntCal20 Northern Hemisphere Radiocarbon Age Calibration Curve (0-55 cal kBP). Radiocarbon 62 (4), pp. 725-757.

Ren, J.; Zhang, S.; Meigs, A.J.; Yeats, R.S.; Ding, R.; Shen, X. 2014. Tectonic controls for transverse drainage and timing of the Xin-Ding paleolake breach in the upper reach of the Hutuo River, north China. Geomorphology, 206, pp. 452–467.

Rhodes, E.J. 2011. Optically stimulated luminescence dating of sediments over the past 250,000 years". Annual Review of Earth and Planetary Sciences 39, pp. 461–488.

Rousseau, D.; Antoine, P.; Hatté, C.; Lang, A.; Zöller, L.; Fontugne, M.; Othman, D.; Luck, J.; Moine, O.; Labonne, M.; Bentaleb, I.; Jolly, D. 2002. Abrupt millennial climatic changes from Nussloch (Germany) Upper Weichselian eolian records during the Last Glaciation. Quaternary Science Reviews, 21, pp. 1577–1582.

Rousseau, D.-D. 1990. Statistical analyses of loess molluscs for paleoecological reconstructions. Quaternary International, 7–8, pp. 81–89.

Rousseau, D.D.; Kukla, G. 1994. Late Pleistocene Climate Record in the Eustis Loess Section, Nebraska, Based on Land Snail As-semblages and Magnetic Susceptibility. Quaternary Research, 42, pp. 176–187.

Rousseau, D.-D.; Sima, A.; Antoine, P.; Hatté, C.; Lang, A.; Zöller, L. 2007. Link between European and North Atlantic abrupt climate changes over the last glaciation. Geophysical Research Letters, 34, 22713.

Ruszkiczay-Rüdiger, Z.; Fodor, L.; Horváth, E.; Telbisz, T. 2007. Folyóvízi, eolikus és neotektonikai hatások szerepe a Gödöllői-dombság felszínfejlődésében – DEM-alapú morfometriai vizsgálat. Földrajzi Közlemények, 131, pp. 319–342.

Schatz, A.-K.; Buylaert, J.-P.; Murray, A.; Stevens, T.; Scholten, T. 2012. Establishing a luminescence chronology for a palaeosol-loess profile at Tokaj (Hungary): A comparison of quartz OSL and polymineral IRSL signals. Quaternary Geochronology 10, pp. 68–74.

Schatz, A.-K.; Scholten, T.; Kühn, P. 2015. Paleoclimate and weathering of the Tokaj (Hungary) loess–paleosol sequence. Palaeogeography, Palaeoclimatology, Palaeoecology 426, pp. 170–182.

Schatz, A.-K.; Zech, M.; Buggle, B.; Gulyás, S.; Hambach, U.; Marković, S.B.; Sümegi, P.; Scholten, T. 2011. The late Quaternary loess record of Tokaj, Hungary: Reconstructing

palaeoenvironment, vegetation and climate using stable C and N isotopes and biomarkers. Quaternary International 240, pp. 52-61.

Schellenberger, A.; Veit, H. 2006. Pedostratigraphy and pedological and geochemical characterization of Las Carreras Loess-paleosol sequence, Valle de Tafi, NW-Argentina. Quaternary Science Reviews, 25, pp. 811–831.

Song, Y.; Guo, Z.; Marković, S.B.; Hambach, U.; Deng, C.; Chang, L.; Wu, J.; Hao, Q. 2018. Magnetic stratigraphy of the Danube loess: A composite Titel-Stari Slankamen loess section over the last one million years in Vojvodina, Serbia. J. Asian Earth Sciences, 155, pp. 68–80.

Stuiver, M.; Reimer, P.J.; Bard, E.; Beck, J.W.; Burr, G.S.; Hughen, K.A.; Kromer, B.; McCormac, F.G.; Van Der Plicht, J.; Spurk, M. 1998. INTCAL98 Radiocarbon age calibration 24,000 - 0 cal BP. Radiocarbon 40, pp. 1041-1083

Stuiver, M.; Reimer, P.J.; Braziunas, T. F. 1998. High-precision radiocarbon age calibration for terrestrial and marine samples. Radiocarbon 40, pp. 1127-1151.

Stuiver, M.; Reimer, P.J. 1993. CALIB rev. 8. Radiocarbon 35, pp. 215-230.

Sun, J.; Liu, T. 2000. Multiple origins and interpretations of the magnetic susceptibility signal in Chinese wind-blown sediments. Earth Planetary Science Letters, 180, pp. 287–296.

Sümegi, P. 2005. Loess and Upper Paleolithic Environment in Hungary: An Introduction to the Environmental History of Hungary Aurea: Nagykovácsi, Hungary, p. 312.

Sümegi, P. 1995. Quatermalacological analysis of Late Pleistocene Loess Sediments of the Great Hungarian Plain. Malacological Newsletter, 1, pp. 79–111.

Sümegi, P.; Hertelendi, E. 1998. Reconstruction of microenvironmental changes in Kopasz Hill loess area at Tokaj (Hungary) between 15.000-70.000 BP years. Radiocarbon, 40. pp. 855-863.

Sümegi, P.; Krolopp, E. 2002. Quatermalacological analyses for modeling of the Upper Weichselian palaeoenvironmental changes in the Carpathian Basin. Quaternary International 91, pp. 53–63.

Sümegi, P.; Rudner, Z.E. 2001. In situ charcoal fragments as remains of natural wild fires in the upper Würm of the Carpathian Basin. Quaternary International 76/77, pp. 165–176.

Sümegi, P.; Törőcsik, T.; Náfrádi, K.; Sümegi, B.P.; Majkut, P.; Molnár, D.; Tapody, R.O. 2016. Radiocarbon dated complex paleoecological and geoarcheological analyses at the Bodrogkeresztúr-Henye Gravettian site (NE Hungary). Archeometriai Műhely 2016/XIII./1.

Sümegi, P.; Gulyás, S.; Molnár, D.; Sümegi, B.P.; Almond, P.; Vandenberghe, J.; Zhou, L.; Pál-Molnár, E.; Törőcsik, T.; Hao, Q.; Smalley, I.; Molnár, M.; Marsi, I. 2018. New chronology of the best developed loess/paleosol sequence of Hungary capturing the past 1.1 ma: Implications for correlation and proposed pan-Eurasian stratigraphic schemes. Quaternary Science Reviews, 191, pp. 144–166.

Sümegi, P.; Gulyás, S.; Molnár, D.; Bozsó, G.; Fekete, I.; Makó, L.; Cseh, P.; Molnár, M.; Sümegi, B.P.; Almond, P.; Zeeden, C.; Törőcsik, T.; Nett, J.; Markó, A.; Lehmkuhl, F. 2021. New chronology and extended palaeoenvironmental data to the 1975 loess profile of Madaras brickyard, South Hungary. Journal of Quaternary Science, 36, pp. 1364–1381.

Sümegi, P.; Gulyás, S.; Molnár, D.; Szilágyi, G.; Sümegi, B.P.; Törőcsik, T.; Molnár, M. 2020. 14C Dated Chronology of the Thickest and Best Resolved Loess/Paleosol Record of the LGM from SE Hungary Based on Comparing Precision and Accuracy of Age-Depth Models. Radiocarbon, 62, pp. 403–417.

Sümegi, P.; Gulyás, S.; Persaits, G.; Páll, D.G.; Molnár, D. 2011. The loess-paleosol sequence of Basaharc (Hungary) revisited: Mollusc-based paleoecological results for the Middle and Upper Pleistocene. Quaternary International, 240, pp. 181–192.

Sümegi, P.; Hertelendi, E. 1998. Reconstruction of microenvironmental changes in Kopasz Hill loess area at Tokaj (Hungary) between 15,000–70,000 BP years. Radiocarbon, 40, pp. 855–863.

Sümegi, P.; Krolopp, E. 2002. Quatermalacological analyses for modeling of the Upper Weichselian palaeoenvironmental changes in the Carpathian Basin. Quaternary International, 91, pp. 53–63.

Sümegi, P.; Molnár, D.; Gulyás, S.; Náfrádi, K.; Sümegi, B.P.; Törőcsik, T.; Persaits, G.; Molnár, M.; Vandenberghe, J.; Zhou, L. 2019. High-resolution proxy record of the environmental response to climatic variations during transition MIS3/MIS2 and MIS2 in Central Europe: The loess-paleosol sequence of Katymár brickyard (Hungary). Quaternary International, 504, pp. 40–55.

Sümegi, P.; Náfrádi, K.; Molnár, D.; Sávai, Sz. 2015. Results of paleoecological studies in the loess region of Szeged-Öthalom (SE Hungary). Quaternary International, 372, pp. 66–78.

Sümegi, P.; Törőcsik, T.; Náfrádi, K.; Sümegi, B.P.; Majkut, P.; Molnár, D.; Tapody, R. 2016. Radiocarbon dated complex paleoecological and geoarcheological analyses at the Bodrogkeresztúr Henye Gravettian site (NE Hungary). Archeometriai Műhely, 8, pp. 31–42.

Sümegi, P.; Molnár, D.; Náfrádi, K.; Makó, L.; Cseh, P.; Törőcsik, T.; Molnár, M.; Zhou, L. 2022. Vegetation and land snail-based reconstruction of the palaeocological changes in the forest steppe eco-region of the Carpathian Basin during last glacial warming. Global Ecology and Conservation 33, e01976

Tan, H.; Ma, H.; Zhang, X.; Lu, H.; Wang, J. 2006. Typical geochemical elements in loess deposits in the Northeastern Tibetan Plateau and its paleoclimatic implications. Acta Geologica Sinica, 80, pp. 110–117.

Újvári, G.; Kovács, J.; Varga, Gy.; Raucsik, B.; Marković, S.B. 2010. Dust flux estimates for the Last Glacial Period in East Central Europe based on terrestrial records of loess deposits: a review. Quaternary Science Reviews, 29, pp. 3157-3166.

Újvári, G.; Kok, J.F.; Varga, G.; Kovács, J. 2016. The physics of wind-blown loess: Implications for grain size proxy interpretations in Quaternary paleoclimate studies. Earth-Science Reviews, 154, pp. 247–278.

Újvári, G.; Molnár, M.; Novothny, Á.; Páll-Gergely, B.; Kovács, J.; Várhegyi, A. 2014. AMS 14C and OSL/IRSL dating of the Dunaszekcső loess sequence (Hungary): Chronology for 20 to 150 ka and implications for establishing reliable age–depth models for the last 40 ka. Quaternary Science Reviews, 106, pp. 140–154.

Újvári, G.; Molnár, M.; Páll-Gergely, B. 2016. Charcoal and mollusc shell 14 C-dating of the Dunaszekcső loess record, Hungary. Quaternary Geochronology, 35, pp. 43–53.

Újvári, G.; Varga, A.; Raucsik, B.; Kovács, J. 2014. The Paks loess-paleosol sequence: A record of chemical weathering and provenance for the last 800ka in the mid-Carpathian Basin. Quaternary International, 319, pp. 22–37.

Vandenberghe, J. 2013. Grazin size of fine-grained windblown sediment: A powerful proxy for process identification. Earth-Science Reviews, 121, pp. 18–30.

Vandenberghe, J.; An, Z.S.; Nugteren, G.; Lu, H.; van Huissteden, K. 1997. New absolute time scale for Quaternary climate in the Chinese Loess region by grain-size analysis. Geology, 25, pp. 35–38.

Vandenberghe, J.; Mucher, H.J.; Roebroeks, W.; Gemke, D. 1985. Lithostratigraphy and Paleoenvironment of the Pleistocene Deposits at Maastricht-Belvédère, Southern Limburg, the Netherlands in Maastricht-Belvédère: Stratigraphy, Palaeoenvironment and Archaeology of the Middle and Late Pleistocene Deposits. Analecta Praehistorica Leidensia, 18, pp. 7–18.

Vandenberghe, J.; Nugteren, G. 2001. Rapid climatic changes recorded in loess successions. Global and Planetary Change, 28, pp. 1–9.

Varga, A.; Újvári, G.; Raucsik, B. 2011. Tectonic versus climatic control on the evolution of a loess-paleosol sequence at Beremend, Hungary: An integrated approach based on paleoecological, clay mineralogical, and geochemical data. Quaternary International, 240, pp. 71–86.

Wentworth, C.K. 1922. A scale of grade and class terms for clastic sediments, The Journal of Geology 30, pp. 377-392.

Wikimedia Commons. Pannonian Basin Geographic Map Blank Cropped. Available online: https://upload.wikimedia.org/wikipedia/commons/2/27/Pannonian_Basin_geographic_map_blank_croped.svg. (accessed on 15 May 2021)

Yang, S.; Li, C.; Yang, D.; Li, X. 2004. Chemical weathering of the loess deposits in the lower Changjiang Valley, China, and paleo-climatic implications. Quaternary International, 117, pp. 27–34.

Zhou, L.P.; Oldfield, F.; Wintle, A.G.; Robinson, S.G.; Wang, J.T. 1990. Partly pedogenic origin of magnetic variations in Chinese loess. Nature, 346, pp. 737–739.

Zhu, R.; Liu, Q.; Jackson, M.J. 2004. Paleoenvironmental significance of the magnetic fabrics in Chinese loess-paleosols since the last interglacial (<130 ka). Earth Planetary Science Letters, 221, pp. 55–69.

DECLARATION OF THE SUPERVISOR

I, Dávid Molnár, hereby confirm that the content of the dissertation is based on the independent work of the doctoral candidate and that he has contributed decisively to the results through his independent creative activity. I consider the entire dissertation to be eligible for support from a professional and academic point of view and recommend its acceptance.

Szeged, 11.07.2023.

.....

Dávid Molnár